

**UCGE Reports
Number 20340**

Department of Geomatics Engineering

**Remote sensing-based framework for forecasting forest
fire danger conditions over boreal forest**

(URL: <http://www.geomatics.ucalgary.ca/graduatetheses>)

by

Musa. Shammi Akther

September 2011



UNIVERSITY OF CALGARY

Remote sensing-based framework for forecasting forest fire danger conditions over
boreal forest

by

Musa. Shammi Akther

A THESIS

SUBMITTED TO THE FACULTY OF GRADUATE STUDIES
IN PARTIAL FULFILMENT OF THE REQUIREMENTS FOR THE
DEGREE OF MASTER OF SCIENCE

DEPARTMENT OF GEOMATICS ENGINEERING

CALGARY, ALBERTA

SEPTEMBER, 2011

© Musa. Shammi Akther 2011

Abstract

Forest fire is an integral part in many forested ecosystems including boreal forests, which influences forest productivity, biodiversity and socio-economy, among others. Here, the potential of three selected satellite (i.e., MODIS)-based variables/indices at 8-day temporal resolution, i.e., surface temperature (T_S), normalized multiband drought index (NMDI) and temperature vegetation wetness index (TVWI) were evaluated in predicting/forecasting the fire danger conditions over boreal forest regions of Alberta during the period 2006-2008. The method was based on the assumption that the fire danger conditions during $i+1$ period would be high if the instantaneous values of: (i) T_S values were either higher or equal; or (ii) NMDI or TVWI values were either lower or equal; in comparison to their respective study area-specific average during i period. The analyses were conducted on the basis of either individual variables or combining all of the three together. The reasonable amounts of fire polygons were fell under the high fire danger conditions for each of the variables individually (i.e., 70.14% for T_S ; 77.26% for NMDI; and 59.73% for TVWI). The combination of all the three individual variables revealed that 95.92% of the fires fell in the categories of “very high” (i.e., all three variables indicated high danger), “high” (i.e., at least two of them indicated high danger), or “moderate” (i.e., at least one of the variables indicated high danger) fire danger classes. These results showed potential applicability of the proposed method in predicting fire danger conditions over the boreal forest regions.

Preface

In the scope of this Thesis, a remote sensing-based framework has been developed in forecasting forest fire danger conditions over the boreal forested regions. The outcomes of this research have been published in a regular fashion, and the details are as follows:

Peer-reviewed Journal Article

- [1] Akther, M.S. and Hassan, Q.K. 2011. Remote sensing based estimates of surface wetness conditions and growing degree days over northern Alberta, Canada. *Boreal Environment Research*, Vol.16. (In press).
- [2] Akther, M.S. and Hassan, Q.K. Remote sensing-based assessment of fire danger conditions over boreal forest. *IEEE Selected Topics in Earth Observation and Remote Sensing* (Accepted).

Proceedings Paper

- [3] Akther, M.S. and Hassan, Q.K. 2010. Spatio-temporal dynamics of surface wetness conditions using remote sensing data over northern Alberta, Canada. *Proceedings of Canadian Geomatics Conference held on 14- 18 June, 2010 at Calgary, Canada. 5p.*

Abstract

- [4] Akther, M.S. and Hassan, Q.K. 2011. Relation between remote sensing-derived variables and forest fire occurrences. *CGU-CSAFM 2011 Scientific Meeting held on May 15-18, 2011 at Banff, AB, Canada.*

Acknowledgements

I would like to thank my supervisor, Dr. Quazi K. Hassan, for his guidance and motivation. Without his enormous support, ideas and illuminating instruction this Thesis could not have reached its present form. I also would like to thank the members of my Thesis examining committee, Dr. Mryka Hall-Beyer, Dr. Ayman Habib and Dr. Derek Lichti.

I would like to acknowledge the various financial supports obtained from: (i) Dr. Quazi K. Hassan's various research grants, (ii) University of Calgary in the form of Faculty of Graduate Studies Scholarship Award, Differential fees and Teaching Assistantships, and (iv) Schulich School of Engineering in the form of a Travel Grant to attend a conference.

I also would like to thank the following agencies for providing the data free of charge: (i) NASA for providing MODIS data; (ii) Alberta Agriculture and Rural Development Department for providing ground-based volumetric soil moisture data; and (iii) Alberta Department of Sustainable Resource Development for providing the fire activity data.

I wish to thank to all of my "Earth Observation for Environment Laboratory" group members for their support, help and encouragement. I also express my love and gratitude to my beloved family members, especially my mother, Mrs. Monowara Haque. Finally, it is worthwhile to thank my loving, supportive, encouraging, and patient husband Kazi Mahmudur Rahman who keeps my spirits up during this programme when it seemed unachievable.

Dedication

*To the loving memory
of
my late father Mohd. Shamsul Haque.*

Table of Contents

Approval Page.....	ii
Abstract.....	iii
Preface.....	iv
Acknowledgements.....	v
Dedication.....	vi
Table of Contents.....	vii
List of Tables.....	ix
List of Figures and Illustrations.....	x
List of Symbols, Abbreviations and Nomenclature.....	xiii
CHAPTER 1: INTRODUCTION.....	1
1.1 Background.....	1
1.2 Problem statement.....	5
1.3 Research objectives.....	8
1.4 Thesis outline.....	9
CHAPTER 2: LITERATURE REVIEW.....	11
2.1 Defining fire danger conditions.....	11
2.2 Causes of forest fire.....	11
2.3 Factors influencing forest fire.....	12
2.4 Methods of SWC Determination.....	14
2.5 Review of remote sensing-based methods in fire danger mapping.....	18
2.6 MODIS data characteristics.....	23
CHAPTER 3: METHODOLOGY.....	26
3.1 Estimation of TVWI.....	27
3.1.1 Description of the study area.....	27
3.1.2 Data Requirements.....	29
3.1.3 Methods.....	30
3.1.3.1 MODIS Data pre processing.....	31
3.1.3.2 Generation of TVWI-values.....	35
3.1.4 Validation.....	39
3.2 Assessment of the remote sensing-based variables in forecasting fire danger conditions.....	40
3.2.1 Description of the study area.....	40
3.2.2 Data Requirements and its Preprocessing.....	43
3.2.2.1 Generation of NMDI maps.....	44
3.2.3 Methods.....	46
3.2.3.1 Analyzing the individual variables of T_s , NMDI, and TVWI in forecasting fire danger conditions.....	48
3.2.3.2. Combining all the three variables in forecasting the fire danger conditions.....	50
3.2.3.3 Generating the fire danger maps for the individual periods of interest.....	50

3.2.4 Validation.....	50
3.2.4.1 Evaluating the capability of the individual variables in forecasting the fire danger conditions.....	51
3.2.4.1 Evaluating the potential of combining all the three variables in forecasting the fire danger conditions.....	52
CHAPTER 4: RESULTS AND DISCUSSION.....	53
4.1 Estimation of TVWI	53
4.2 Assessment of the remote sensing-based variables in forecasting fire danger conditions.....	61
4.2.1 The capability of the individual variables of T _s , NMDI, and TVWI in forecasting fire danger conditions.....	61
4.2.1.1 The temporal dynamics of the study area-specific average values for the variables.....	61
4.2.1.2 The capability of the individual variables of T _s , NMDI, and TVWI in forecasting fire danger conditions.....	63
4.2.2 The potential of combining all the three variables in forecasting the fire danger conditions.....	67
4.2.2.1 Fire danger maps for the individual periods of interest.....	69
CHAPTER 5: CONCLUSIONS AND FUTURE WORK.....	71
5.1 Summary.....	71
5.2 Contribution to science.....	72
5.3 Future works.....	72
REFERENCES.....	74
APPENDIX I.....	86
APPENDIX II.....	87
APPENDIX III.....	89
APPENDIX IV.....	101
APPENDIX V.....	122

List of Tables

Table 2.1: MODIS specifications	24
Table 2.2: Characteristics of MODIS spectral bands.....	25
Table 3.1: Time periods of MODIS 8-day composites data	32
Table 3.2: Characteristics of natural sub regions over the study area	42
Table 4.1: % of data lower/ higher than the mean values over the study area.....	63
Table 4.2: No. of fire within ± 3 standard deviation for the variables.....	66
Table 4.3: % of data under each of the fire danger condition categories upon combining all of three variables.....	68
Table AII.1: Values of dryline1 (θ_{dry1}) and slope and intercept of the dryline2 (θ_{dry2}) for estimating TVWI	87
Table AII.2: Description of the quadratic fits ($y = a_1x^2 + a_2x + a_3$) to the variables of T_S / NMDI / TVWI as a function of DOY	88

List of Figures and Illustrations

Figure 1.1: 15 terrestrial ecozones of Canada.....	2
Figure 1.2: Extent of boreal forest across Canada	4
Figure 1.3: Schematic diagram of the Forest Fire Weather Index	6
Figure 1.4: Schematic diagram of the proposed framework.....	9
Figure 2.1: Triangular diagram of the major factors responsible for the forest fire danger.....	13
Figure 3.1: (a) Location of the province of Alberta in Canada, (b) The extent of the study area	28
Figure 3.2: Schematic diagram of the methodology of estimating TVWI	30
Figure 3.3: Conceptual diagram illustrated the calculations of TVWI as a function of θ_s and NDVI	38
Figure 3.4: The extent of the study area with the natural sub regions falling under the area of interest.....	41
Figure 3.5: Simulated canopy spectra at different leaf water content.....	45
Figure 3.6: Schematic diagram of the methods of assessing the remote sensing-based variables in forecasting fire danger conditions	47
Figure 3.7: Conceptual diagram of forecasting forest fire danger as a function of MODIS-derived variables (i.e., T_s , NMDI and TVWI).....	49
Figure 4.1: Example of scatter plot of θ_s vs. NDVI and the corresponding dry and wet edges during the day of year 153-160 in 2006.....	53
Figure 4.2: The temporal dynamics of the study area-specific average values for the variable of (a) T_s , (b) NMDI and (c) TVWI during the fire seasons	55
Figure 4.3: Deviation between the averaged ground-based measurements of VSM and TVWI for the period 2006-2008	57
Figure 4.4: Spatial dynamics of 2006-2008 averaged TVWI and its relative frequency distribution	60
Figure 4.5: The temporal dynamics of the study area-specific average values for the variable of (a) T_s , (b) NMDI and (c) TVWI during the fire seasons	62

Figure 4.6: Frequency distribution of the fires on the basis of the “study area-specific average \pm 3 standard deviation” values.....	64
Figure 4.7: An example fire danger mapping for the period 25 June-02 July, 2008 produced by combining all of three variables of T_s , NMDI, and TVWI.....	70
Figure AIII.1: Fire danger mapping for the period 17 May-24 May, 2006.....	90
Figure AIII.2: Fire danger mapping for the period 26 June-03 July, 2006.....	91
Figure AIII.3: Fire danger mapping for the period 04 July-11 July, 2006	92
Figure AIII.4: Fire danger mapping for the period 28 July-04 August, 2006	93
Figure AIII.5: Fire danger mapping for the period 17 May-24 May, 2007	94
Figure AIII.6: Fire danger mapping for the period 26 June-03 July, 2007.....	95
Figure AIII.7: Fire danger mapping for the period 04 July-11 July, 2007	96
Figure AIII.8: Fire danger mapping for the period 28 July-04 August, 2007	97
Figure AIII.9: Fire danger mapping for the period 16 May-23 May, 2008	98
Figure AIII.10: Fire danger mapping for the period 03 July-10 July, 2008	99
Figure AIII.11: Fire danger mapping for the period 27 July-03 August, 2008	100
Figure AIV.1: The spatial model showing the formulated workflow with data inputs to produce mosaicked images	102
Figure AIV.2: The spatial model showing the formulated workflow with data inputs to produce stacked images	104
Figure AIV.3: The spatial model showing the formulated workflow with data inputs to produce the binary images	105
Figure AIV.4: The spatial model showing the formulated workflow with data inputs to produce the total cloud free number images	106
Figure AIV.5: The spatial model showing the formulated workflow with data inputs to produce the mean and sum mean deviation images.....	107
Figure AIV.6: The spatial model showing the formulated workflow with data inputs to produce the average deviation images	108
Figure AIV.7: The spatial model showing the formulated workflow with data inputs to produce the cloud corrected images.....	109

Figure AIV.8: The spatial model showing the formulated workflow with data inputs to produce the NDVI images	110
Figure AIV.9: The spatial model showing the formulated workflow with data inputs to produce the NMDI images.....	111
Figure AIV.10: The spatial model showing the formulated workflow with data inputs to produce the atmospheric pressure images	112
Figure AIV.11: The spatial model showing the formulated workflow with data inputs to produce the potential temperature images	113
Figure AIV.12: The spatial model showing the formulated workflow with data inputs to produce the stack image of NDVI and potential temperature	114
Figure AIV.13: The ERDAS built-in model interface of Creating Feature Space Image.....	115
Figure AIV.14: The ERDAS built-in model interface of converting pixel values to ASCII	116
Figure AIV.15: The spatial model showing the formulated workflow with data inputs to produce the TVWI images	118
Figure AIV.16: The spatial model showing the formulated workflow with data inputs to calculate the global mean and standard deviation.....	119
Figure AIV.17: The spatial model showing the formulated workflow with data inputs to produce the fire danger maps	121

List of Symbols, Abbreviations and Nomenclature

List of Symbols

<u>Symbol</u>	<u>Definition</u>
α	Prestley-Taylor's parameters
ϕ	combined effects of α and Budyko-Thronwaite-Mather's wetness parameters
ρ	Surface Reflectance
θ	Soil moisture
θ_s	Potential Surface Temperature
C_{ab}	Chlorophyll content
C_m	Leaf dry matter content
C_p	Specific heat capacity
C_w	Water content
g	Earth-surface gravitational acceleration
L	Temperature lapse rate
N	Leaf internal structure
P_0	Average pressure at mean sea level
R	Gas constant
T_0	Sea level standard temperature
T_a	Air Temperature
T_s	Surface Temperature
Z	Elevation above mean sea level

List of Abbreviations

<u>Abbreviation</u>	<u>Definition</u>
ARD	Agriculture and Rural Development
AVHRR	Advanced Very High Resolution Radiometer
BUI	Buildup index
DC	Drought code
DMC	Duff moisture
DOY	Day of Year
EVI	Enhanced Vegetation Index
FFMC	Fine fuel moisture code
FWI	Forest Fire Weather Index
GIS	Geographic Information Systems
ISI	Initial spread index
LAI	Leaf area index
LP DAAC	Land processes distributed active archive center
MODIS	Moderate Resolution Imaging spectroradiometer
MSG	Meteosat Second Generation
NASA	National Aeronautics and Space Administration
NDVI	Normalized Difference Vegetation Index
NDWI	normalized difference water index
NIR	Near infrared
NMDI	Normalized Multiband Drought Index
NOAA	National Oceanic and Atmospheric Administration
NRC	National Resource Canada
SAIL	Scattering Arbitrary Inclined Leaves
SEVIRI	Spinning Enhanced Visible and InfraRed Imager
SRD	Sustainable Resource Development
SWC	Surface Wetness Condition
SWIR	Shortwave infrared
TVWI	Temperature Vegetation Wetness Index
UTM	Universal Transverse Mercator
VARI	Visible atmospherically resistant index
VI	Vegetation Index
VIgreen	vegetation index green
VSM	Volumetric Soil Moisture
WDI	Water deficit index

CHAPTER 1: INTRODUCTION

1.1 Background

Canada is divided into 15 terrestrial ecozones on the basis of landforms, soil types, water features, climate, vegetation, flora and fauna as shown in Figure 1.1. Among these, 11 of the ecozones are forest-dominant (NRC, 2011a), that include: Taiga Cordillera, Boreal Plains, Taiga Plains, Hudson Plains, Boreal Cordillera, Boreal Shield, Taiga Shield, Atlantic Maritime, Pacific Maritime, Mixedwood Plains, Montane Cordillera. It is interesting to note that the boreal ecozones (that include Boreal Plains, Boreal Cordillera and Boreal Shield ecozones) occupy approximately 35% of Canada's total landmass (NRC, 2011b). Thus it would be important for us to study the dynamics of these ecozones for maximizing their benefits.

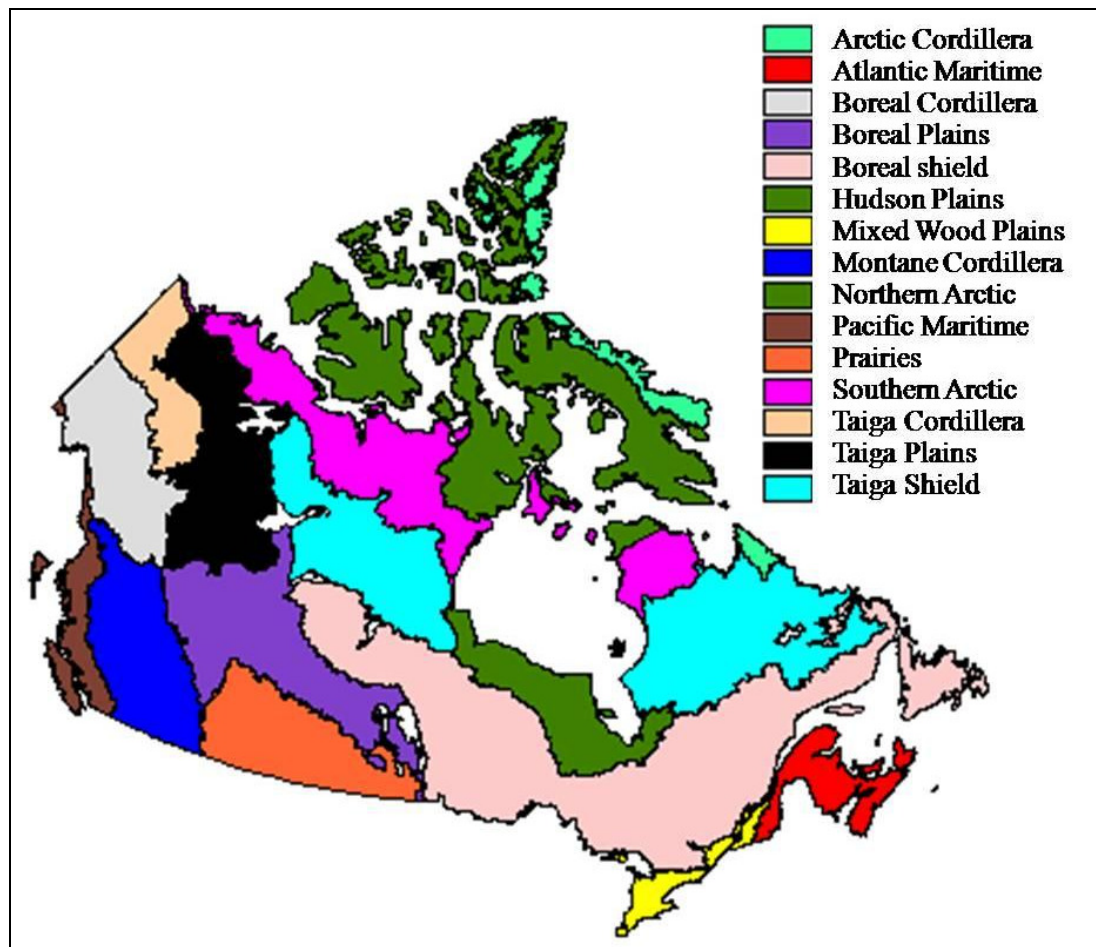


Figure 1.1: 15 terrestrial ecozones of Canada (Source: Ecozones, SC, 2011)

In general, the boreal ecozones and their forest (called boreal forest hereafter) are significantly impacted by different natural disturbances, such as, forest fires, forest insect outbreaks, landslides, ice storms, wind storms among others. Among these disturbances, the forest fire is one of the most important ones (NRC, 2011c). The forest fire impacts us in numerous ways: (i) economic loss due to burning of the trees and properties adjacent to the location of fire, (ii) releasing enormous amounts of CO₂ into the atmosphere, (iii) health hazard due to smoke, and (iv) loss of human life in fighting large fires, among

others. Conversely, there are a number of benefits: (i) controls the disease and insects, (ii) controls stand species and communities, (iii) influences wildlife habitat patterns and populations, (iv) exposes the mineral soils to support regeneration of the trees, (v) more exposure to the incident solar radiation, (vi) release of seeds for certain tree-species, and (vii) small fires are extremely helpful in reducing the excessive loading of the dead vegetation, that helps to control the large fires. As per the Canadian historical record, there are about 9000 forest fires per annum that burn 2.1 million hectares of forests on an average (NRC, 2011b). Note that the large fires dominate the total burned areas (i.e., fires greater than 200 ha represent 97% of area burned). Figure 1.2 shows the extent of boreal forest along with the provincial boundaries and the forest fire occurrences over Canada during the period 1980-1989.

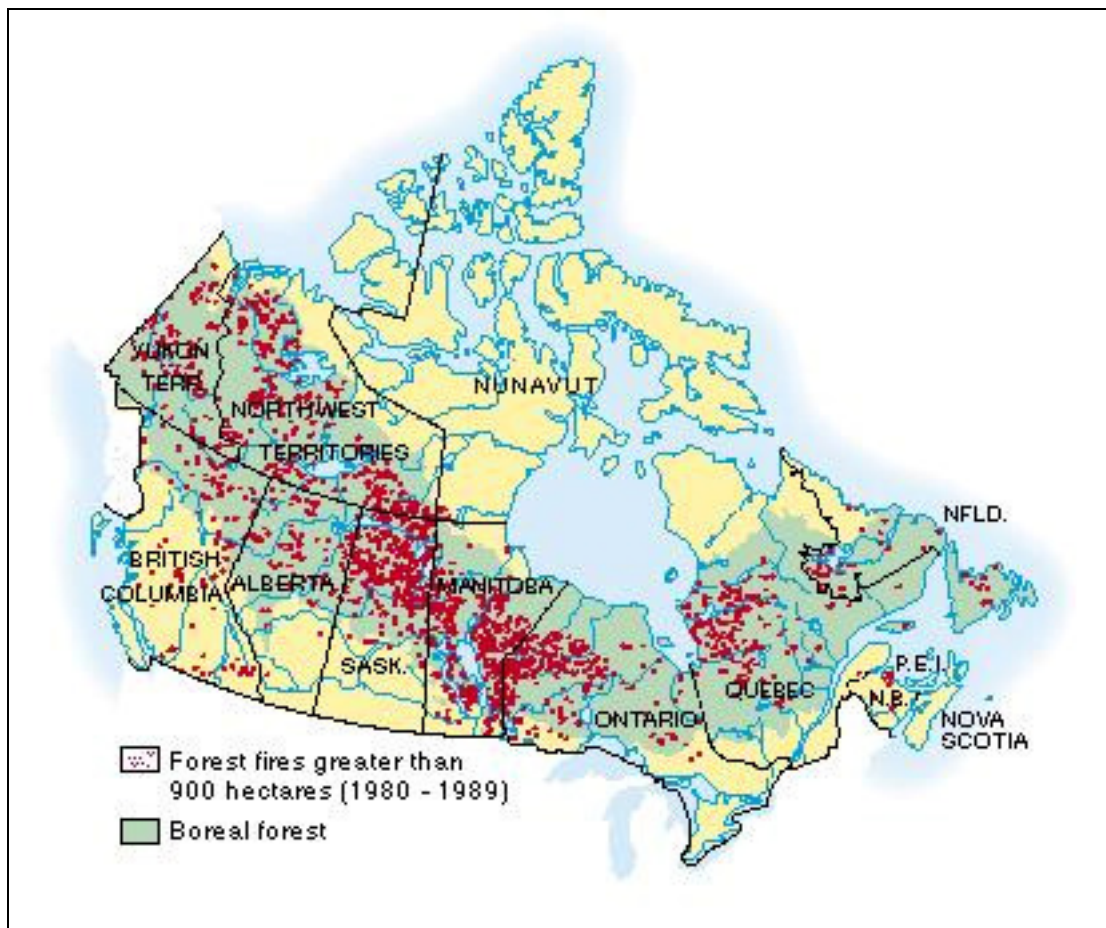


Figure 1.2: Extent of boreal forest with the provincial boundaries and forest fire occurrences across Canada (Source: The Atlas of Canada, NRC, 2011 b)

The Canadian province of Alberta [where boreal forest occupies approximately 58% of the area (Dowing and Pettapiece 2006)], on average about 1400 fires occurred each year with a total of 135 thousand hectares of area burned over the years 2000-2009 (SRD, 2011a). So, it is very important to investigate the probability of fire occurrence or pre-fire forest conditions.

Several factors are responsible for the occurrence of the forest fires. Some of the critical factors are weather (e.g., temperature, precipitation, wind speed, soil moisture, and atmospheric moisture, among others) and fuel conditions (Flannigan et al. 2000, Carvalho et al. 2008, Flannigan et al. 2009, Krawchuk et al. 2009). Along with these, it also requires a source of ignition that includes lightning and human induced fires.

1.2 Problem statement

In Canadian context, the forest fire danger is determined using the Forest Fire Weather Index (FWI: a component of Canadian Forest Fire Danger Rating System) system (Van Wagner 1987); and illustrated in Figure 1.3. It computes three fuel moisture codes: Fine Fuel Moisture Code (FFMC), Duff Moisture Code (DMC), Drought Code (DC) and three fire behavior indices: Initial Spread Index (ISI), Buildup Index (BUI), and Fire Weather Index (FWI) (NRC, 2011d). The FFMC is the ratings of the moisture content of litter and other cured fine fuels and indicate the relative ease of ignition and the flammability of fine fuel. This is the fast drying layer with a time lag of 12 hours and derived as a function of temperature, relative humidity, rain and wind. DMC is an indication of fuel consumption in moderate duff layers and medium-size woody material and represents the average moisture content of loosely compacted organic layers of moderate depth. DC is the average moisture content of deep, compact organic layers which is an indicator of seasonal drought effects on forest fuels and the amount of smoldering in deep duff layers and large logs (NRC, 2011d). The DMC and the DC are the slow drying code with time lags of 12 and 25 days respectively. On the other hand, the fire behavior indices represent the rate of fire spread, the fuel available for combustion, and the frontal fire intensity. The

higher numbers of all components indicate the increases of fire danger conditions (NRC, 2011d).

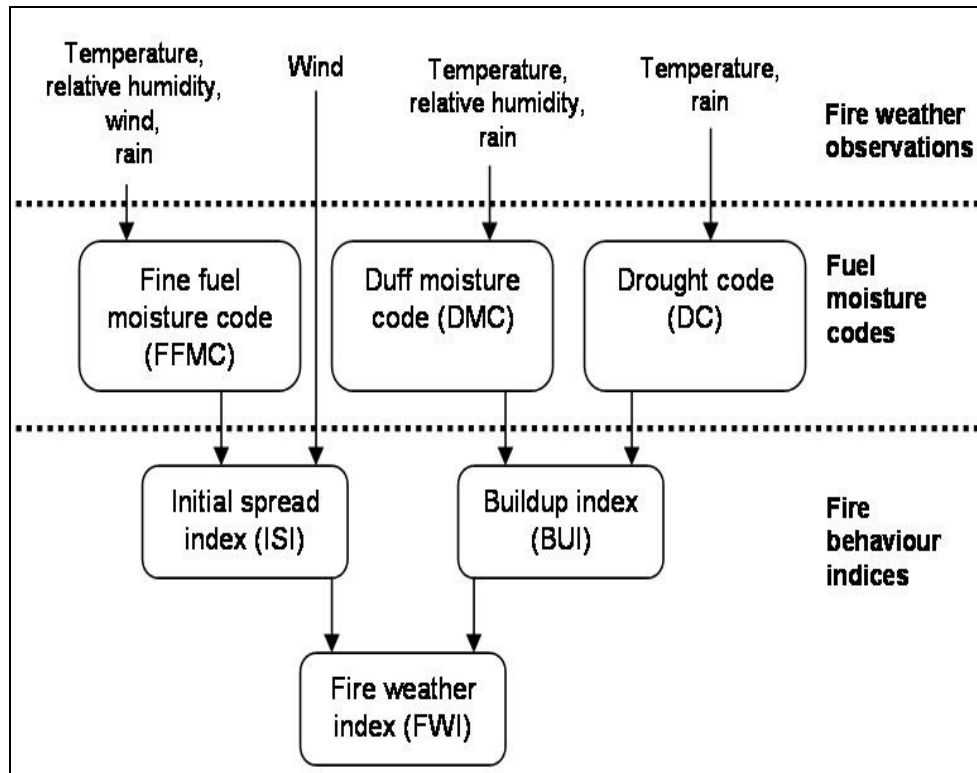


Figure 1.3: Schematic diagram of the Forest Fire Weather Index (adopted from Van Wagner, 1987)

The FWI system uses gridded maps of several weather variables from the previous day's, that include noon-time measurements of air temperature, relative humidity, and wind speed; and rainfall accumulated over 24-hour period) to generate the components. The gridded weather maps were produced by interpolating the weather data between stations using the Geographic Information Systems (GIS) techniques.

In theory, different interpolation techniques (e.g. kriging, inverse distance weighing, natural neighbour etc.) generate different maps of a particular output even using the same input dataset (Lam 1983). The uncertainty associated with interpolation techniques can potentially be reduced by incorporating more point-based measurements of the required weather variables, which is expensive and also difficult to acquire in the remote areas of the landscape. In addition, not only the weather conditions, but also the presence of fuel (i.e., vegetation composition) and its status are important in describing fire danger conditions (Johnson 1992, Mallinis et al 2008).

In order to address the limitation of interpolation techniques and also incorporate fuel conditions, the remote sensing-based methods can be employed to generate continuous surfaces for the variables of interest (Leblon et al. 2007, Stenberg et al. 2008, Anttliia and Kairesalo 2010, Sekhon et al. 2010).

In general, the remote sensing-based methods are used in monitoring the fire danger conditions (e.g., Gu et al. 2008, Wang et al. 2008, Wang et al. 2009), these have been evaluated against the fire danger conditions during the same period of fire occurrences. Thus, it would be worthwhile to develop a remote sensing-based framework to determine the probability of fire occurrence or pre-fire forest conditions in estimating the spatial dynamics to aid better fire management practices.

1.3 Research Objectives

In the scope of this Thesis, the potential of several Moderate Resolution Imaging Spectroradiometer (MODIS)-based variables/indices in forecasting fire danger conditions were evaluated over the agriculture and forest dominated regions in the Canadian province of Alberta. Figure 1.4 shows the schematic diagram of the proposed framework.

In the development of this framework, there were two main objectives,

- (i) implementing the existing temperature-vegetation wetness index (TVWI: an indirect method to estimate the surface wetness conditions; Hassan et al. 2007b) approach over the topographically-variable agriculture and forest dominated northern portion of Canadian province of Alberta,
- (ii) integrating the weather and fuel condition to develop a framework to forecast the fire danger condition. The variables were: surface temperature (T_s), normalized multiband drought index (NMDI: a measure of vegetation water index which express the fuel condition) (Wang and Qu 2007, Wang et al. 2008); and TVWI.

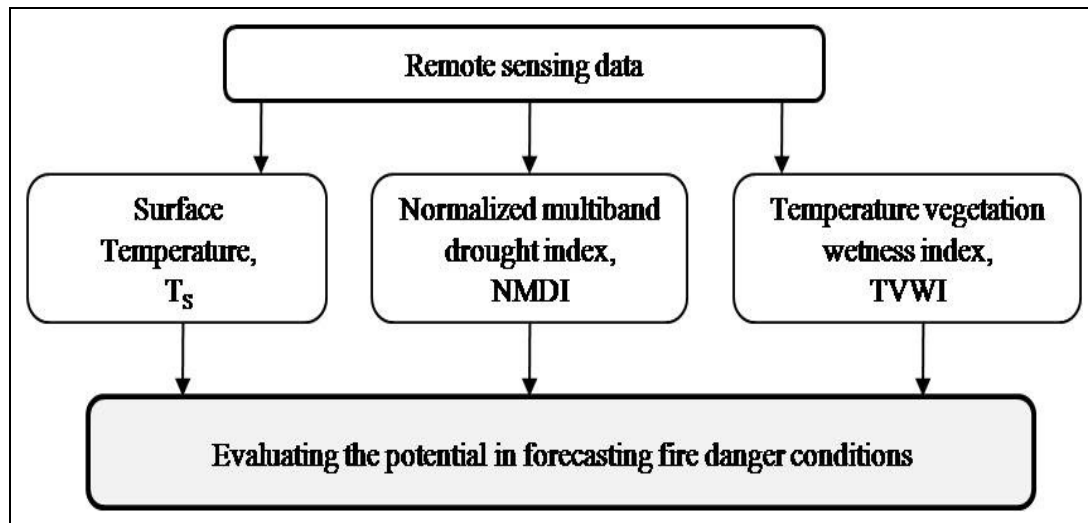


Figure 1.4: Schematic diagram of the proposed framework

1.4 Thesis Outline

This Thesis consists of five chapters. Chapter one provides background information, problem statement, and objectives of the research.

Chapter two provides literature review on the influencing factors causing fires to occur. It also presents the existing remote sensing-based methods in determining the various aspects of the forest fire danger conditions.

Chapter three describes the methodology of the study. It includes estimation of the remote sensing-based variables and assessment of the variables in forecasting fire danger conditions.

Chapter four provides the results from the findings of this research along with brief discussion.

Chapter five summarizes the key findings of the research, the scientific contribution of the research, and the scope of the future directions.

CHAPTER 2: LITERATURE REVIEW

2.1 Defining fire danger conditions

The fire danger condition is the state of the surrounding environment that controls the fire behaviour, i.e., how the fuel ignites, flame develops, and fire spreads (Wotton, 2009).

Such danger conditions may be determined as a function of the interaction among some of the physical and biological environmental components (Countryman 1972). Those include the conditions of weather and fuel in particular.

2.2 Causes of forest fire

There are two major reasons behind the occurrence of forest fires, namely, i) lightning-caused fire, and ii) human-caused fire. Lightning is the primary natural cause of forest fires and the sources of the human-caused fires may include arson, sparks from the machineries of forest industry, passing trains, prescribed burn, recreation (unattended or out-of-control campfires, lighted cigarettes etc.), human negligence (people sometimes leave behind the sources of ignition like a camp fire), residents (burning grass, brush or rubbish etc.) among others.

During the period 2000-2009, in Alberta 43% of wildfires were caused by lightning (that burned ~ 66% of total burn-area), and human-caused fires were 57% (that burned ~34% of total burn-area) (SRD, 2011a). The lightning-caused fires burned the major portion of the total burn-area, as sometimes they occur in remote areas and go undetected. Thus, the

lightning-caused fires may sustain for a relatively longer period of time before being detected by firefighting authorities.

2.3 Factors influencing forest fire

The factors that influence the forest fire danger are a combination of both static and dynamic characteristics of a particular location. Those factors vary spatially and temporally across the landscape. According to the classic fire environment triangle, the three principal elements that affect the forest fire behaviour are (Countryman 1972):

- (i) *weather conditions*: it involves surface temperature, rainfall amounts and duration, relative humidity, cloud cover, and wind speed and direction, among others.
- (ii) *fuel characteristics*: the type of fuel, quantity, fuel moisture condition are the fuel characteristics that influence the fire behaviour.
- (iii) *topographic characteristics*: it involves slope, steepness, aspect, elevation among, others..

Among the elements, the topography of a particular landscape is a static factor which increases the rate of spread and intensity of the ignited fire. So, for early warning of fire occurrence the weather condition and fuel condition are the key variables. The source of ignition that causes fires is also an essential component for fire occurrences. It initiates the fire phenomenon with the favorable fire danger condition. Figure 2.1 shows the fire triangle which includes the source of ignition, weather condition and fuel condition to explain the precondition of the forest fire occurrence.

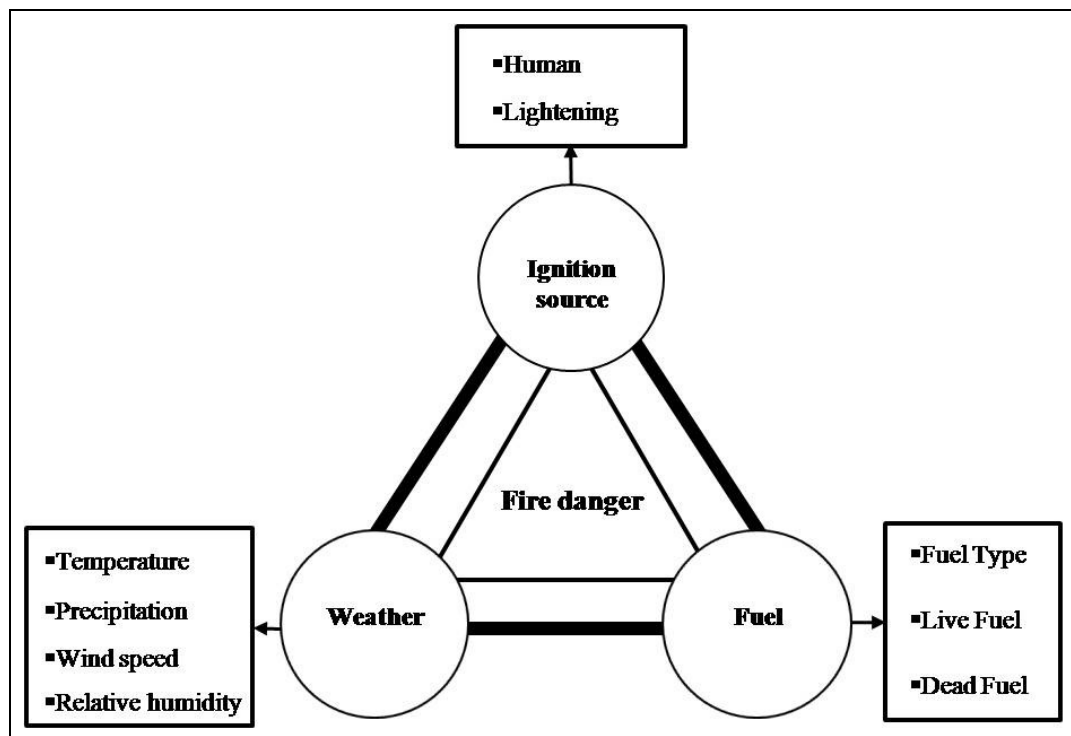


Figure 2.1: Triangular diagram of the major factors responsible for the forest fire danger

Among all the factors mentioned above, some of the critical variables representing both weather and fuel conditions were investigated. Those include: surface wetness conditions (SWC: an indirect way of estimating soil moisture), temperature (or surface temperature), and live fuel moisture conditions.

2.4 Methods of SWC Determination

Soil moisture is the amount of water in the soil column available for the plant uptake which is a primary indicator which expresses the drought condition as well as forest fire danger condition. It is also a very essential variable for the vegetation growth and many plant functions (e.g., photosynthesis, transpiration, both plant and soil respiration, and in-plant water and nutrient movements etc.) (Flanagan and Johnson 2005, Hari and Nojd 2009). The weather and precipitation patterns also depend on soil moisture (Fennessey and Shukla, 1999). So, it is essential to estimate the soil moisture to understand the drought condition as well as fire danger conditions (i.e., probability of fire occurrence). Soil moisture is highly variable both spatially and temporally (Brocca et al. 2010).

SWC can be measured precisely at point locations using either direct or indirect methods. The direct methods are known as gravimetric method and volumetric method. In gravimetric method, soil moisture is derived from the changes in mass of the sample of soil weighted before and after drying. The sample of the soil is taken using coring devices or augers at specific depths and locations. Similarly, in volumetric method the soil sample is taken with a known volume core sampler or with a tube auger and estimated the amount of water present in soil sample by drying it in the oven. These methods are labor-intensive, time consuming and destructive (i.e., a sample of soil can only use once to estimate the soil moisture as the soil sample cannot be taken at exactly the same location more than one time). Thus in order to capture the temporal variability of soil moisture the alternative is the use of indirect methods, which are non-destructive in nature. Some of the commonly used indirect methods are: neutron scattering, Gamma Ray Attenuation,

time domain reflectometry, frequency domain reflectometry, and ThetaProbe etc. (Seneviratne et al., 2010, Chow et al. 2009). The neutron scattering method uses a radioactive source of fast (high-energy) neutrons which are lowered into a borehole, and the moisture content of the soil measured by counting the slowed down or thermalized neutron density which are backscattered by the collisions with hydrogen nuclei. The gamma ray attenuation method is also a radioactive technique where the moisture content is determined from the wet density changes measured by the gamma transmission technique. On the other hand, the time domain reflectometry and frequency domain reflectometry are the electromagnetic techniques which have ability to determine accurately the permittivity (dielectric constant) of the soil on the soil moisture content from wave propagation. The Theta Probe type ML2x method uses the impedance of a sensing rod by measuring a standing wave. This method is used by Alberta Agriculture and Rural Development Department (ARD, 2010). It acquires the volumetric soil moisture (VSM: % of volume of soil moisture at 5 cm, 20 cm, 50 cm and 100 cm depth of the soil profile) inserting the instrument horizontally into the soil. The sensors can be inserted in the holes which are previously prepared using any kind of adequate soil drill device. It also can install by covering the sensor in soil up to maximum 5 m depth.

However, the ground-based methods fail to provide the spatial variability, which is important to understand the dynamics at landscape scale. One of the feasible alternatives are the employment of remote sensing-based methods, which have already been proven to address the spatial dynamics for the variable of interest (Stenberg *et al.* 2008, Anttlia and Kairesalo 2010, Sekhon *et al.* 2010).

For the last two decades, visible and thermal infrared remote sensing data have been widely used to determine soil moisture indirectly as a means of SWC. In most of instances, these depend upon the relationships between vegetation index (VI) and actual surface temperature (T_s) (Nemani et al. 1993, Carlson 2007, Li et al. 2009, Patel et al. 2009). The T_s is an indicator of water stress due to an inverse relationship between transpiration and leaf temperature. The transpiration decreases from water deficit which increases the leaf temperature consequently increases the air temperature and surface temperature. According to this concept, a two dimensional scatter plot of T_s -VI usually assumes a triangular (Carlson 2007; Sandholt et al. 2002) or trapezoidal shape (Moran et al. 2004, Petropoulos et al. 2009). The edges of these shapes are considered in the formulation of SWC. In general, the negative slope of the T_s -VI diagram describes the water availability with respect to the vegetation conditions, e.g., (i) high SWC-values are found over relatively dense vegetation with low T_s -values; and (ii) low SWC-values are, on the other hand, found over sparse vegetation with high T_s -values. In particular to describing the VI component, most of the instances, the normalized difference vegetation index [NDVI: as a function of surface reflectance-values from red and near infrared spectral bands] is used using the following expression (Rouse et al. 1974):

$$NDVI = \frac{\rho_{NIR} - \rho_{Red}}{\rho_{NIR} + \rho_{Red}} \quad (2.1)$$

where, ρ is the surface reflectance for the near infrared (NIR) and red spectral bands.

The T_S -VI space can be formulated by use of either daily-level or composites. However, Venturini et al. (2004) emphasized on the uncertainty of the daily-values of remote sensing-based T_S as a result of atmospheric conditions. They also mentioned that the use of multiday (e.g., 14 or 16-day) composite of T_S would not be useful for their proposed method of determining ϕ (i.e., the combined effects of Priestley-Taylor's parameters α and Budyko-Thornwaite-Mather's wetness parameters) as part of estimating evapotranspiration by using T_S -VI relations. In contrast, other researchers (e.g., Patel et al., 2010; Chen et al., 2010) used composites in the T_S -VI approach in determining SWC regimes; and demonstrated its effectiveness.

Despite the wider acceptability of the T_S -VI methods, the major limitation is its applicability over topographically variable terrain as the elevation influences the T_S (Carlson 2007). The T_S decreases with increases of elevation due to the atmospheric pressure drops. Another fact is that the T_S -VI methods has not widely used over vegetated regions. The limitation of topographic variability first addressed by Hassan et al. (2007b) by transforming the T_S into potential surface temperature (θ_S : defined as the temperature considering that the site lies at the mean sea level) to eliminate the influence of elevation on T_S ; and then combined with NDVI [the method described as temperature vegetation wetness index (TVWI)] (Hassan et al. 2007b, Hassan and Bourque 2009) over forest dominated humid region in Canadian Atlantic Maritime Ecozone. The scatter plots of NDVI- T_S are created either triangular or trapezoidal form and the slope of the NDVI- T_S space is related to surface soil moisture and evapotranspiration and provides valuable information on surface and vegetation water stress. However, the TVWI approach

requires further validation over other ecozones to determine its wider applicability and need to evaluate the applicability in explaining the forest fire danger condition.

2.5 Review of remote sensing-based methods in fire danger mapping

In most of the instances, remote sensing-based vegetation and water indices are commonly used in understanding forest fire danger conditions. These indices are based on the surface reflectance characteristics observed in the visible and infrared spectral bands acquired by the satellite sensors. Some of the commonly used indices are NDVI (see Eq. 2.1), enhanced vegetation index (EVI), vegetation index green (VIgreen), visible atmospheric resistant index (VARI), and normalized difference water index (NDWI); and their formulations are as follows:

- Enhanced vegetation index (EVI) (Huete et al 2002):

$$EVI = 2.5 * \frac{\rho_{NIR} - \rho_{Red}}{\rho_{NIR} + \rho_{Red} - \rho_{Blue} + 1} \quad (2.2)$$

where, ρ is the surface reflectance for the near-infrared, red and blue spectral bands.

- Vegetation index green (VIgreen) (Gitelson et. al 2002)

$$VI_{green} = \frac{\rho_{Green} - \rho_{Red}}{\rho_{Green} + \rho_{Red}} \quad (2.3)$$

where, ρ is the surface reflectance for the green and red spectral bands.

- Visible atmospherically resistant index (VARI) (Gitelson et. al 2002)

$$VARI = \frac{\rho_{Green} - \rho_{Red}}{\rho_{Green} + \rho_{Red} - \rho_{Blue}} \quad (2.4)$$

where, ρ is the surface reflectance for the green, red and blue spectral bands.

- Normalized difference water index (NDWI) (Gao 1996)

$$NDWI = \frac{\rho_{NIR} - \rho_{SWIR}}{\rho_{NIR} + \rho_{SWIR}} \quad (2.5)$$

where, ρ is the surface reflectance for the near-infrared and short wave infrared (SWIR) spectral bands. This index is calculated using a water absorption band SWIR band, thus it may be more closely related to live fuel moisture than the vegetation indexes (Dennison et al. 2005).

These remote sensing-based vegetation and water indices could assess the extent of the drought condition. Thus, many researchers have used these indices to understand the forest fire conditions. Some of such examples are as follows:

- *determining Canadian FWI codes*: The AVHRR-derived NDVI and T_s images were used in the determination of the codes of the Canadian FWI system (e.g., fine fuel moisture content, duff moisture code, drought code, buildup index, and

fire weather index code) using (Leblon et al. 2001, Oldford et al. 2006, Leblon et al. 2007). The correlations between NDVI and FWI variables (that include FFWC, DMC, DC, BUI, FWI) revealed that they were having similar seasonal variation but no direct relationship between NDVI and fuel moisture conditions were observed. It would be due to the fact that NDVI would be more directly related to vegetation greenness rather than vegetation drought conditions (Leblon et al. 2001). Despite this, the stepwise multiple regression models of predicted DC in spring of 1995 were found to be reasonable (i.e., adjusted R^2 in the range 0.34 to 0.75) over broad forest cover types of the northern Alberta and the southern Northwest Territories, Canada (Oldford et al. 2006).

- *determining live fuel moisture conditions*: The live fuel moisture conditions were also determined as a function of NDVI and T_s (Chuvienco et al. 2004, García 2008) or a set of vegetation greenness indices [i.e., NDVI, enhanced vegetation index (EVI), vegetation index green (VIgreen), visible atmospherically resistant index (VARI)] and vegetation wetness indices [i.e., normalized difference water index (NDWI) using infrared and short wave infrared reflectance-values centered at 1240, 1640, and 2130 nm] (Dennison et al. 2005, Dasgupta et al. 2007, Peterson et al. 2008). The greenness indices are sensitive to changes in vegetation chlorophyll absorption as well as changes in water content (Peterson et al. 2008).
- *determining dead fuel moisture conditions*: Dead fuel moisture was determined by combining MSG–SEVIRI derived weather variables of air temperature (T_a) and relative humidity (Nieto 2010). Note that air temperature was calculated on the basis of exploiting relations between NDVI and T_s data; on the other hand relative

humidity was determined upon considering the relations between vapour pressure and precipitable water. The precipitable water content was estimated with the thermal infrared bands of Spinning Enhanced Visible and InfraRed Imager (SEVIRI) using a split-window algorithm.

- *dynamic forest fire index*: The dynamic fire risk index (DFRI) was determined as a function of NDVI and the Static Fire Risk Index (SFRI) on La Palma Island, Spain. SFRI was developed from the area specific variables (e.g., slope, elevation, solar insolation hours, proximity to main road, vegetation cover type) using a logistic regression model. The DFRI for the Tenerife Island was determined as a function of Water Stress Index (WSI) and SFRI. The WSI was derived using AVHRR-NDVI, MODIS-NDVI, and MODIS-EVI data. The analysis revealed that the risk index could be applicable as a fire risk indicator (Hernández-Leal et al. 2008).
- *fire potential index*: In other studies (Schneider 2008, Huesca 2009), the indices of NDVI, VARI, and NDWI were also applied as a proxy to live fuel moisture in determining fire potential index. It was found that the use of both VARI and NDWI were having better capabilities of understanding live fuel moisture in comparison to that of NDVI.

Apart from the above, another index, normalized multiband drought index (NMDI; Wang and Qu 2007, Wang et al. 2008, Wang et al 2009), was also used in understanding the drought conditions. It can be calculated as follows (Wang et al. 2008):

$$\text{NMDI} = \frac{\rho_{860\text{nm}} - (\rho_{1640\text{nm}} - \rho_{2130\text{nm}})}{\rho_{860\text{nm}} + (\rho_{1640\text{nm}} - \rho_{2130\text{nm}})} \quad (2.6)$$

where, ρ is the surface reflectance-values for the corresponding NIR band (centered at 860 nm) and SWIR bands (centered at 1640 and 2130 nm). However, NMDI was not applied in understanding the forest fire danger related issues previously.

In general, the above mentioned remote sensing-derived indices are used in monitoring the fire danger conditions as they have been evaluated according to the values of estimated remote sensing based variables at the same period/time of fire occurrences. So, usually the previous developed methods were not the forecasting of forest fire, but rather then monitoring of forest fire. So, to forecast the fire danger the pre-fire environmental conditions should evaluate.

It is worthwhile to mention that a limited number of remote sensing-based studies have been conducted in the determination of the probability of fire occurrence or pre-fire forest conditions. For example:

- Vidal and Devaux-Ros (1995) calculates water deficit index (WDI) by combining NDVI and the difference between T_s and T_a ; and shows its effectiveness in predicting the onset of fires ;
- Oldford et al. (2003) demonstrated qualitatively for 18 no. of fire events (i.e., occurred only during the month of July in 1994 over Canadian northern boreal

forests) that the average T_S -values were having positive incremental trends as the date of fire occurrences approached; and

- Guangmeng and Mei (2004) also reported similar findings as Oldford et al. (2003) on the basis of analyzing 12 no. of fires, that occurred during April and May in 2003 in Northeast China.

2.6 MODIS data characteristics

MODIS is one of the widely used satellite sensors that scientists are using to study global and regional phenomena since 1999. Due to its high temporal and low to medium spatial resolution, it is very commonly used sensors in the different fields of scientific research, including oceanography, environmental science, atmospheric science among others.

It is a key scientific instrument of both Terra and Aqua satellites, launched on 18 December 1999 and 4 May 2002 respectively by National Aeronautics and Space Administration (NASA). In the morning, the Terra's orbit passes around the Earth across the equator from north to south. On the other hand, the Aqua's orbit passes in the afternoon across south to north over the equator.

The MODIS on both Terra and Aqua acquires data in 36 spectral bands ranging the wavelength from 0.4 μm to 14.4 μm over a 2330 km swath and every one to two days it views the entire Earth's surface. The Scan Mirror Assembly of the instruments uses continuously rotating double-sided scan mirror to scan ± 55 degrees. The detailed specifications of the MODIS sensors and the characteristics of MODIS spectral bands are

shown in Tables 2.1 and 2.2. The initial MODIS data format is Hierarchical Data Format (HDF). The temporal resolutions of different MODIS data products are: daily, 8-day, 16-day, monthly, quarterly, and yearly as well.

Table 2.1: MODIS specifications (LP DAAC, 2011)

Parameters	Details
Orbit	705 km, 10:30 a.m. descending node (Terra) or 1:30 p.m. ascending node (Aqua), sun-synchronous, near-polar, circular
Scan Rate	20.3 rpm, cross track
Swath Dimensions	2330 km (cross track) by 10 km (along track at nadir)
Quantization	12 bit
Spatial Resolution	250 m (bands 1-2) 500 m (bands 3-7) 1000 m (bands 8-36)
Repeat period	1-2 days
Design Life	6 years

Table 2.2: Characteristics of MODIS spectral bands (LP DAAC, 2011)

No. of Band	Reflected bandwidth range (μm)	Emitted bandwidth range (μm)	Primary use	Pixel size (m)
1	0.620–0.670	-	Absolute land cover transformation, vegetation chlorophyll	250
2	0.841–0.876	-	Cloud amount, vegetation land cover transformation	250
3	0.459–0.479	-	Soil/vegetation differences	500
4	0.545–0.565	-	Green vegetation	500
5	1.230–1.250	-	Leaf/canopy differences	500
6	1.628–1.652	-	Snow/cloud differences	500
7	2.105–2.155	-	Cloud & land properties	500
8	0.405–0.420	-	Chlorophyll	1000
9	0.438–0.448	-	Chlorophyll	1000
10	0.483–0.493	-	Chlorophyll	1000
11	0.526–0.536	-	Chlorophyll	1000
12	0.546–0.556	-	Sediments	1000
13	0.662–0.672	-	Atmosphere, sediments	1000
14	0.673–0.683	-	Chlorophyll fluorescence	1000
15	0.743–0.753	-	Aerosol properties	1000
16	0.862–0.877	-	Aerosol & atmospheric properties	1000
17	0.890–0.920	-	Aerosol & atmospheric properties	1000
18	0.931–0.941	-	Aerosol & atmospheric properties	1000
19	0.915–0.965	-	Aerosol & atmospheric properties	1000
20	-	3.660–3.840	Sea surface temperature	1000
21	-	3.929–3.989	Forest fires & volcanoes	1000
22	-	3.929–3.989	Cloud & surface temperature	1000
23	-	4.020–4.080	Cloud & surface temperature	1000
24	-	4.433–4.498	Cloud fraction, troposphere temperature	1000
25	-	4.482–4.549	Cloud fraction, troposphere temperature	1000
26	1.360–1.390	-	Cloud fraction, troposphere temperature	1000
27	-	6.535–6.895	Mid troposphere humidity	1000
28	-	7.175–7.475	Upper troposphere humidity	1000
29	-	8.400–8.700	Surface temperature	1000
30	-	9.580–9.880	Total ozone	1000
31	-	10.780–11.280	Cloud/surface temp., forest fires, volcanoes	1000
32	-	11.770–12.270	Cloud Height, forest fires & volcanoes, surface temperature	1000
33	-	13.185–13.485	Cloud fraction, cloud height	1000
34	-	13.485–13.785	Cloud fraction, cloud height	1000
35	-	13.785–14.085	Cloud fraction, cloud height	1000
36	-	14.085–14.385	Cloud fraction, cloud height	1000

CHAPTER 3: METHODOLOGY

This chapter is divided into two major components:

- (i) Estimation of TVWI: The TVWI was estimated to capture the variability of SWC over the study area primarily using MODIS based 8-day composites. The specific aims were:
 - implementing the TVWI approach over the topographically-variable agriculture and forest dominated northern portion of Canadian province of Alberta,
 - assessing it's ability of capturing the ground-based volumetric soil moisture (VSM) in different layers. ; and
- (ii) Assessment of the remote sensing-based variables of T_s , NMDI and TVWI in forecasting fire danger conditions, which had the following specific objectives:
 - capability of the individual variables of T_s , NMDI, and TVWI in forecasting fire danger conditions; and
 - potential of combining all the three variables in forecasting the fire danger conditions, and finally generate the fire danger maps for the individual periods of interest.

3.1 Estimation of TVWI

3.1.1 Description of the study area

The extent of the study area is shown in Figure 3.1 with a background of MODIS-derived land cover map (i.e., MOD12Q1 v.004; annual 1 km composite of 2004 MODIS images projected as UTM Zone 12 NAD 83). Geographically it lies between 53–60 °N latitude and 110–120 °W longitude. It falls into the northern portion of the Canadian province of Alberta. It can be characterized as topographically variable (i.e., average elevation varies from 225 m to 1750 m above sea level) with the dominance of agriculture and forest land cover types (see Figure 3.1 for more details). The average annual temperature across the study area varies between -3.6 to +2.3 °C. The mean annual precipitation varies between 300-900 mm (Dowing and Pettapiece 2006).

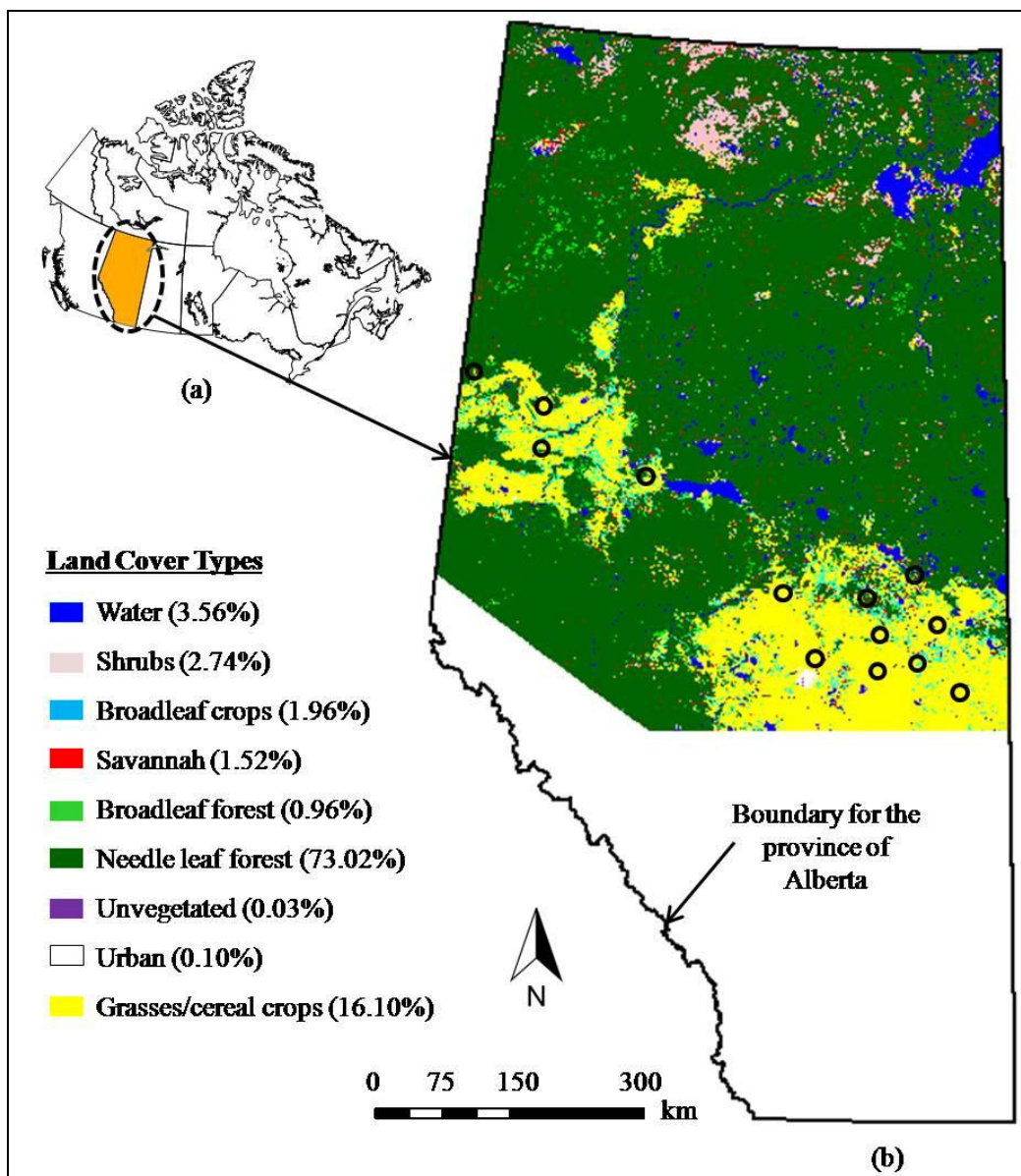


Figure 3.1: (a) Location of the province of Alberta in Canada; (b) The extent of the study area with a land cover map in the background derived from annual composite of 2004 MODIS images. Hollow circles are representing the locations where the ground-based soil moisture data were acquired.

3.1.2 Data requirements

In this study, MODIS-based products were used which were freely available from the Land Processes Distributed Active Archive Center (LP DAAC: a component of NASA's earth observing system data and information system) (LP DAAC, 2010).

Those included:

- (i) MOD11A2 v.005 : 8-day composites of T_S (generated by averaging the clear-sky daytime T_S -values during an 8-day period) at 1 km resolution during the months May-September for the period 2006-2008;
- (ii) MOD09Q1 v.005: 8-day composites of red (620–670 nm) and near infrared (NIR: 841–876 nm) surface reflectance at 250 m resolution during May-September for the period 2006-2008.

A digital elevation model (DEM) of the study area was also used which was generated from 3-arc second resolution height point-data. This DEM data was freely available from NASA Shuttle Radar Topography Mission archive (SRTM, 2009).

In addition, the ground-based measurements of VSM of 13 stations at 5 cm, 20 cm, 50 cm and 100 cm depth of the same period of remote sensing data were acquired using Theta Probe type ML2x freely available from Alberta Department of Agriculture and Rural Development (ARD, 2010).

3.1.3 Methods

Figure 3.2 shows the schematic diagram of the methodology of estimating TVWI. It has four major components: (i) data pre-processing, (ii) estimating TVWI-values, and (iii) comparing the TVWI-values with the ground-based measurements.

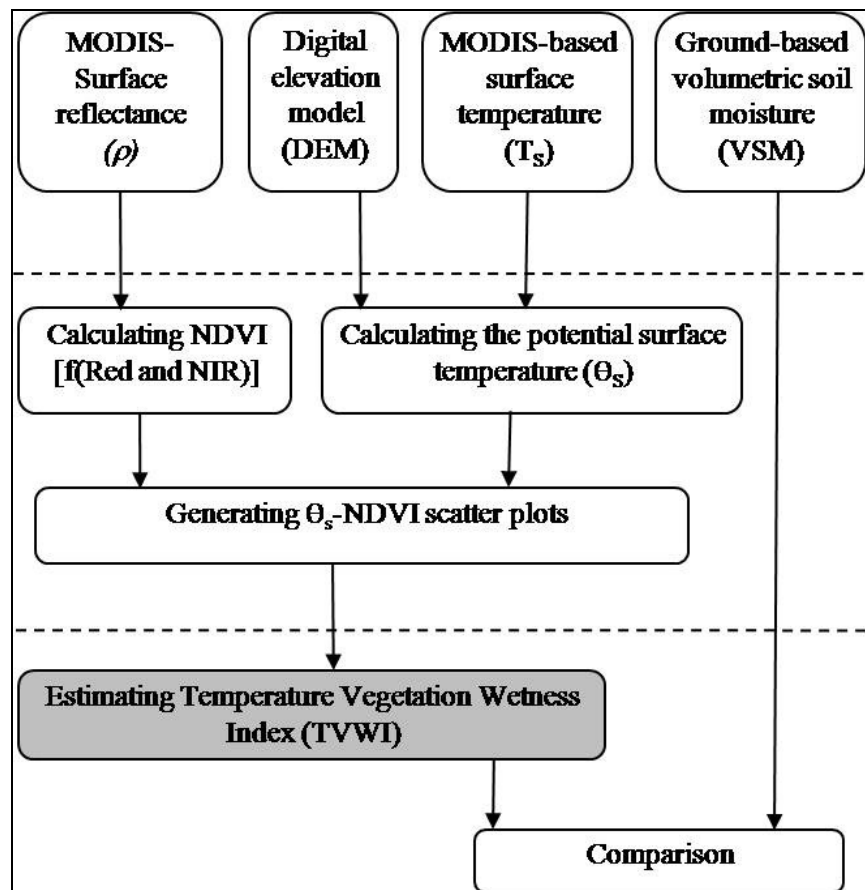


Figure 3.2: Schematic diagram of the methodology of estimating TVWI

3.1.3.1 MODIS data pre-processing

The MODIS data pre processing was performed in four steps: data downloading, data reprojection, image mosaicking and employing the cloud correction algorithm.

Data downloading: The MODIS T_S and surface reflectance data were downloaded from the Land Processes Distributed Active Archive Center (LP DAAC, 2010) in Hierarchical Data Format (HDF). In order to cover the entire study area, it was required to download two adjacent image frames. A total of 52 images were downloaded to generate the 26 periodical data for T_S and surface reflectance over each year. Table 3.1 gives the details of the periods and their respective DOY of MODIS 8-day composites.

Data reprojection: The downloaded raw images of T_S and surface reflectance were in sinusoidal projection (sinusoidal grid tiling) system. The data were reprojected using the MODIS Re-Projection Tool v4.0 software (MRT, 2010) into Universal Transverse Mercator zone 12 (UTM12) with North American Datum of 1983 (NAD83). It would be worthwhile to mention that these images were in produced in Geo-TIFF format.

Table 3.1: Time periods of MODIS 8-day composites data

<i>Pe rio ds</i>	<i>DOY</i>	<i>Dates in 2006/2007</i>	<i>Dates in 2008</i>	<i>Pe rio ds</i>	<i>DOY</i>	<i>Dates in 2006/2007</i>	<i>Dates in 2008</i>
1	97-104	07 Apr -14 Apr	06 Apr -13 Apr	14	201-208	20 Jul-27 Jul	19 Jul-26 Jul
2	105-112	15 Apr -22 Apr	14 Apr -21 Apr	15	209-216	28 Jul-04 Aug	27 Jul-03 Aug
3	113-120	23 Apr -30 Apr	22 Apr -29 Apr	16	217-224	05 Aug-12 Aug	04 Aug-11 Aug
4	121-128	01 May-08 May	30 Apr-07 May	17	225-232	13 Aug-20 Aug	12 Aug-19 Aug
5	129-136	09 May-16 May	08 May-15 May	18	233-240	21 Aug-28 Aug	20 Aug-27 Aug
6	137-144	17 May-24 May	16 May-23 May	19	241-248	29 Aug-05 Sep	28 Aug-04 Sep
7	145-152	25 May-01 Jun	24 May-31 May	20	249-256	06 Sep-13 Sep	05 Sep-12 Sep
8	153-160	02 Jun-09 Jun	01 Jun-08 Jun	21	257-264	14 Sep-21 Sep	13 Sep-20 Sep
9	161-168	10 Jun-17 Jun	09 Jun-16 Jun	22	265-272	22 Sep-29 Sep	21 Sep-28 Sep
10	169-176	18 Jun-25 Jun	17 Jun-24 Jun	23	273-280	30 Sep-07 Oct	29 Sep-06 Oct
11	177-184	26 Jun-03 Jul	25 Jun-02 Jul	24	281-288	08 Oct-15 Oct	07 Oct-14 Oct
12	185-192	04 Jul-11 Jul	03 Jul-10 Jul	25	289-296	16 Oct-23 Oct	15 Oct-22 Oct
13	193-200	12 Jul-19 Jul	11 Jul-18 Jul	26	297-305	24 Oct-31 Oct	23 Oct-30 Oct

Image mosaicking: Each data period consists of two scenes in GEO-TIFF format. These two scenes were mosaicked together to create the respective desired images. The resulting image was then clipped to the boundaries of Alberta. All of these processes were carried out using ERDAS Imagine (ERDAS, 2011).

Employing the cloud correction algorithm: As MODIS is an optical sensor, thus it has limitations in observing the surface because clouds obscure the track visible/ NIR surface reflectance data or T_s data. Some of the pixels of the 8-day MODIS images used in producing the composites were contaminated by cloud. Usually the contaminated pixels cover approximately 5-10% over the period and area of study. So, the removal of those cloud pixels was very vital in this study. In order to correct those, an image correction technique was used to fill the cloud contaminated pixels in both surface reflectance and T_s time series images. The algorithm was initially developed by Hassan et al. 2007a. The method was evaluated by considering the cloud-free pixels as cloud contaminated pixels and calculated the considered contaminated pixel values using the cloud correction algorithm (Hassan et al. 2007a). The comparison of those estimated cloud-free values and the actual values of their respective pixels of the T_s revealed a strong relation ($r^2=88.3\%$) between the estimated and actual surface temperatures. Mathematically, it was as follows:

$$A = \frac{\sum_{i=1}^{i=n} \bar{X}(i) - X(i)}{m}, \text{ and} \quad (3.1)$$

$$B_n = \bar{X}(n) - A, \quad (3.2)$$

where,

$\bar{X}(i)$ is mean value of either T_S or surface reflectance for each of their respective 8-day composites for a specific year for the entire image [where i ($=1,2,\dots,n$) is the 8-day period of interest and n =the total number of 8-day composite images involved per year];

$X(i)$ represents the time series of image-based T_S and surface reflectance values for a specific year for cloud-contaminated pixels taking into account only T_S and surface reflectance values from cloud-free composites,

m is the total number of cloud-free pixels from individual composite images available for a specific year for a cloud-contaminated pixel,

A is the average temporal deviation of either T_S or surface reflectance from their respective $\bar{X}(i)$ for a specific cloud-contaminated pixel of interest, and

B_n is the estimated 8-day means of either T_S or surface reflectance for individual cloud-contaminated pixels.

3.1.3.2 Generation of TVWI-values

The estimation of TVWI was performed in three steps proposed by Hassan *et al.* (2007b): calculating NDVI, converting the T_S into (θ_S ; defined as the temperature considering that the site lies at the mean sea level); and scatter plots of θ_S -NDVI and estimate of TVWI.

The surface reflectance images (MOD09Q1) were used to calculate the NDVI as a function of red and NIR reflectance using the Eq. 2.1 using an ERDAS model. The conversion of T_S into θ_S was as follows:

- Calculation of atmospheric pressure (p) over the study area at each of the pixels according to their respective point elevations of the acquired DEM according to the ideal gas law:

$$p = p_0 \left(1 - \frac{L \cdot z}{T_0} \right)^{\frac{g \cdot M}{R \cdot L}}, \quad (3.3)$$

where,

p is the atmospheric pressure,

p_0 is the standard atmospheric pressure at mean sea level (=101.3 kPa),

z is the elevation above mean sea level (in m),

L is the temperature lapse rate (= 0.0065 K/m)

R is the gas constant (= 8.31447 J/ mol•K)

g is the earth-surface gravitational acceleration (= 9.80665 m/s²)

M is the molar mass of dry air (= 0.0289644 kg/mol)

T_0 is the sea level standard temperature

The simplified equation of this ideal gas law (equation 4), assuming 20 °C and a standard atmosphere were used to calculate the atmospheric pressure (Allen et. al. 1998):

$$p = 101.3 \left[\frac{293 - 0.0065z}{293} \right]^{5.26}, \quad (3.4)$$

- Calculation of potential surface temperature, θ_s (in K) using the following equation:

$$\theta_s = T_s \left[\frac{p_o}{p} \right]^{R/C_p}, \quad (3.5)$$

where,

T_s is the surface temperature (in K),

R is the gas constant ($=287 \text{ J kg}^{-1} \text{ K}^{-1}$),

C_p is the specific heat capacity of air ($\sim 1004 \text{ J kg}^{-1} \text{ K}^{-1}$), and

θ_s is the potential surface temperature (in K).

To determine the TVWI for each period the NDVI and potential temperature were scatter plotted against each other. In ERDAS it was done by stacking and clipping each pair of images for each period. The resulting Feature Space Images were then converted to ASCII data format. This data were then plotted in Microsoft excel.

Figure 3.3 shows the conceptual diagram of estimating the TVWI-values. The upper boundary of the θ_S is c_1 and the lower boundary is θ_{wet} . The lower θ_S is required to reach in $TVWI=0$ with increase of NDVI. Both of the dry edge (i.e., θ_{dry}) and wet edge (i.e., θ_{wet}) would describe the available water stress in relation to vegetation conditions. Along the θ_{dry} , water would be most likely unavailable in supporting the evapotranspiration. The values of TVWI would have a minimum value of 0. On the other hand, along the θ_{wet} , water would be unrestricted in supporting the evapotranspiration, thus the values of TVWI would have a maximum value of 1.

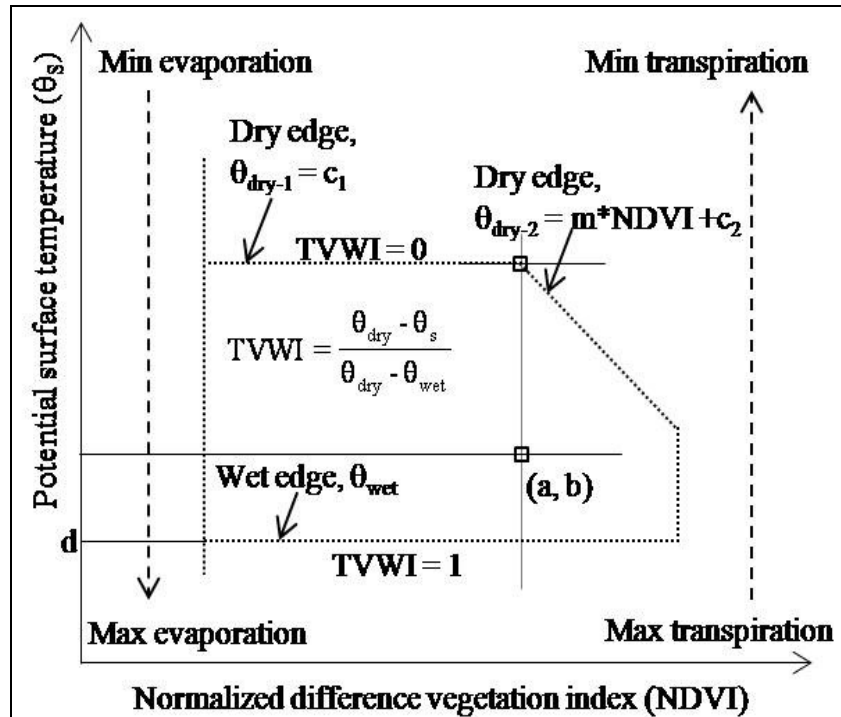


Figure 3.3: Conceptual diagram illustrating the calculations of TVWI as a function of θ_s and NDVI. Both of the dry edge (i.e., θ_{dry}) and wet edge (i.e., θ_{wet}) would describe the available water conditions in relation to vegetation conditions. c_1 is the dry edge for θ_{dry-1} ; m and c_2 are the slope and intercept for θ_{dry-2} , respectively [Modified after Hassan et al., 2007b]

The θ_{dry} was calculated by the following equation:

$$\theta_{dry} = \begin{cases} NDVI \geq a & m*NDVI+c_2 \\ NDVI < a & c_1 \end{cases} \quad (3.6)$$

$$\theta_{wet} = d$$

Finally, the TVWI was calculated using the following expression (Hassan et al. 2007b; Hassan and Bourque 2009):

$$TVWI = \frac{\theta_{dry} - \theta_s}{\theta_{dry} - \theta_{wet}}, \quad (3.7)$$

where, TVWI is a dimensionless entity and θ_{dry} , θ_{wet} , and θ_s are all in K.

3.1.4 Validation

In this study, a total of 60 TVWI images (at each 8-day intervals) were generated during 2006-2008. The TVWI-values were extracted at 13 stations (where the ground-based VSM data were acquired; see Figure 3.1 for location information). Then, the average TVWI-value for each of the 8-day intervals was calculated. In a similar way, the ground-based measurement of VSM for each of the 8-day period of interest was also averaged. Finally, the VSM values with the TVWI values were compared both qualitatively and quantitatively in terms of D (% of deviation).

$$D = \frac{(M_{ground} - P) \times 100}{M_{ground}} \quad (3.8)$$

where, M_{ground} = Ground-based measurement, and

P = Predicted value.

3.2 Assessment of the remote sensing-based variables in forecasting fire danger conditions

3.2.1 Description of the study area

Figure 3.4 shows the extent of the study area, which falls in the northern portion of the Canadian province of Alberta with an area of approximately 429,065 km². It expands in the range 54–60 °N latitude and 110–120 °W longitude. On the basis of climate, soil, and vegetation types, the study area has been divided into ten natural sub-regions (see Figure 3.4 for more detail). Among the sub-regions, eight (central mixedwood, dry mixedwood, northern mixedwood, sub-arctic, Peace-Athabasca delta, lower boreal highlands, Athabasca plain, and upper boreal highlands) of them fall within boreal natural region (Dowing and Pettapiece 2006). The study area is mainly over the boreal forest natural region and forest dominated with deciduous, mixedwood, and coniferous forests with widespread wetlands. It is mainly topographically variable (i.e., average elevation varies from 225 m to 950 m above sea level) with the dominance of boreal forest types. In general, the study area is characterized by cold (i.e., mean annual temperature varies between -3.6 °C and +1.8 °C) and relatively dry (i.e., mean annual precipitation varies between 376.8 mm and 588.4 mm) climatic conditions (see Table 3.2 for more details); (Dowing and Pettapiece 2006).

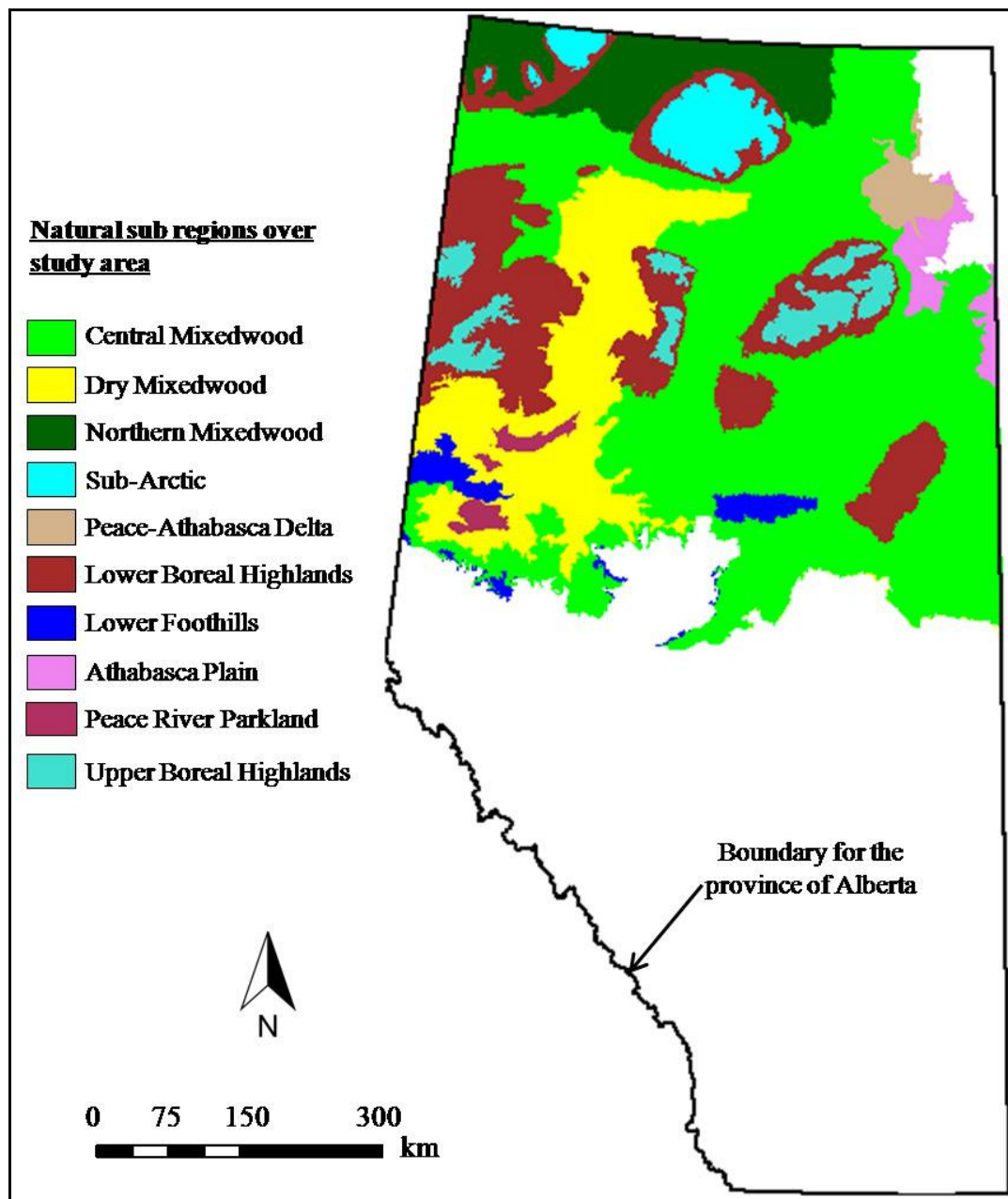


Figure 3.4: The extent of the study area with the natural sub regions falling under the area of interest.

Table 3.2: Characteristics of natural subregions over the study area

<i>Natural subregion</i>	<i>Average elevation above sea level (m)</i>	<i>Mean annual precip. (mm)</i>	<i>Mean annual temp. (°C)</i>	<i>Main vegetation types</i>
Central Mixedwood	525 (200-1050)	477.5	0.2	Closed-canopy mixedwood: dominant-aspen, white spruce & black spruce
Dry Mixedwood	600 (225-1225)	460.6	1.1	Aspen forests with shrubby understories, some white spruce, jack pine
Northern Mixedwood	350 (150-650)	386.8	-2.5	Forested by pure or mixed aspen, white spruce and black spruce stands
Boreal Subarctic	825 (575-1000)	512.3	-3.6	Open, stunted black spruce forests with some jack pine hybrids
Peace Athabasca Delta	225 (200-250)	376.8	-1.4	Aquatic, shoreline, meadow, shrub and marsh vegetation in the lowlands
Lower Boreal Highlands	675 (400-1050)	495.2	-1	Mixed forests (aspen, balsam poplar, black & white spruce, paper birch)
Athabasca Plain	300 (200-650)	428.3	-1.2	Dry jack pine forests, dunes largely unvegetated
Upper Boreal Highlands	825 (650-1150)	534.5	-1.5	Coniferous forests: jack pine hybrids, black spruce
Peace river parkland	625 (300-800)	450.2	1.5	Remnant aspen clones and continuous forest: California oat grass, porcupine grass, Jack pine, willow.
Lower Foothills	950 (650-1625)	588.4	1.8	Mixedwood forests (aspen-lodgepole pine–white spruce)

3.2.2 Data requirements and its pre-processing

In this study, the MODIS-based 8-day composites of T_s images at 1 km resolution (i.e., MOD11A2 v.005); and surface reflectance images at 500 m resolution [i.e., MOD09A1 v.005; acquired over the spectral bands of near infrared (NIR): 841–876 nm, shortwave infrared (SWIR): 1628- 1652 nm), and SWIR: 2105- 2155 nm among others] were used (LP DAAC, 2010). The surface reflectance images were used to generate NMDI-maps. In addition, the MODIS-derived 8-day composites of TVWI-images were acquired, which were developed in an earlier study. All of these data were acquired during the fire seasons (i.e., April-October) of 2006-2008, which fell in between 97-297 day of year (DOY).

Apart from the satellite data, two databases (i.e., a non-spatial and another geospatial one) were also acquired that described the fire occurrences in the study area during the fire seasons of 2006-2008. Both of the databases were freely available from Alberta Sustainable Resource Development (SRD, 2011b). The non-spatial (in Microsoft excel worksheet format) database contained information about all of the fire events with their respective start dates and fire names. There were total of 3375 fires with ~220,564 hectares of area burned found in the non-spatial database. On the other hand, the geospatial database contained information about a portion of the fire events, and described them in the form of polygons (geospatial vector data in shapefile format). The major limitation of the geospatial database was that it had no fire start dates in its attributes. In order to bring the start dates of the fires, the non-spatial database was merged with the attributes of the geospatial database according to the name of each fire over the study period and area; and obtained 368 fires caused by both lightning (254) and

humans (114). The 368 fires represented ~76% of the total burn areas in the non-spatial database and among them ~74% of the areas were burned only by lightning.

3.2.2.1 Generation of NMDI maps

The chlorophyll content only affects MODIS visible bands and has no effect on NIR and SWIR. On the other hand, the water content (C_w) affects MODIS SWIR bands centered at 1240 nm, 1640 nm, and 2130 nm. The simulated effect of leaf water content on canopy reflectance (using the leaf radiative transfer model-PROSPECT and canopy reflectance model-SAIL) is shown in Figure 3.5 (Wang and Qu 2007). It illustrated that the MODIS SWIR bands centered at 1640 nm and 2130 nm were sensitive to the moisture change considering the values of chlorophyll content (C_{ab}) =40, leaf dry matter content (C_m) =0.01, leaf internal structure $N=1.3$, soil moisture (θ) = 0.25 and leaf area index LAI=2 (Wang and Qu 2007).

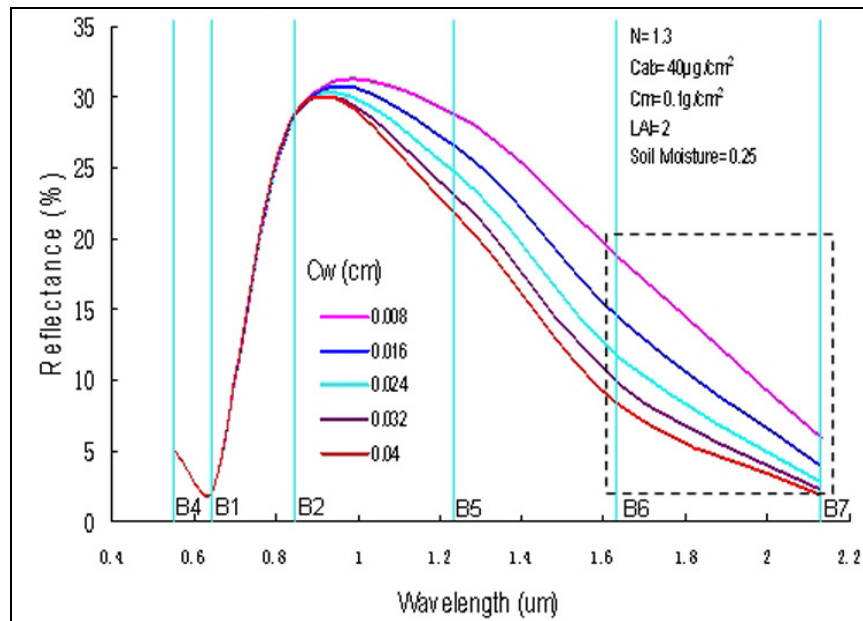


Figure 3.5: Simulated canopy spectra at different leaf water content (after Wang and Qu 2007)

Based on the vegetation water content spectral signatures (Wang and Qu 2007), The NMDI uses the difference between two liquid water absorption bands (1640 nm and 2130 nm) which are vegetation water sensitive bands, instead of using a single liquid water absorption band as does the NDWI. The differences between two water absorption bands in response to leaf water content provide the potential to estimate vegetation water. In this study, the 8-day composites of NMDI-maps were calculated at 500 m resolution using Eq. 2.8.

3.2.3 Methods

Figure 3.6 shows the schematic diagram describing the methods of assessing the remote sensing-based variables in forecasting fire danger conditions. The major components of the methods were: (i) analyzing the individual variables of T_s , NMDI, and TVWI in forecasting fire danger conditions; (ii) combining all the three variables in forecasting the fire danger conditions; and (iii) generating the fire danger maps for the individual periods of interest.

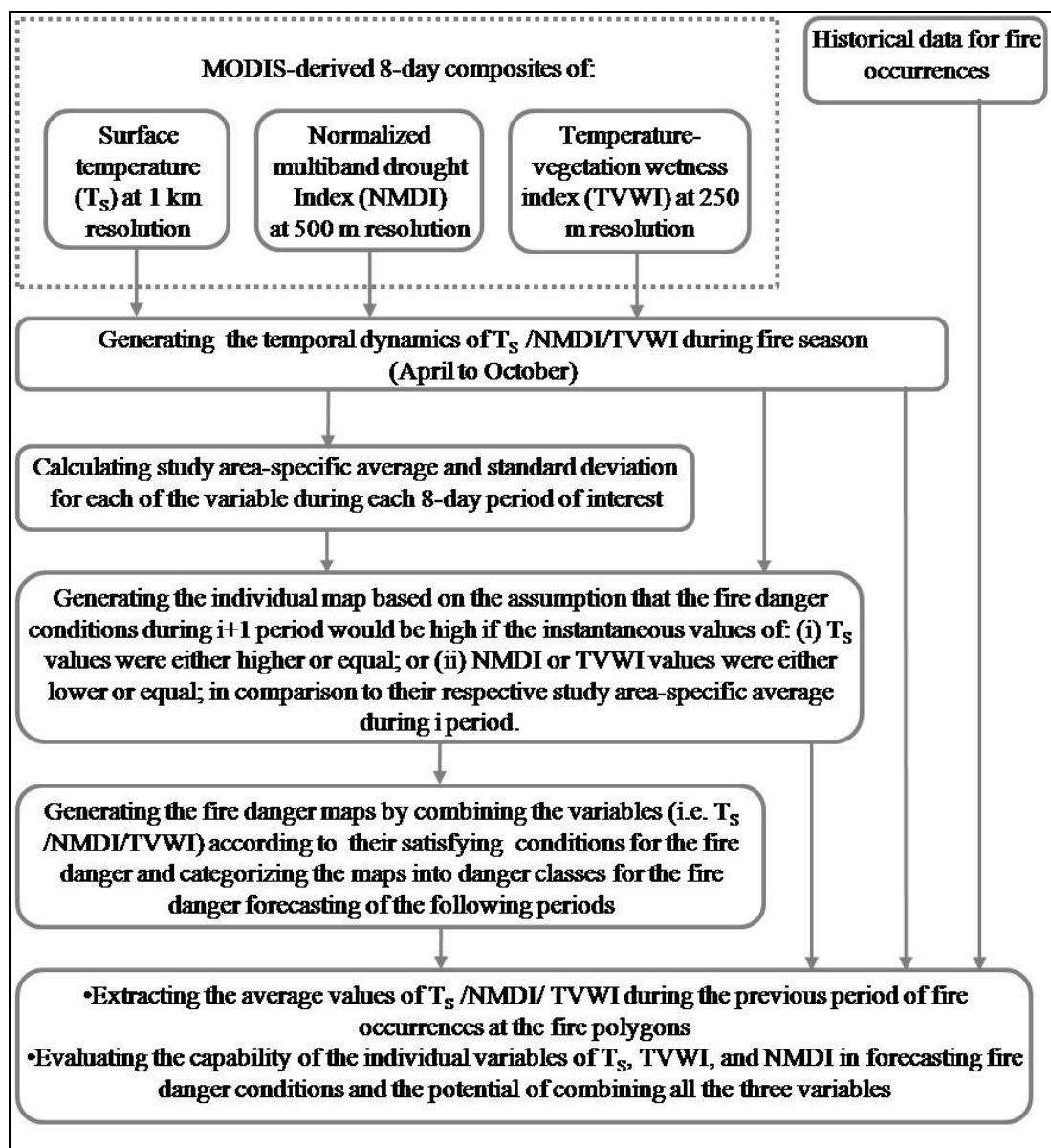


Figure 3.6: Schematic diagram of the methods of assessing the remote sensing-based variables in forecasting fire danger conditions

3.2.3.1 Analyzing the individual variables of T_s , NMDI, and TVWI in forecasting fire danger conditions

Figure 3.7 illustrates the concept of forecasting forest fire danger as a function of MODIS-derived three variables (i.e., T_s , NMDI and TVWI). During each of the 8-day period, it required to calculate the study area-specific average-values [i.e., $\overline{T_s(i)}$, $\overline{NMDI(i)}$ and $\overline{TVWI(i)}$] for each of the variables; and their generalized patterns are also shown in Fig. 3. The values of both $\overline{T_s(i)}$ and $\overline{NMDI(i)}$ would start to increase from the onset of the fire season and reach to a maximum at height of the growing season before start to decrease again (Wang et al. 2009, Hassan et al. 2007a). On the other hand, the values of $\overline{TVWI(i)}$ would relatively higher both at the onset and end of the fire season as the surface could be more wet due to relatively lower temperature regimes. In order to forecast fire danger conditions during $i+1$ period, the instantaneous values of the variables at a given pixel during i period (i.e., $T_{s(i)}$ / $NMDI_{(i)}$ / $TVWI_{(i)}$) were compared with their respective average-values (i.e., $\overline{T_s(i)}$, $\overline{NMDI(i)}$ and $\overline{TVWI(i)}$). For example, the fire danger would be considerably high if the one or more of the following conditions were to exist:

- $T_{s(i)} \geq \overline{T_s(i)}$, as high temperature might favour the fire to initiate;
- $NMDI_{(i)} \leq \overline{NMDI(i)}$, as low moisture in the vegetation might support the fire occurrences; and
- $TVWI_{(i)} \leq \overline{TVWI(i)}$, as low values of surface wetness conditions might also support the fire to ignite.

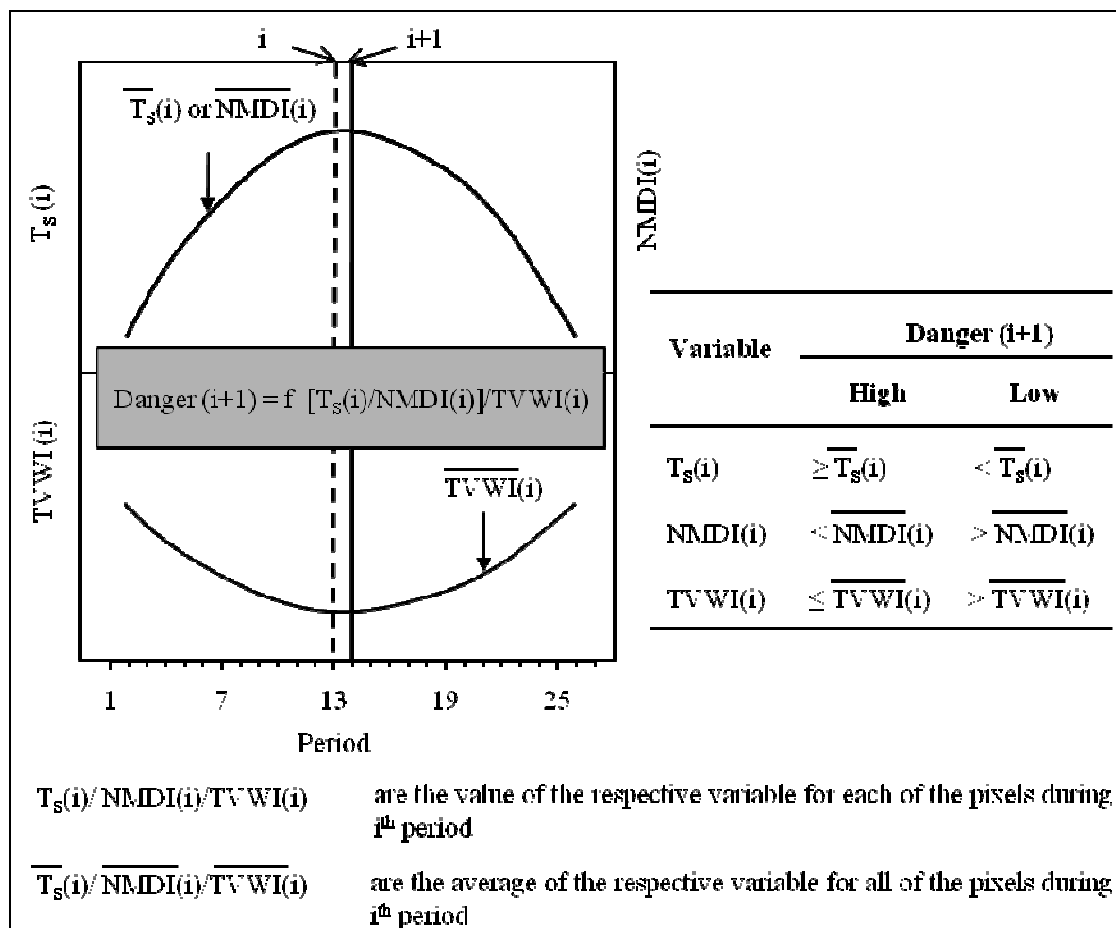


Figure 3.7: Conceptual diagram of forecasting forest fire danger as a function of MODIS-derived variables (i.e., T_s , NMDI and TVWI)

3.2.3.2 Combining all the three variables in forecasting the fire danger conditions

These were formulated by integrating the outcomes of the individual variables (i.e., whether fire danger conditions were “high” or “low” as discussed in the above section) for each pixel.

3.2.3.3 Generating the fire danger maps for the individual periods of interest

Finally, the fire danger maps were generated upon combining all of the three variables according to their satisfying condition to four fire danger classes; i.e.,

- (i) very high: if all the three variables indicated that the fire danger would be high;
- (ii) high: if at least two of the three variables indicated that the fire danger would be high;
- (iii) moderate: if at least one of the three variables indicated that the fire danger would be high; and
- (iv) low: if all of the three variables indicated that the fire danger would be low.

3.2.4 Validation

In order to evaluate the above mentioned concept, the calculated average-values of the variables of T_s , NMDI, and TVWI during i period for each of the fire polygons were evaluated both individually and also combinedly in understanding the fire danger conditions.

3.2.4.1 Evaluating the capability of the individual variables in forecasting the fire danger conditions

In terms of individual variables, the average data of the each variable were extracted from the previous period of fire occurrences within each fire polygons and evaluated as follows:

- It was determined that how many cases the average values of a particular variable (i.e., average-value at i period for each of fire polygon occurred during $i+1$ period) fell under the high or low fire danger categories in compare to their study area-specific average during i period according to the assumption described in the section 3.2.3.1.
- Both of the high and low danger categories, were further divided into six classes on the basis of study area-specific average and the standard deviation-values in the range of “average \pm 3 standard deviation” for each of the variable. Then quantified how many fires were occurred within each standard deviation interval for the variable of interest. This particular analysis was carried out to understand spatially whether the warmer or less moist conditions would favor more fires to occur or not.

3.2.4.2 Evaluating the potential of combining all the three variables in forecasting the fire danger conditions

It was also evaluated whether the combination of the three variables would enhance the capability of describing fire danger conditions in compare to the individual variables.

These were formulated by integrating the outcomes of the individual variable (i.e., whether fire danger conditions were “high” or “low” for each of fire polygons. The “% of the cases” were then determined which fell under each of the fire danger classes.

CHAPTER 4: RESULTS AND DISCUSSION

4.1 Estimation of TVWI

Figure 4.1 shows an example scatter plot of θ_S -NDVI for day of year (DOY) in between 153-160 in 2006. In general, the trapezoidal shape was observed upon generating the scatter plots of θ_S -NDVI for each of the 8-day periods.

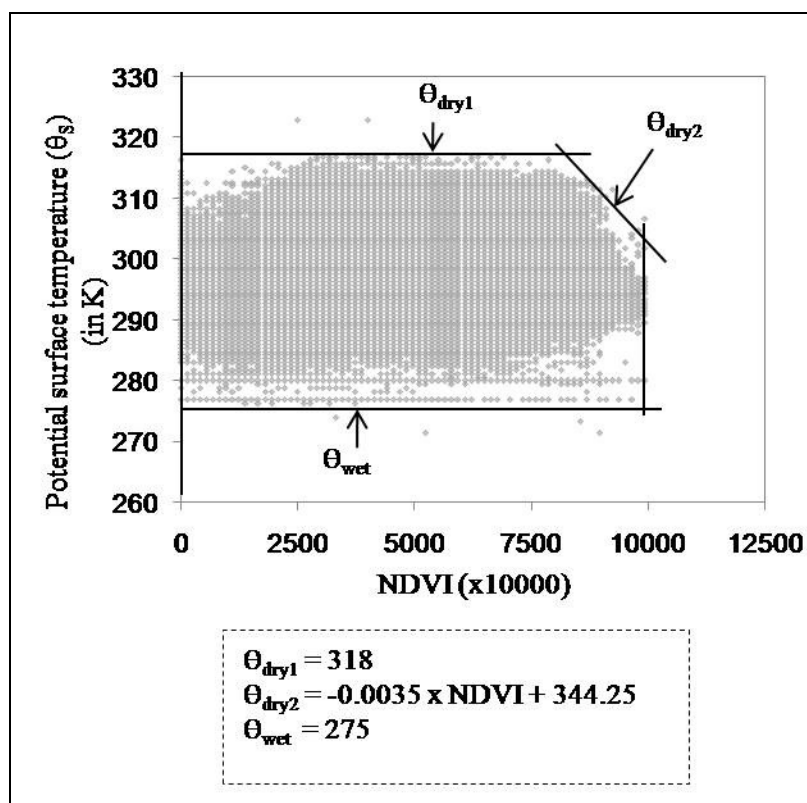


Figure 4.1 Example of scatter plot of θ_S vs. NDVI and the corresponding dry and wet edges during the day of year 153-160 in 2006.

The value of θ_{dry1} was 318; and the slope and intercept of θ_{dry2} were -0.0035 and 344.25 respectively. The value of θ_{wet} was considered to be a constant of 275 K similar to other studies (Hassan *et al.* 2007b). As it was important to establish the same baseline in determining the maximum values of TVWI (=1) across the whole data series, and also the value of 275 K was quite enough to support evapotranspiration. The values of θ_{dry1} , θ_{dry2} (i.e., both the slope and intercept) of 8-day average according to DOY over the year 2006 to 2008 were given in Appendix II.

The temporal dynamics of TVWI and VSM at 5 cm, 20 cm, 50 cm and 100 cm depth of the soil were plotted during the period 2006-2008 (see Figure 4.2 for details). A analysis revealed that TVWI-values were in better agreement with VSM at 50 cm and 100 cm depths rather than 5 cm or 20 cm. Similar observations were also reported in the literature (Su *et al.* 2003). The rationale behind such phenomenon could be explained from the relations between high evapotranspiration demand (that reflects TVWI as described in Figure 3.3) and SM at deeper layers. The available SM in the upper soil layers (i.e., at 5-20 cm) would quickly be depleted due to higher evapotranspiration demand, and such demand would then be supported by the upward movement of the SM from deeper layers (≥ 50 cm) (Lawrence *et. al* 2007, Shuttleworth 1988).

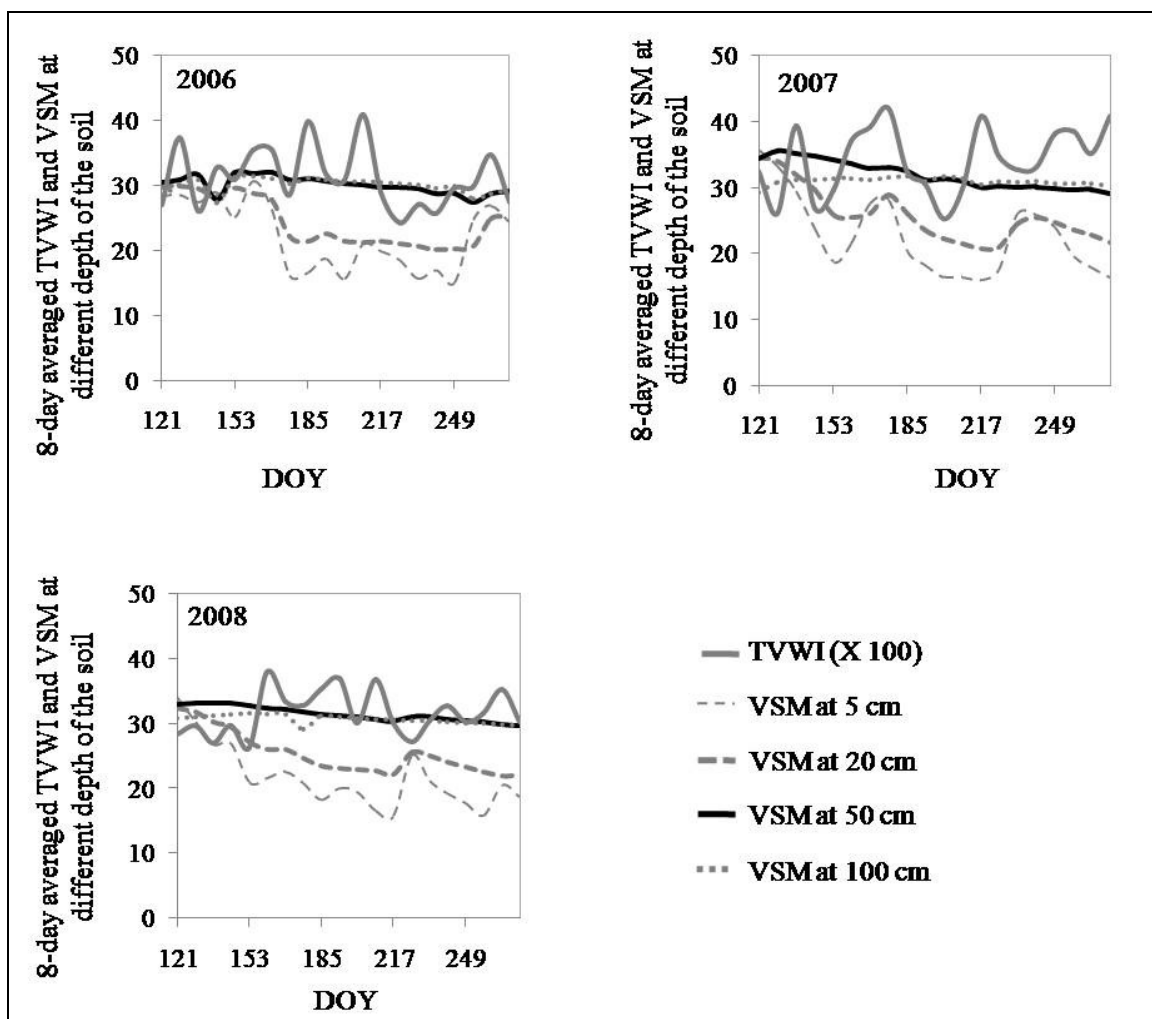


Figure 4.2: Temporal dynamics of 8-day averaged TVWI and VSM at different depths of the soil during the day of year 121-273 for the period 2006-2008

Thus, the quantitative evaluation between TVWI and VSM was further performed at 50 cm depths during 2006-2008 periods as shown in Figure 4.3. It revealed that the deviation was within $\pm 20\%$ for 80% of the times in 2006, 65% of the times in 2007, and 100% of the times in 2008. On an average, 81.67% of the times, the % of deviation of the TVWI and VSM within $\pm 20\%$ were observed for the period of interest.

Note that the $\pm 20\%$ deviation between remote sensing-based and ground-based estimates would be considered as quite acceptable in the event of analyzing climate-driven variables (Hassan and Bourque 2010). Besides, relatively higher deviation (i.e., $> \pm 20\%$) also could be expected as the ground-based measurements were at a point location, while remote sensing-based estimates were an average values over $250 \times 250 \text{ m}^2$.

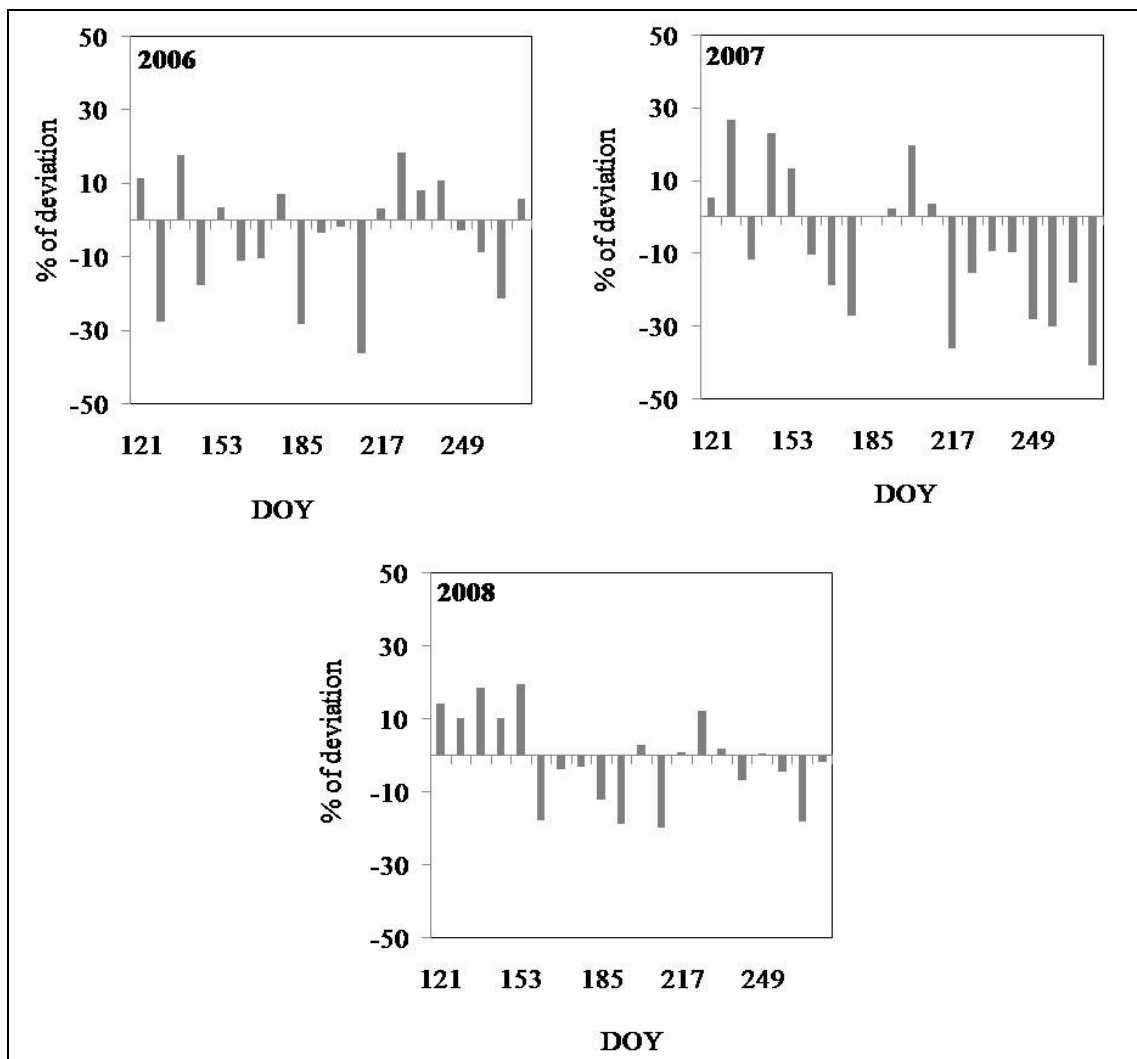


Figure 4.3: Deviation between the averaged ground-based measurements of VSM and TVWI for the period 2006, 2007 and 2008.

A map illustrating the spatial distribution of the averaged TVWI and its respective relative frequency distributions is shown in Figure 4.4. It was found that ~98.04% of the times the TVWI-values fell in the range of 0.2-0.6; with an average and standard deviation of ~0.44 and ~0.083 respectively. The distinct spatial patterns of TVWI are summarized as follows:

- The higher TVWI values were found in the sub regions of the northern part of the study area. It was associated with the lower temperature regimes. It would be the case as the temperature gradually decreases in this particular direction in the northern hemisphere (Hassan et al. 2007a, Sekhon et al. 2010).
- Usually, the TVWI values were higher in the regions which had higher elevation in comparison to their surrounding subregion. For an example, both the dry mixedwood and lower foothills natural subregions are extended up to the southern portion of the Alberta as shown in Figure 4.4. The average elevation of the natural subregions of dry mixedwood and lower foothills are 600 m and 950 m above mean sea level respectively. It was observed that the TVWI values were higher in lower foothills than dry mixedwood.
- The Peace-Athabasca Delta is a boreal wetland located in northeastern Alberta. This natural subregion is composed of low-lying areas, such as, aquatic land and shoreline. The area of this subregion covered with meadow, shrub and marsh vegetation which is able to retain soil moisture. This might be the reason for observing higher TVWI values over some portion of the natural subregion. In

contrast, some of the areas have lower TVWI values (See Figure 4.4). This was due to the presence of lake over that area where the reflectance of red and NIR spectral bands were very low. Thus the estimated NDVI values were near to zero and indicate the absence of vegetation.

- In general, the lower TVWI-values were mainly observed over agriculture-dominant areas, whereas the higher TWVI-values were observed over forest-dominant regions. It might be related to the fact that forest-dominated dense vegetation would be able to retain water in the different layers of ground in greater extent in compare to the relatively less vegetated agricultural areas. Usually the upper layer soil moisture of the agriculture-dominant areas would evaporate quickly with high air and surface temperature.

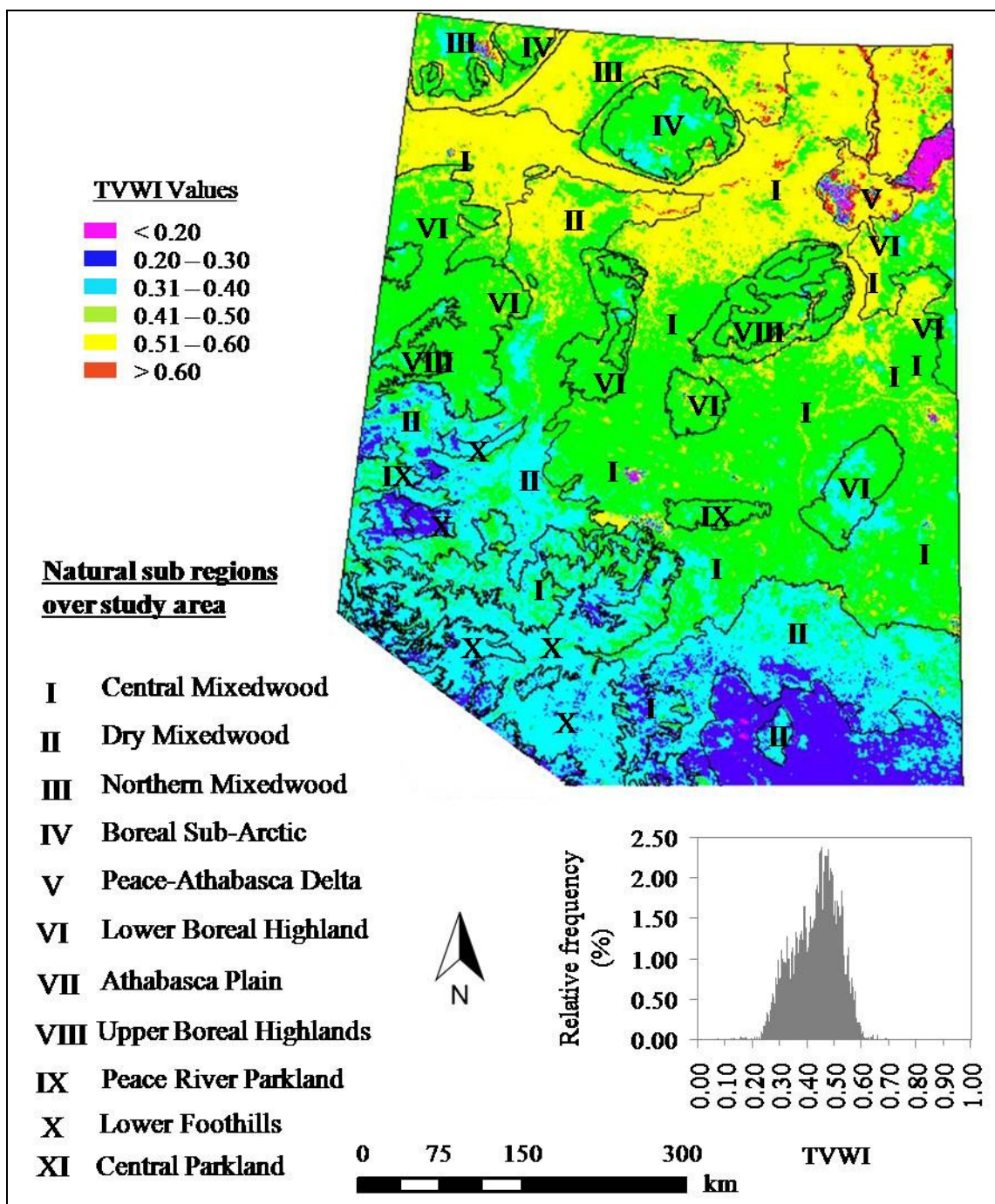


Figure 4.4: Spatial dynamics of 2006-2008 averaged TVWI and its relative frequency distribution with natural sub regions over study area

4.2 Assessment of the remote sensing-based variables in forecasting fire danger conditions

4.2.1 *The capability of the individual variables of T_s , NMDI, and TVWI in forecasting fire danger conditions*

4.2.1.1 The temporal dynamics of the study area-specific average values for the variables

Figure 4.5 shows the temporal dynamics of the study area-specific average values for the variable of T_s , NMDI, and TVWI during the fire seasons (i.e., in between 97-297 DOY) for the period 2006-2008. All of the variables revealed distinct temporal patterns that coincided with the generalized patterns of the variables which were assumed in developing the proposed method (see Figure 3.7). Quadratic fits to the variables as a function of DOY were found to have strong relations (i.e., T_s : $r^2 \sim 0.84\text{--}0.88$, NMDI: $r^2 \sim 0.67\text{--}0.83$ during 121-273 DOY, and TVWI: $r^2 \sim 0.74\text{--}0.80$; see Appendix II for more details).

Note that both at earlier and later part of the season (values are not shown in Figure 4.5) the NMDI-values were relatively high. It would be associated with wetness resulted from snow melting earlier in the season and snow accumulation later on. A similar pattern was also observed in other vegetation wetness indices (e.g., NDWI) over boreal forested region (Sekhon et al. 2010).

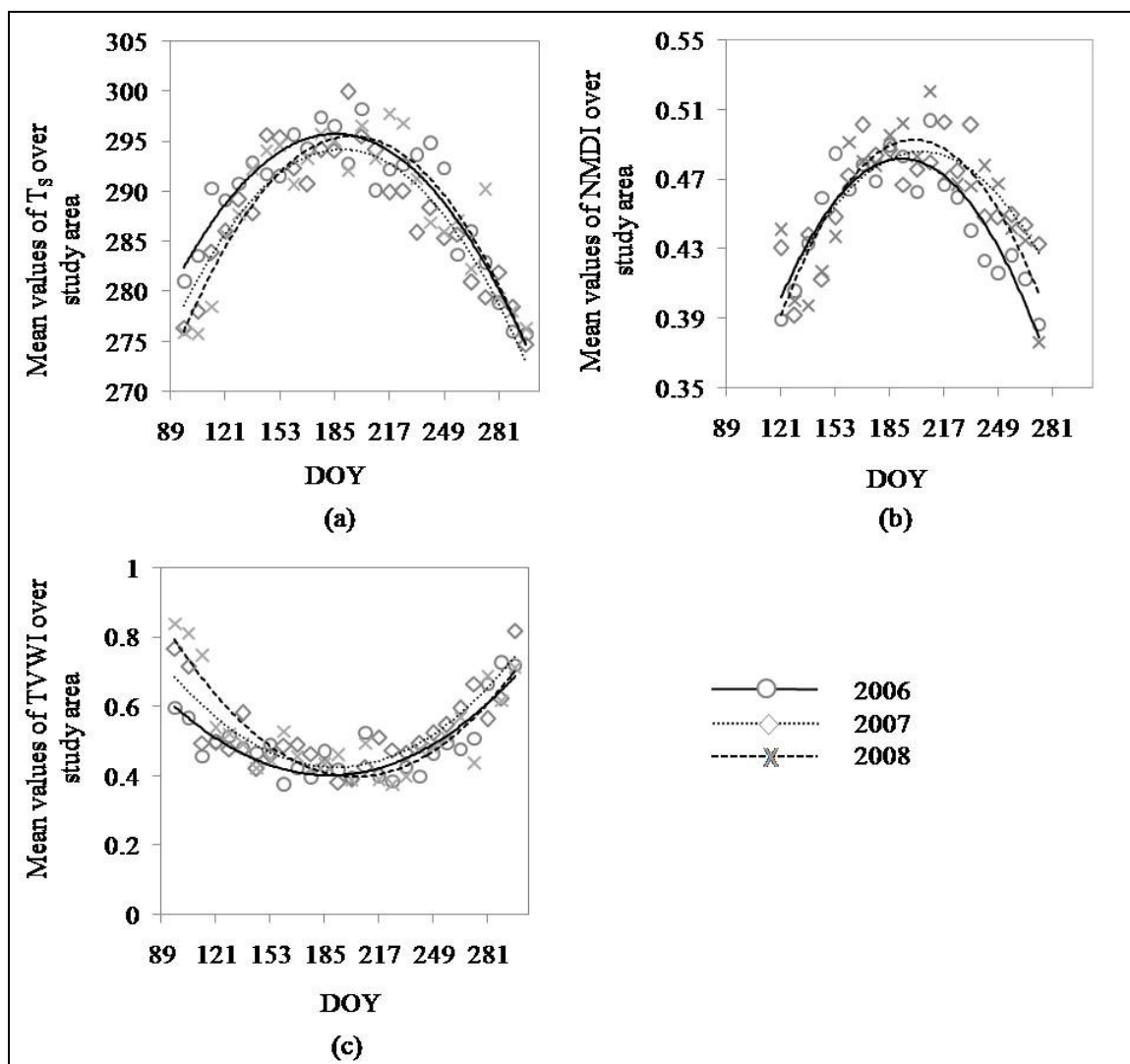


Figure 4.5: The temporal dynamics of the study area-specific average values for the variable of (a) T_s , (b) NMDI and (c) TVWI during the fire seasons (i.e., in between 97-297 DOY) for the period 2006-2008.

4.2.1.2 The capability of the individual variables of T_s , NMDI, and TVWI in forecasting fire danger conditions

Figure 4.6 illustrates the comparison between the fire polygon-specific average-values of the variables and their respectively study area-specific averages during i period while the fires occurred in the following period. It was found that reasonable amounts of fire polygons fell under the high fire danger category [i.e., 70.14% when $T_s(i) \geq \overline{T_s(i)}$; 77.26% when $NMDI_{(i)} \leq \overline{NMDI(i)}$; and 59.73% when $TVWI_{(i)} \leq \overline{TVWI(i)}$] during the period 2006-2008 (see details in Table 4.1).

Table 4.1: % of data lower/ higher than the mean values over the study area for the variables (i.e. T_s / NMDI/ TVWI; extracted from the fire polygons one period before fire occurrence)

<i>Variables</i>	<i>Conditions</i>	<i>% of data</i>			
		<i>2006</i>	<i>2007</i>	<i>2008</i>	<i>2006-2008</i>
Temp	Higher than average	68.71	58.69	77.24	70.14
	Lower than average	31.29	41.31	22.76	29.86
NMDI	Higher than average	27.48	20.65	21.38	22.74
	Lower than average	72.52	79.35	78.62	77.26
TVWI	Higher than average	29.01	47.83	46.90	40.27
	Lower than average	70.99	52.17	53.10	59.73

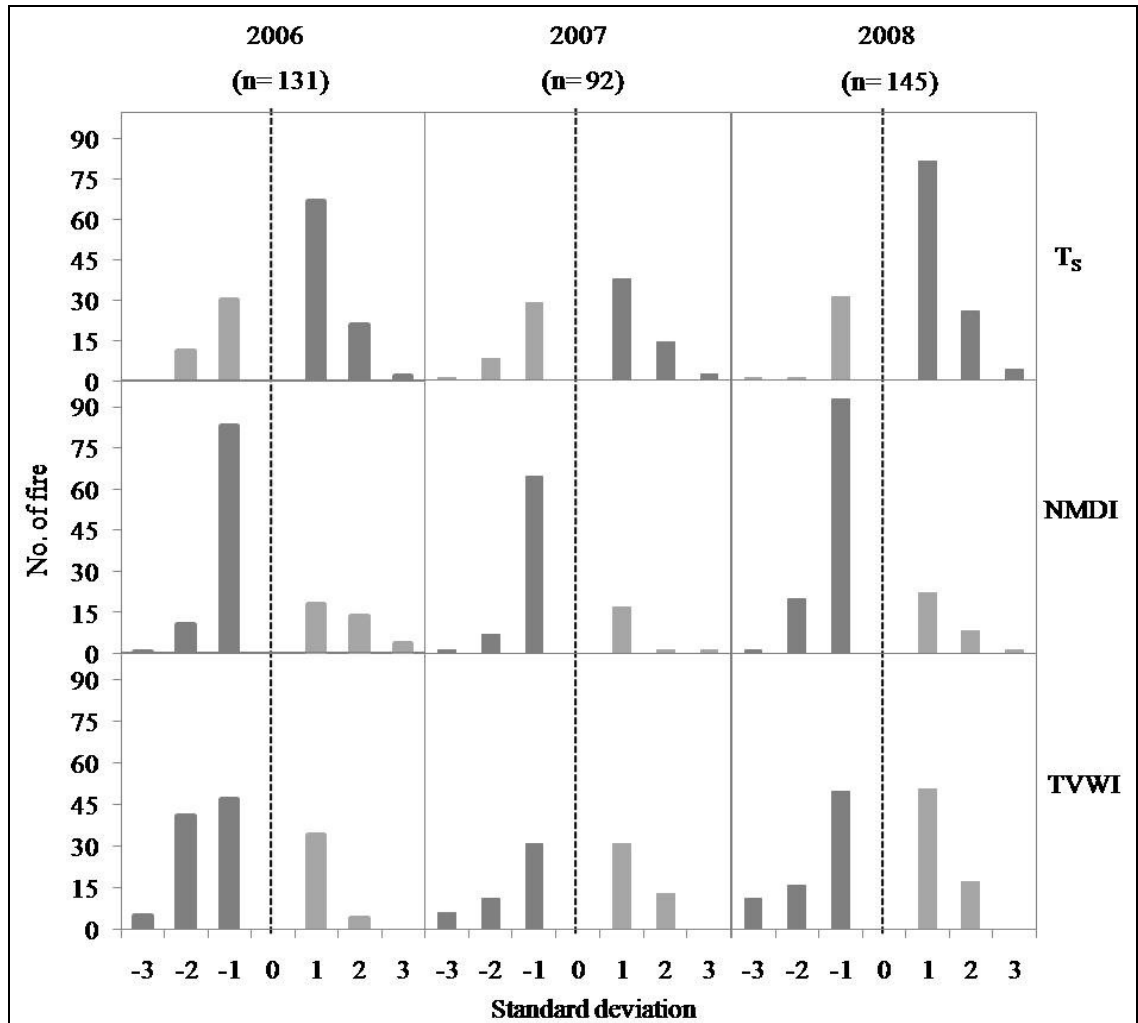


Figure 4.6: Frequency distribution of the fires on the basis of the “study area-specific average \pm 3 standard deviation” values.

In general, the finding about T_S in predicting fire danger provided better quantification in comparison to other studies (Oldford et al. 2003, Guangmeng and Mei 2004). On the other hand, it was not possible to compare performance for the both NMDI and TVWI, as their implementation in predicting danger conditions were so far not found in the literature. The discrepancies associated with high danger categories for each of the variables and fire polygons category [i.e., 29.86% when $T_S(i) \geq \overline{T_S}(i)$; 22.74% when $NMDI_{(i)} \leq \overline{NMDI}(i)$; and 40.27% when $TVWI(i) \leq \overline{TVWI}(i)$] might be attributed due to one or more of the other influencing factors, such as, precipitation, wind speed, topography, fuel cover types, etc. (Leblon et al. 2001, Oldford et al. 2003, Desbois and Vidal 2006, Ardakani et al. 2011) which were not included in this study.

Further, the fire danger classes were analyzed upon categorizing on the basis of study area-specific average and the standard deviation-values (see Table 4.2 and Figure 4.6 for more details). However, it didn't reveal clear association with the states of the variables (in terms of deviating from the study area-specific average values) and the number of fire occurrences. For example, most of the fires were found to be within "average \pm 1 standard deviation" category, which indicated either more warmer or less surface/vegetation wet/moist conditions didn't favour the fires to initiate. Similar situations (e.g., drier condition didn't correspond with high number of fire occurrences) were also reported elsewhere (e.g., Bartsch et al. 2009).

Table 4.2: No. of fire within ± 3 standard deviations for the variables (i.e. Ts/ NMDI/ TVWI) estimated from the mean values of the study area and the average values of the variables extracted within the fire polygons one period before fire occurrence

<i>Year</i>	<i>Variable</i> <i>Standard deviation</i>	<i>-3</i>	<i>-2</i>	<i>-1</i>	<i>1</i>	<i>2</i>	<i>3</i>
		<i>No. of fire</i>					
2006	Ts	0	11	30	67	21	2
	NMDI	1	11	83	18	14	4
	TVWI	5	41	47	34	4	0
2007	Ts	1	8	29	38	14	2
	NMDI	1	7	65	17	1	1
	TVWI	6	11	31	31	13	0
2008	Ts	1	1	31	82	26	4
	NMDI	1	20	93	22	8	1
	TVWI	11	16	50	51	17	0

4.2.2 The potential of combining all the three variables in forecasting the fire danger conditions

Upon combining the three individual variables in predicting fire danger conditions, it was found that the predictability was enhanced to a greater extent (see Table 4.3 for more details). On an average, total 95.92% of the fires were found that fell in the categories of very high to moderate fire danger classes (i.e. 36.68% data were in very high, 36.41% data were in high and 22.83% data were in moderate danger class) during the period 2006-2008. It would be associated with the fact that the combination of weather and fuel conditions should predict the danger conditions better in comparison to individual ones. 4.08% of the fires were found to be in the low danger class (i.e., none of the variables were in favour of fire occurrences), which might be associated with other influencing factors mentioned earlier.

Table 4.3: % of data under each of the fire danger condition categories upon combining all of three variables (i.e. T_S / NMDI/ TVWI; extracted over the fire polygons one period prior to the fire occurrences) during the period 2006-2008.

<i>Year</i>	<i>No. of the variables satisfying the fire danger condition</i>	<i>Fire danger classes</i>	<i>% of data</i>
2006	All	Very High	39.69
	At least 2	High	35.11
	At least 1	Moderate	22.91
	None	Low	2.29
2007	All	Very High	35.87
	At least 2	High	27.17
	At least 1	Moderate	28.26
	None	Low	8.70
2008	All	Very High	34.48
	At least 2	High	43.45
	At least 1	Moderate	19.31
	None	Low	2.76
2006-2008	All	Very High	36.68
	At least 2	High	36.41
	At least 1	Moderate	22.83
	None	Low	4.08

4.2.2.1 Fire danger maps for the individual periods of interest

Figure 4.7 shows an example fire danger mapping for the period 25 June-02 July, 2008 produced by combining all of three variables of T_S , NMDI, and TVWI from the previous period 17 June 17-June 24 2008. Also areas around two of the fire polygons were zoomed to illustrate detailed danger conditions, which were fell within very high danger class. Over the entire study area, approximately ~45% of areas were observed that fell under “very high” to “high” danger categories. More fire danger maps are included in the Appendix.

Further analysis of the high danger category (i.e., ~31% of the entire study area) revealed that the combinations of either T_S and TVWI, or T_S and NMDI produced high amount danger conditions (i.e., ~16% for T_S and TVWI, and ~10% for T_S and NMDI of the entire study area). On the other hand, the combination of NMDI and TVWI were able to capture ~ 5% of the entire study area. These observations might be related to fact that the two combinations (i.e., T_S and TVWI; and T_S and NMDI) were representing both the weather and fuel condition, the remaining combination of NMDI and TVWI were representing primarily fuel conditions. In case of moderate danger class (where at least one of the variable indicated the high fire danger condition), NMDI was the dominant variable (i.e., ~15% of the entire study area). It might be the case as NMDI would be directly related to the fuel moisture conditions (i.e., one of the most critical factors for the fire initiation) (Oldford et al. 2006). It would be worthwhile to note that fires would only occur over the moderate-to-very high danger classes if there would be a source of ignition.

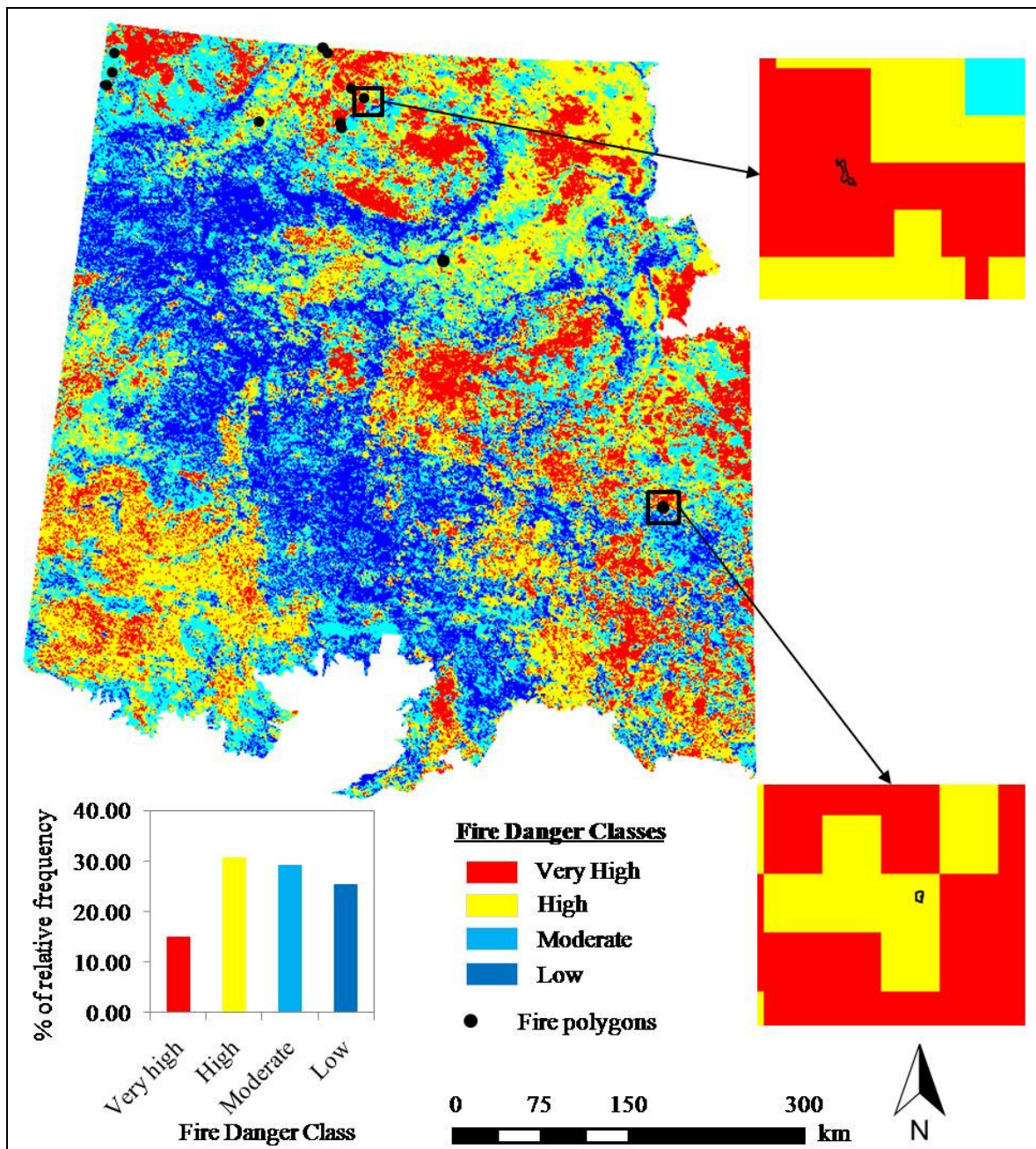


Figure 4.7: An example fire danger mapping for the period 25 June-02 July, 2008 produced by combining all of three variables of T_s , NMDI, and TVWI from the previous period 17 June 17-June 24 2008. Illustrations of the fire danger around the two fire polygons were delineated in the zoomed section.

CHAPTER 5: CONCLUSIONS AND FUTURE WORK

5.1 Summary

In this Thesis, the effectiveness of TVWI-approach was demonstrated in capturing the spatial dynamics of surface wetness conditions over agriculture and forest-dominant regions. It could be used as an indirect way of determining soil moisture conditions, as the deviation between TVWI-values and ground-based VSM were found within $\pm 20\%$ for 81.67% of the cases. Thus, the finding would be encouraging for others in determining moisture regimes in soil over other areas by use of remote sensing-based techniques as demonstrated here.

A MODIS-based simple protocol was also demonstrated for forecasting forest fire danger conditions and its implementation over boreal forest-dominant regions. It employed 8-day composite of variables/indices (i.e., T_s /NMDI/TVWI) during i period to forecast fire danger during $i+1$ period. The results showed that the individual variables of T_s , NMDI and TVWI could be used to predict the fire danger reasonably where NMDI had the best capabilities. The integration of these three variables revealed that the forecasting might be enhanced, i.e., ~95.92% of the fires fell in the “very high” to “moderate” fire danger classes during the period 2006-2008. Despite the agreements, it is suggested that the proposed methods should be evaluated prior to implementing in other ecosystems across the world according to the variables of that particular ecosystems except for the similar boreal forested regions like this study area.

5.2 Contribution to science

The main contributions resulted from this Thesis are as follows:

- Initially, TVWI method was developed and implemented over humid, tempered forest-dominated and topographically-variable landscape in eastern Canada) (Hassan et. al. 2007b). Here, this method was implemented over boreal forest-dominant regions and demonstrated its applicability.
- In previous research, T_s was used in the prediction of fire danger and evaluated qualitatively (Oldford et al. 2003, Guangmeng and Mei 2004). Here, it was used and quantified quantitatively.
- Both TVWI and NMDI were used to quantify the forest fire danger conditions for the first time.
- The concept of integrating of the variables of T_s , NMDI, and TVWI in predicting forest fire danger conditions are unique and applied over the fire prone boreal forested regions.

5.3 Future work

Despite the effectiveness of the proposed method of combining the variables of T_s , NMDI, and TVWI in predicting fire danger conditions; it is needed to consider the following issues in order to potentially enhance its capability:

- Other important weather variables, in particular precipitation and relative humidity, are quite often used in the framework of danger mapping systems (Van Wagner 1987); so thus it would be worthwhile to investigate.

- The incorporation of lightning data during $i+1$ period with our fire danger map from the i period could be interesting to investigate in determining the degree of agreements of our danger map with the fire occurrences.
- The current temporal scale (i.e., 8-day) remains a bit challenging from operational point of view. As in practice fire danger maps are operationally produced at daily-level as a function of weather variables acquired at point-locations across the landscape. Thus, it requires to develop methods to forecasting at much finer temporal scales (e.g., 2-4 days of intervals).
- The dynamics of fire occurrences significantly differ from ecosystem-to-ecosystem (Ardakani et al. 2011). Thus it is strongly recommend to evaluate the proposed methods prior to implementing in other ecosystems

References

- Allen, R.G., Pereira, L.S., Raes, D., and Smith, M. 1998. *Crop evapotranspiration: guide-lines for computing crop water requirements*. Food and Agriculture Organizations of the United Nations, Rome, Italy, ISBN 92-5-104219-5. 290p.
- Anttila, S. and Kairesalo, T. 2010. Mean and variance estimations with different pixel sizes: case study in a small water quality monitoring area in southern Finland. *Boreal Environmental Research*, 15:335-346.
- Ardakani, A. S., Zoj, M. J. V., Mohammadzadeh, A. and Mansourian, A. 2011. Spatial and temporal analysis of fires detected by MODIS data in northern Iran from 2001 to 2008, *IEEE Journal of Selected Topics in Applied Earth Observations and Remote Sensing*, 4(1): 216-225.
- Bajocco, S., Rosati, L. and Ricotta, C. 2010. Knowing fire incidence through fuel phenology: A remotely sensed approach, *Ecological Modelling*, 221(1): 59–66.
- Bartsch, A., Balzter, H. and George, C. 2009. The influence of regional surface soil moisture anomalies on forest fires in Siberia observed from satellites. *Environmental Research Letters*, 4: 045021.
- Brocca, L., Melone, F., Moramarco, T. and Morbidelli, R. 2010. Spatial-temporal variability of soil moisture and its estimation across scales. *Water Resources Research*, 46: W02516.

- Carlson, T. 2007. An overview of the "Triangle Method" for estimating surface evapotranspiration and soil moisture from satellite imagery. *Sensors*, 7: 1612–1629.
- Carvalho, A., Flannigan, M. D., Logan, K. A., Miranda, I. and Borrego, C. 2008. Fire activity in Portugal and its relationship to weather and the Canadian Fire Weather Index System, *International Journal of Wild land Fire*, 17: 328–338.
- Chen, C.-F., Son, N.-T., Chang, L.-Y. and Chen, C.-C. 2010. Monitoring of soil moisture variability in relation to rice cropping systems in the Vietnamese Mekong Delta using MODIS data. *Applied Geography*, 31: 463-475.
- Chow, L., Xing, Z., Rees, H.W., Meng, F., Monteith, J. and Stevens, L. 2009. Field performance of nine soil water content sensors on a sandy loam soil in New Brunswick, Maritime Region, Canada. *Sensors*, 9: 9398-9413.
- Chuvieco, E. D., Cocero, D., Riano, P., Martin, J., Martínez-Vega, J.de la. Riva, and Pérezd, F. 2004. Combining NDVI and surface temperature for the estimation of live fuel moisture content in forest fire danger rating, *Remote Sensing of Environment*, 92: 322-331.
- Countryman, C.M., 1972. *The Fire Environment Concept*. USDA Forest Service, Pacific Southwest Forest and Range Experiment Station, Berkeley. 12 pp.
- Dasgupta, S., Qu, J. J., Hao, X. and Bhoi, S. 2007. Evaluating remotely sensed live fuel moisture estimations for fire behavior predictions in Georgia, USA, *Remote Sensing of Environment*, 108: 138-150.

- Dennison, P. E., Roberts, D. A., Peterson, S. H. and Rechel, J. 2005. Use of normalized difference water index for monitoring live fuel moisture, *International Journal of Remote Sensing*, 26(5):1035–1042.
- Desbois, N. and Vidal, A. 1996. Real time monitoring of vegetation flammability using NOAA-AVHRR thermal infrared data, *EARSel Advances in Remote Sensing*, 4(4-XI): 25-32.
- Downing, D. J. and Pettapiece, W. W. 2006. *Natural Regions and Subregions of Alberta*. Alberta, Canada: Pub. No. T/852, Natural Regions Committee, Government of Alberta.
- Eagleman, J. R. and Lin, W.C. 1976. Remote sensing of soil moisture by a 21-cm passive radiometer. *Journal of Geophysical Research*, 81:3660-3666.
- Fennessey, M. J., and Shukla, J., 1999. Impact of initial soil wetness on seasonal atmospheric prediction. *Journal of Climate*, 12: 3167-3180.
- Flanagan, L. B. and Johnson, B. G. 2005. Interacting effects of temperature, soil moisture and plant biomass production on ecosystem respiration in a northern temperate grassland. *Agricultural and Forest Meteorology*, 130: 237–253.
- Flannigan, M. D., Stocks, B. J. and Wotton, B.M. 2000. Climate change and forest fires, *The Science of the Total Environment*, 262: 221-229.
- Flannigan, M., Stocks, B., Turetsky, M. and Wotton, M. 2009. Impacts of climate change on fire activity and fire management in the circumboreal forest, *Global Change Biology*, 15: 549–560.

- García, M., Chuvieco, E., Nieto, H. and Aguado, I. 2008. Combining AVHRR and meteorological data for estimating live fuel moisture content, *Remote Sensing of Environment*, 112: 3618- 3627.
- Gitelson, A. A., Kaufman, Y. J., Stark, R., & Rundquist, D. 2002. Novel algorithms for estimation of vegetation fraction, *Remote Sensing of Environment*, 80: 76–87.
- Gu, Y., Hunt, E., Wardlow, B., Basara, J. B., Brown, J. F. and Verdin, J. P. 2008. Evaluation of MODIS NDVI and NDWI for vegetation drought monitoring using Oklahoma Mesonet soil moisture data, *Geophysical Research Letters*, 35: L22401.
- Guangmeng, G. and Mei, Z. 2004. Using MODIS land surface temperature to evaluate forest fire risk of northeast China, *IEEE Geoscience and Remote Sensing Letters*, 1(2): 98-100.
- Hari, P. and Nojd, P. 2009. The effect of temperature and PAR on the annual photosynthetic production of Scots pine in northern Finland during 1906-2002. *Boreal Environmental Research*, 14 (suppl.A):5-18.
- Hassan, Q.K. and Bourque, C.P.-A. 2009. Potential species distribution of balsam fir based on the integration of biophysical variables derived with remote sensing and process-based methods, *Remote Sensing*, 1:393–407.
- Hassan, Q.K. & Bourque, C.P.-A. 2010. Spatial enhancement of MODIS-based images of leaf area index: application to the boreal forest region of northern Alberta, Canada. *Remote Sensing*, 2: 278-289.

- Hassan, Q.K., Bourque, C.P.-A., Meng, F.-R. and Richards, W. 2007a. Spatial mapping of growing degree days: an application of MODIS-based surface temperatures and enhanced vegetation index. *Journal of Applied Remote Sensing*, 1: 013511.
- Hassan, Q.K., Bourque, C.P.-A., Meng, F.-R. and Cox, R.M. 2007b. A wetness index using terrain-corrected surface temperature and normalized difference vegetation index derived from standard MODIS products: an evaluation of its use in a humid forest-dominated region of eastern Canada. *Sensors*, 7: 2028–2048.
- Hernández-Leal, P. A., González-Calvo, A., Arbelo, M., Barreto, A. and Alonso-Benito, A. 2008. Synergy of GIS and remote sensing data in forest fire danger modeling, *IEEE Journal of Selected Topics in Applied Earth Observations and Remote Sensing*, 1(4): 240-247.
- Huesca, M., Litago, J., Palacios-Orueta, A., Montes, F., Sebastián-López, A. and Escribano, P. 2009. Assessment of forest fire seasonality using MODIS fire potential: A time series approach, *Agricultural and Forest Meteorology*, 149: 1946–1955.
- Huete, A., Didan, K., Miura, T., Rodriguez, E.P., Gao, X. & Ferreira, L.G. 2002. Overview of the radiometric and biophysical performance of the MODIS vegetation indices. *Remote Sensing of Environment*, 83: 195-213.
- Johnson, E. A. 1992. *Fire and vegetation dynamics*. Studies from the North American boreal forests. New York, USA: Cambridge University Press, p 129.

- Krawchuk, M. A., Cumming, S. G. and Flannigan, M. D. 2009. Predicted changes in fire weather suggest increases in lightning fire initiation and future area burned in the mixedwood boreal forest, *Climatic Change*, 92: 83–97.
- Lam, Nina Siu-Ngan. 1983. Spatial interpolation methods: a review, *Cartography and Geographic Information Science*, 10(2): 129-150.
- Lawrence, D. M., Thornton, P. E., Oleson, K. W. and Bonan, G. B. 2007. The partitioning of evapotranspiration into transpiration, soil evaporation, and canopy evaporation in a GCM: impacts on land-atmosphere interaction, *Journal of Hydrometrology*, 8: 862-880.
- Leblon, B., Alexander, M., Chen, J. and White, S. 2001. Monitoring fire danger of northern boreal forests with NOAA-AVHRR NDVI images, *International Journal of Remote Sensing*, 22(14): 2839-2846.
- Leblon, B., García, P. A. F., Oldford, S., Maclean, D. and Flannigan, M. 2007. Using cumulative NOAA-AVHRR spectral indices for estimating fire danger codes in northern boreal forests, *International Journal of Applied Earth Observation and Geoinformation*, 9: 335-342.
- Li, Z.-L., Tang, R., Wan, Z., Bi, Y., Zhou, C., Tang, B., Yan, G. and Zhang, X. 2009. A review of current methodologies for regional evapotranspiration estimation from remotely sensed data, *Sensors*, 9: 3801-3853.
- Mallinis, G., Mitsopoulos, I. D., Dimitrakopoulos, A. P., Gitas, I. Z. and Karteris, M. 2008. Local-scale fuel-type mapping and fire behavior prediction by employing high-resolution satellite imagery, *IEEE Journal of Selected Topics in Applied Earth Observations and Remote Sensing*, 1(4): 230-239.

- Moran, M. S., Watts, J. M., Peters-Lidard, C. D. and McElroy, S. A. 2004. Estimating soil moisture at the watershed scale with satellite-based radar and land surface models. *Canadian Journal of Remote Sensing*, 30(5):805-826.
- Nemani, R., Pierce, L., Running, S., Goward, S. 1993. Developing satellite-derived estimates of surface moisture status. *Journal of Applied Meteorology*, 32: 548–557.
- Nieto, H., Aguado, I., Chuvieco, E. and Sandholt, I. 2010. Dead fuel moisture estimation with MSG–SEVIRI data. Retrieval of meteorological data for the calculation of the equilibrium moisture content, *Agricultural and Forest Meteorology*, 150: 861–870.
- Oldford, S., Leblon, B., Gallant, L. and Alexander, M. E. 2003. Mapping pre-fire forest conditions with NOAA-AVHRR images in northern boreal forests, *Geocarto International*, 18(4): 21-32.
- Oldford, S., Leblon, B., Maclean, D. and Flannigan, M. 2006. Predicting slow-drying fire weather index fuel moisture codes with NOAA-AVHRR images in Canada's northern boreal forests, *International Journal of Remote Sensing*, 27(18): 3881–3902.
- Parviainen, M., Luoto, M. and Heikkinen, R. K. 2010. NDVI-based productivity and heterogeneity as indicators of plant-species richness in boreal landscapes. *Boreal Environmental Research*, 15:301-318.
- Patel, N.R., Anapashsha, R., Kumar, S., Saha, S.K. and Dadhwal, V.K. 2009. Assessing potential of MODIS derived temperature/vegetation condition index (TVDI) to infer soil moisture status. *International Journal of Remote Sensing*, 30: 23–39.

- Peterson, S. H., Roberts, D. A. and Dennison, P. E. 2008. Mapping live fuel moisture with MODIS data: A multiple regression approach, *Remote Sensing of Environment*, 112: 4272–4284.
- Petropoulos, G., Carlson, T.N., Wooster, M.J. and Islam, S. 2009. A review of T_S-VI remote sensing based methods for the retrieval of land surface energy fluxes and soil surface moisture. *Progress in Physical Geography*, 33(2): 1-27.
- Sandholt, I., Rasmussen, K. and Andersen, J. 2002. A simple interpretation of the surface temperature/vegetation index space for assessment of surface moisture status. *Remote Sensing of Environment*, 79: 213-224.
- Schindler, D.W., and Lee, P.G. 2010. Comprehensive conservation planning to protect biodiversity and ecosystem services in Canadian boreal regions under a warming climate and increasing exploitation, *Biological Conservation*, 143: 1571–1586.
- Schneider, P., Roberts, D. A. and Kyriakidis, P. C. 2008. A VARI-based relative greenness from MODIS data for computing the Fire Potential Index, *Remote Sensing of Environment*, 112:1151-1167.
- Sekhon, N.S., Hassan, Q.K. and Sleep, R.W. 2010. Evaluating potential of MODIS-based indices in determining "snow gone" stage over forest-dominant regions. *Remote Sensing*, 2: 1348-1363.
- Seneviratne, S. I., Corti, T., Davin, E. L., Hirschi, M., Jaeger, E. B., Lehner, I., Orlowsky, B., and Teuling, A. J. 2010. Investigating soil moisture-climate interactions in a changing climate: a review, *Earth-Science Reviews*, 99:125–161.
- Shuttleworth, W. J. 1988. Evaporation from Amazonian rainforest. *Proc. Roy. Soc. London* 233: 321-346.

- Stenberg, P., Rautiainen, M., Manninen, T., Voipio, P. and Mottus, M. 2008. Boreal forest leaf area index from optical satellite images: model simulations and empirical analyses using data from central Finland. *Boreal Environmental Research*, 13:433-443.
- Su, Z., Yacob, A., Wen, J., Roerink, G., He, Y., Gao, B., Boogaard, H. and Diepen, C. V. 2003. Assessing relative soil moisture with remote sensing data: theory, experimental validation, and application to drought monitoring over the North China Plain. *Physics and Chemistry of the Earth*, 28:89-101.
- Van Wagner, C. E.; Pickett, T. L. 1985. *Equations and FORTRAN program for the Canadian Forest Fire Weather Index System*. Canadian Forest Service, Ottawa, ON. Forestry Technical Report 33, p. 25.
- Van Wagner, C.E. 1987. *Development and structure of the Canadian forest fire weather index*. Ottawa, Ontario, Canada: Forestry technical report 35, Government of Canada, Canadian Forestry Service, Petawawa National Forestry Institute, p.48.
- Venturini, V., Bisht, G., Islam, S. and Jiang, L. 2004. Comparison of evaporative fractions estimated from AVHRR and MODIS sensors over South Florida. *Remote Sensing of Environment*, 93 :77–86.
- Vidal, A. and Devaux-Ros, C. 1995. Evaluating forest fire hazard with a Landsat TM derived water stress index, *Agricultural and Forest Meteorology*, 77: 207-224.
- Wang, L. and Qu, J. J. 2007. NMDI: A normalized multi-band drought index for monitoring soil and vegetation moisture with satellite remote sensing, *Geophysical Research Letter*, 34: L20405.

- Wang, L., Qu, J. J., Hao, X. and Zhu, Q. 2008. Sensitivity studies of the moisture effects on MODIS SWIR reflectance and vegetation water indices, *International Journal of Remote Sensing*, 29(24):7065-7075.
- Wang, L., Qu, J. J. and Hao, X. 2008. Forest fire detection using the normalized multi-band drought index (NMDI) with satellite measurements, *Agricultural and Forest Meteorology*, 148: 1767-1776.
- Wang, L., Qu, J. J., Xiaoxiong, X. and Hao, X. 2009. Analysis of seven-year moderate resolution imaging spectroradiometer vegetation water indices for drought and fire activity assessment over Georgia of the United States, *Journal of Applied Remote Sensing*, 3:033555.
- Wotton, B. M. 2009. Interpreting and using outputs from the Canadian Forest Fire Danger Rating System in research applications, *Environmental and Ecological Statistics*, 16:107-131.

Web References

- ARD, 2010. Alberta Agriculture and Rural Development Department,
<http://www.agric.gov.ab.ca/app116/stationview.jsp>, last accessed on 5 June 2010.
- ERDAS, 2011. ERDAS imagine, <http://www.erdas.com/products.aspx>, last accessed on 25 August, 2011.
- LP DAAC, 2010. The Land Processes Distributed Active Archive Center,
https://lpdaac.usgs.gov/lpdaac/products/modis_products_table, last accessed on 25 August 2010.
- LP DAAC, 2011. The Land Processes Distributed Active Archive Center, MODIS Overview, https://lpdaac.usgs.gov/lpdaac/products/modis_overview, last accessed on 11 July, 2011.
- MRT, 2010. MODIS Reprojection Tool,
https://lpdaac.usgs.gov/lpdaac/tools/modis_reprojection_tool, last accessed on 30 August 2010.
- NRC, 2010. Natural Resource Canada, The state of Canada's forest, Annual report 2010.
<http://cfs.nrcan.gc.ca/pubwarehouse/pdfs/31835.pdf>, last accessed on, 2011.
- NRC, 2011 a. Natural Resource Canada, Forest ecosystems of Canada.
<http://ecosys.cfl.scf.nrcan.gc.ca/classification/intro-ecozone-eng.asp>, last accessed on 02 September, 2011.
- NRC, 2011b. Natural Resource Canada, The Atlas of Canada.
http://atlas.nrcan.gc.ca/site/english/learningresources/theme_modules/borealforest/index.html, last accessed on 02 July, 2011.

- NRC, 2011 c. Natural Resource Canada, Boreal forest, Natural disturbances,
<http://canadaforests.nrcan.gc.ca/article/borealnaturaldisturbances>, last accessed on
22 August, 2011.
- NRC, 2011d. Natural Resources Canada, Canadian Forest Fire Weather Index System.
http://cwfis.cfs.nrcan.gc.ca/en_CA/background/summary/fwi, last accessed on 05
July, 2011.
- SRD, 2011a. Sustainable Resource Development, Government of Alberta,
[http://www.srd.alberta.ca/Wildfire/WildfireStatus/HistoricalWildfireInformation/
10-YearStatisticalSummary.aspx](http://www.srd.alberta.ca/Wildfire/WildfireStatus/HistoricalWildfireInformation/10-YearStatisticalSummary.aspx), last accessed on 20 March, 2011.
- SRD, 2011b. Sustainable Resource Development, Government of Alberta,
[http://www.srd.alberta.ca/Wildfire/WildfireStatus/HistoricalWildfireInformation/
HistoricalWildfireDatabase.aspx](http://www.srd.alberta.ca/Wildfire/WildfireStatus/HistoricalWildfireInformation/HistoricalWildfireDatabase.aspx), last accessed on 28 March, 2011.
- SRTM, 2009. NASA Shuttle Radar Topography Mission archive,
<http://srtm.csi.cgiar.org/>, last accessed on 20 July 2009.
- SC, 2011. Ecozones, Statistics Canada, [http://www.statcan.gc.ca/ads-annonces/11-509-
x/ecozones-eng.htm](http://www.statcan.gc.ca/ads-annonces/11-509-x/ecozones-eng.htm), last accessed on 25 August 2011.

APPENDIX I

Permission from published Journal

The permission procedure of the journal of “Boreal Environmental Research” for the published paper namely “Remote sensing based estimates of surface wetness conditions and growing degree days over northern Alberta Canada” is given below:

According to the journal (<http://www.borenv.net/> last visited 22 July 2011):

“The author(s) may reproduce or re-use parts of their original material first published in Boreal Environment Research without permission”

APPENDIX II

Table AII.1: Values of dryline1 (θ_{dry1}) and slope and intercept of the dryline2 (θ_{dry2}) for estimating TVWI during the year 2006 to 2008.

DOY	θ_{dry1}			θ_{dry2}					
	2006	2007	2008	2006		2007		2008	
				Slope	Inter- cept	Slope	Inter- cept	Slope	Inter- cept
121-128	314.0	307.00	309.50	-0.0045	339.25	-0.0037	328.95	-0.0040	331.49
129-136	320.0	312.00	312.00	-0.0025	332.97	-0.0049	341.82	-0.0069	357.38
137-144	320.0	318.00	319.00	-0.0065	367.61	-0.0045	345.45	-0.0100	392.00
145-152	316.5	320.00	317.00	-0.0027	335.79	-0.0040	347.20	-0.0062	361.31
153-160	318.0	323.50	320.00	-0.0035	344.25	-0.0019	335.57	-0.0090	392.38
161-168	317.0	320.50	320.00	-0.0050	356.50	-0.0045	353.58	-0.0091	393.64
169-176	318.0	316.50	318.50	-0.0056	361.88	-0.0053	359.03	-0.0074	379.92
177-184	321.0	324.00	320.00	-0.0072	381.67	-0.0063	369.00	-0.0124	395.00
185-192	326.0	318.00	321.50	-0.0067	382.00	-0.0052	360.43	-0.0021	335.80
193-200	315.5	326.00	317.00	-0.0028	336.22	-0.0047	361.16	-0.0071	375.59
201-208	323.0	320.50	319.00	-0.0048	360.74	-0.0024	335.64	-0.0069	376.75
209-216	319.5	318.50	328.00	-0.0045	351.36	-0.0073	377.80	-0.0059	365.15
217-224	313.0	318.00	322.00	-0.0053	354.29	-0.0054	359.08	-0.0038	351.33
225-232	313.0	314.00	318.50	-0.0031	335.61	-0.0062	363.23	-0.0105	397.75
233-240	317.5	305.00	311.50	-0.0039	346.02	-0.0029	328.04	-0.0021	326.53
241-248	317.0	311.50	308.00	-0.0043	349.14	-0.0061	360.59	-0.0026	327.06
249-256	317.0	307.00	305.50	-0.0048	353.00	-0.0071	364.14	-0.0061	355.74
257-264	302.0	309.50	310.00	-0.0022	316.88	-0.0063	358.88	-0.0036	337.00
265-272	305.5	301.50	303.00	-0.0039	334.67	-0.0031	324.48	-0.0050	342.00
273-280	301.0	302.50	311.00	-0.0030	322.63	-0.0055	348.92	-0.0089	385.67

Table AII.2: Description of the quadratic fits ($y = a_1x^2 + a_2x + a_3$) to the variables of T_S / NMDI / TVWI as a function of DOY during the period 2006-2008.

Variables	Year	a₁	a₂	a₃	r²
T_S	2006	-0.001	0.627	237.5	0.88
	2007	-0.001	0.692	228.6	0.85
	2008	-0.002	0.785	218.7	0.84
NMDI	2006	-2.00E-05	0.006	-0.099	0.83
	2007	-1.00E-05	0.004	-0.016	0.67
	2008	-2.00E-05	0.006	-0.156	0.70
TVWI	2006	2.00E-05	-0.009	1.252	0.74
	2007	3.00E-05	-0.011	1.486	0.75
	2008	4.00E-05	-0.014	1.847	0.80

APPENDIX III

Fire Danger Maps

Some of the sample fire danger maps are presented here. During the period 2006-2008, 4 (four) such sample maps for each of the each year are included. The zoomed sections are the illustrations of the fire danger around the fire polygons

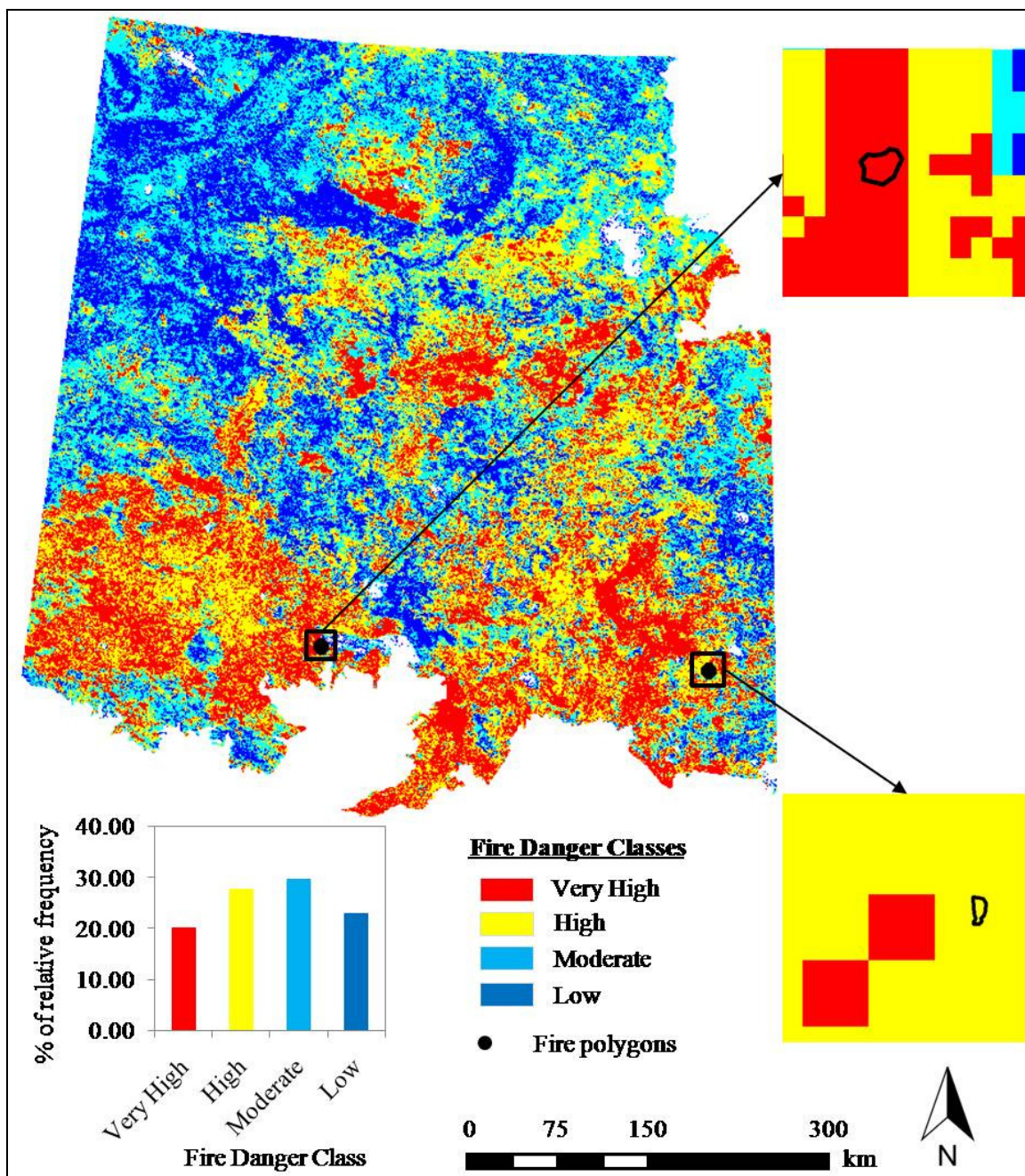


Figure AIII.1: Fire danger mapping for the period 17 May-24 May, 2006 produced by combining all of three variables of T_S , NMDI, and TVWI from the previous period 9 May-16 May 2006.

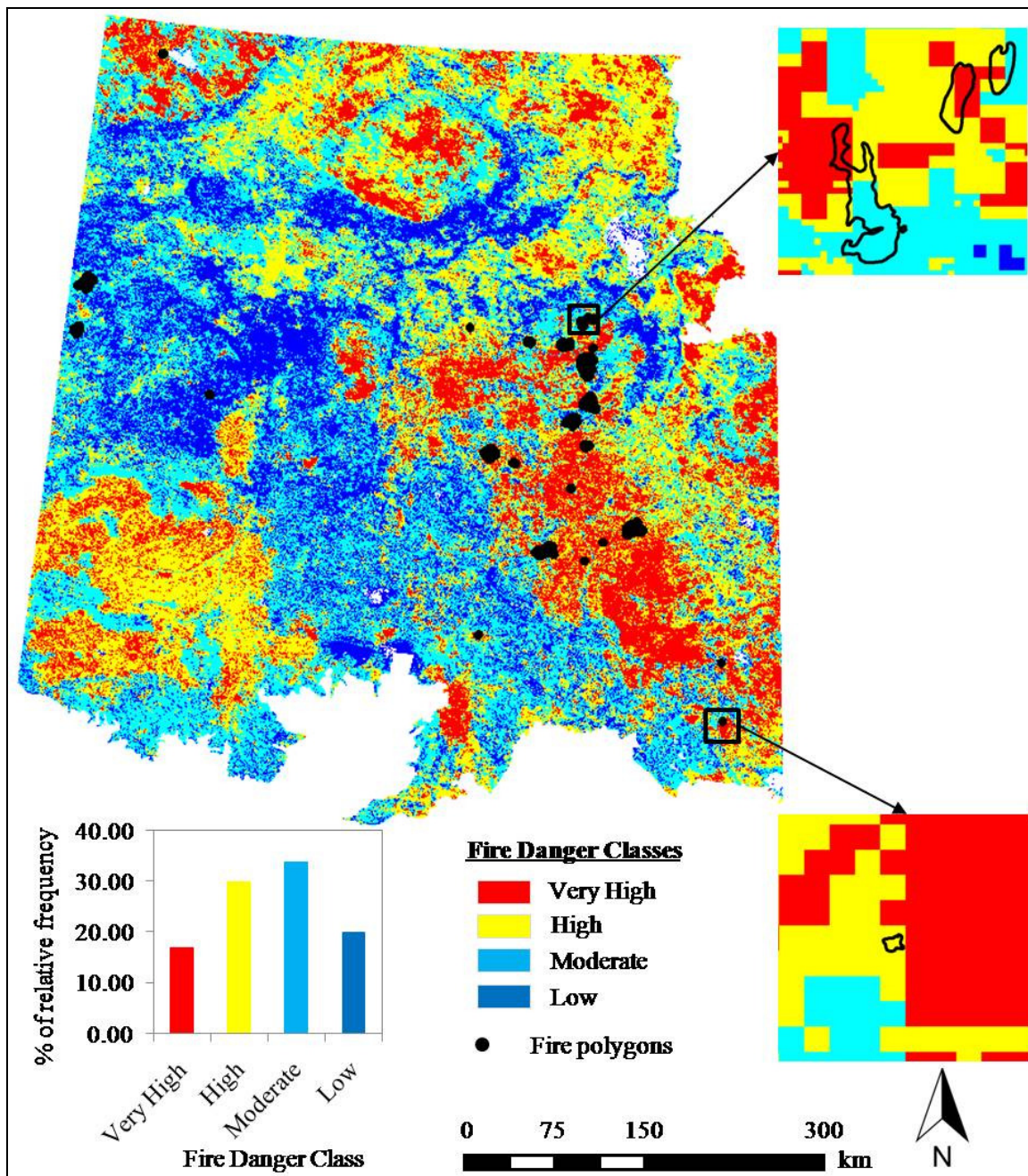


Figure AIII.2: Fire danger mapping for the period 26 June-03 July, 2006 produced by combining all of three variables of T_S , NMDI, and TVWI from the previous period 18 June-25 June 2006.

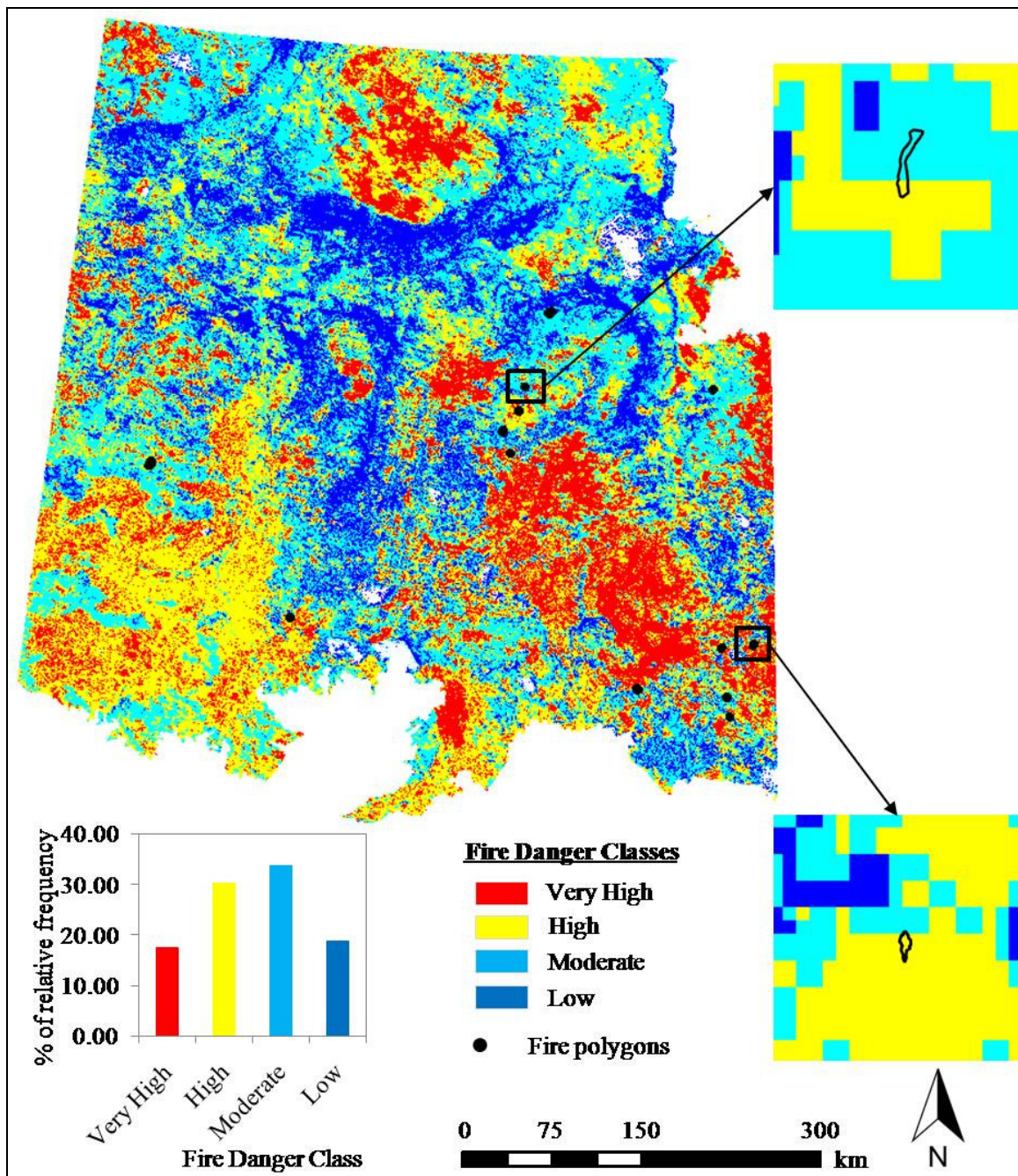


Figure AIII.3: Fire danger mapping for the period 04 July-11 July, 2006 produced by combining all of three variables of T_s , NMDI, and TVWI from the previous period 26 June-03 July 2006.

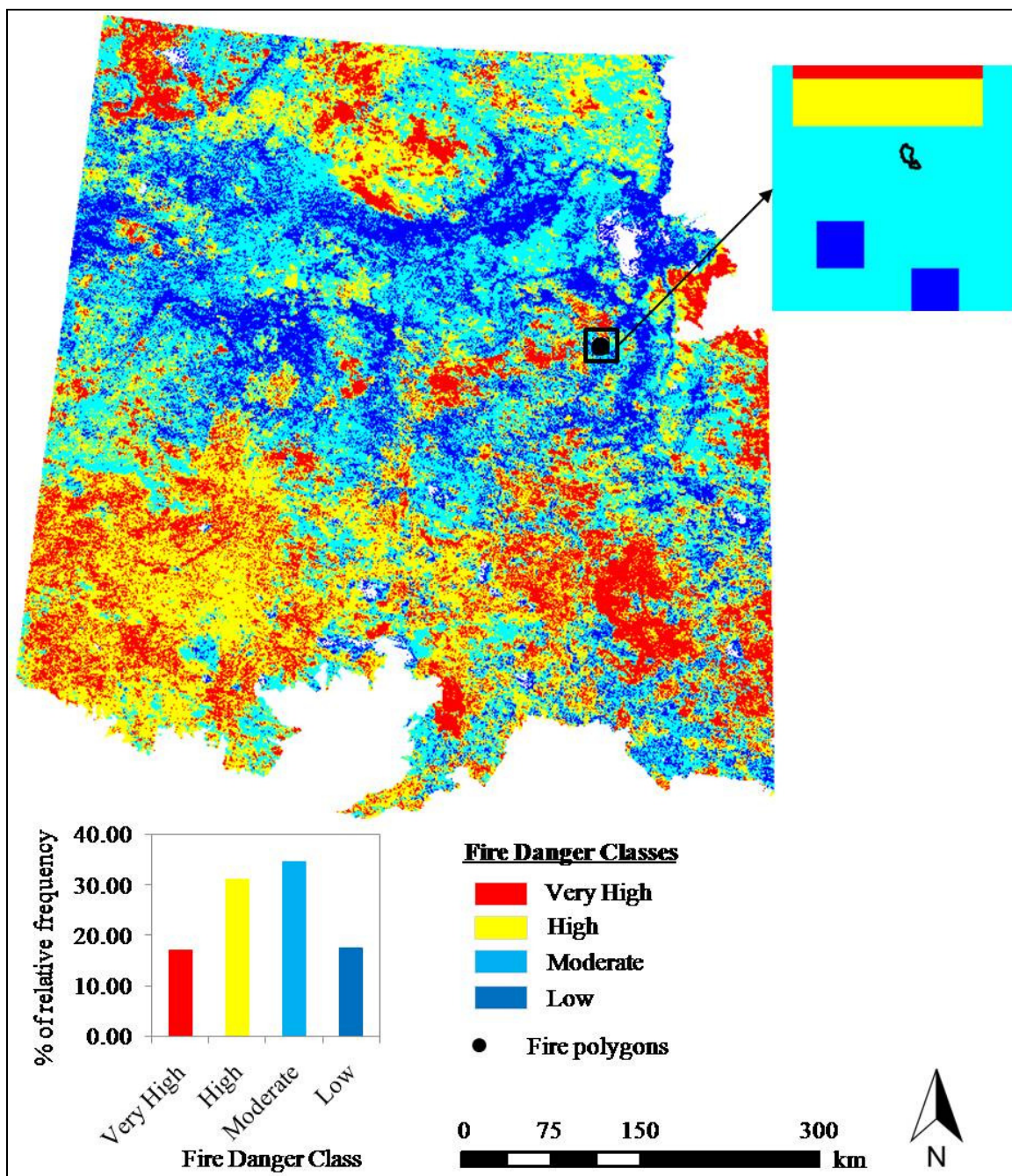


Figure AIII.4: Fire danger mapping for the period 28 July-04 August, 2006
 produced by combining all of three variables of T_s , NMDI, and TVWI from the
 previous period 20 July-27 July 2006.

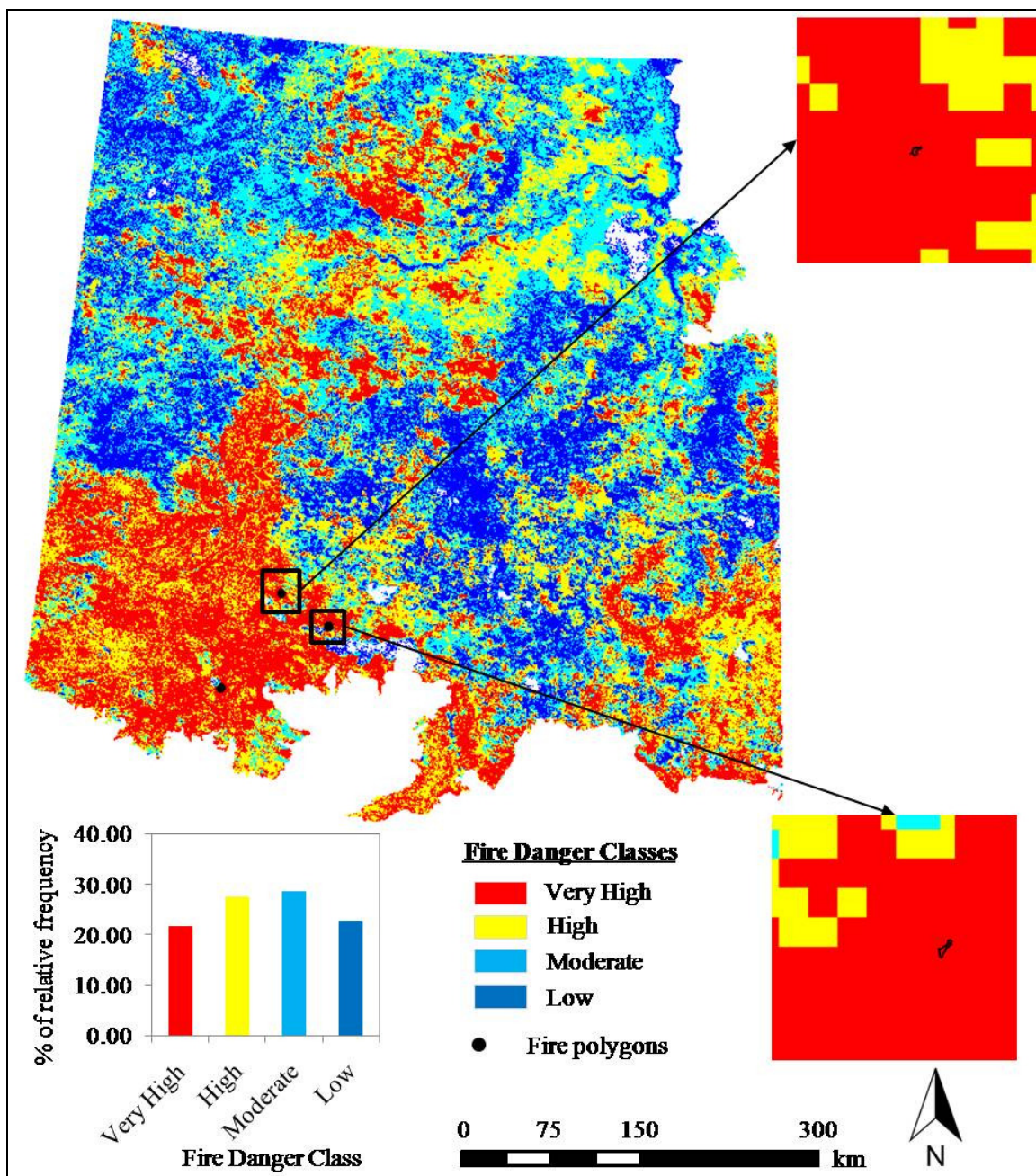


Figure AIII.5: Fire danger mapping for the period 17 May-24 May, 2007 produced by combining all of three variables of T_s , NMDI, and TVWI from the previous period 9 May-16 May 2007.

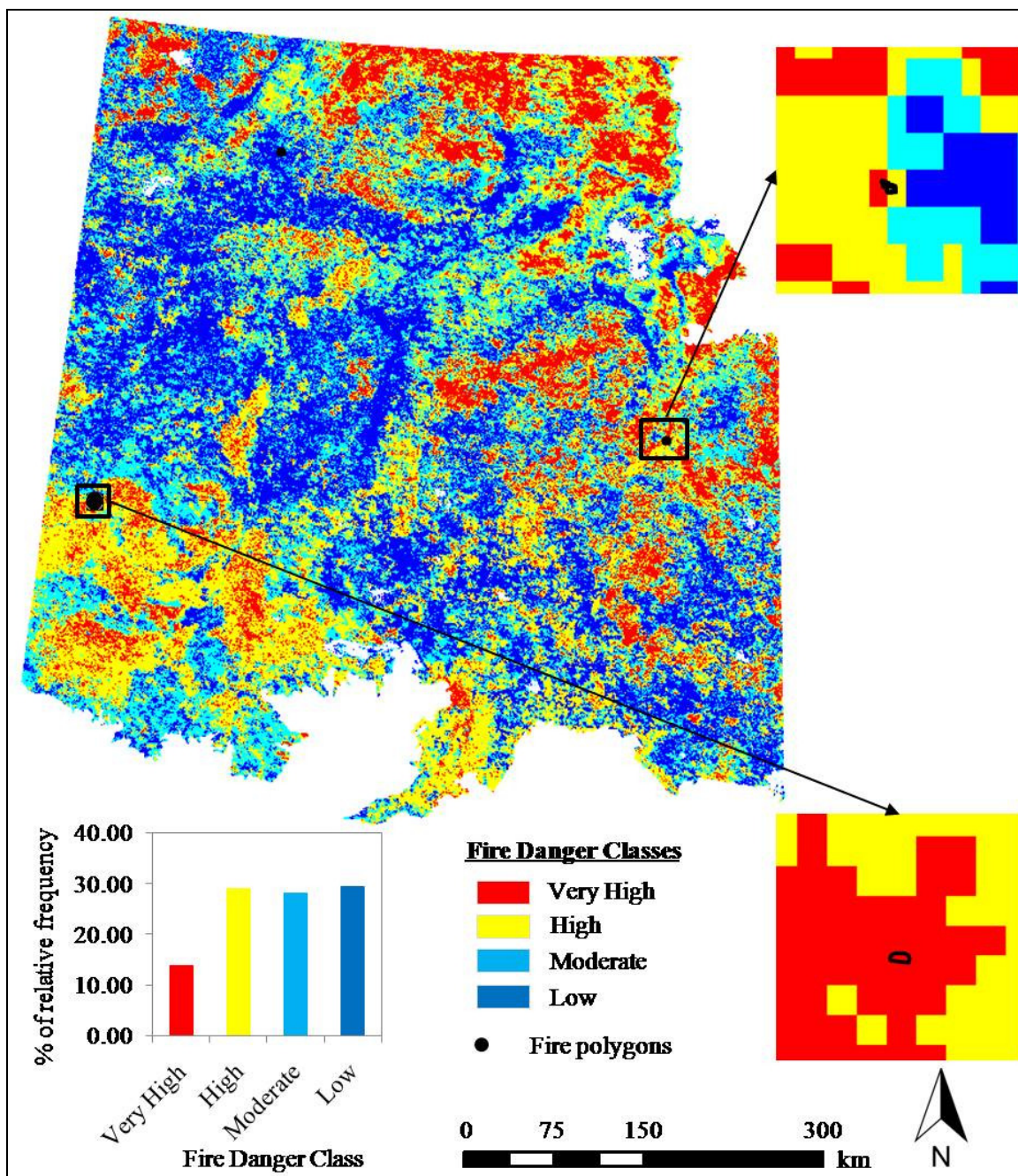


Figure AIII.6: Fire danger mapping for the period 26 June-03 July, 2007 produced by combining all of three variables of T_s , NMDI, and TVWI from the previous period 18 June-25 June 2007.

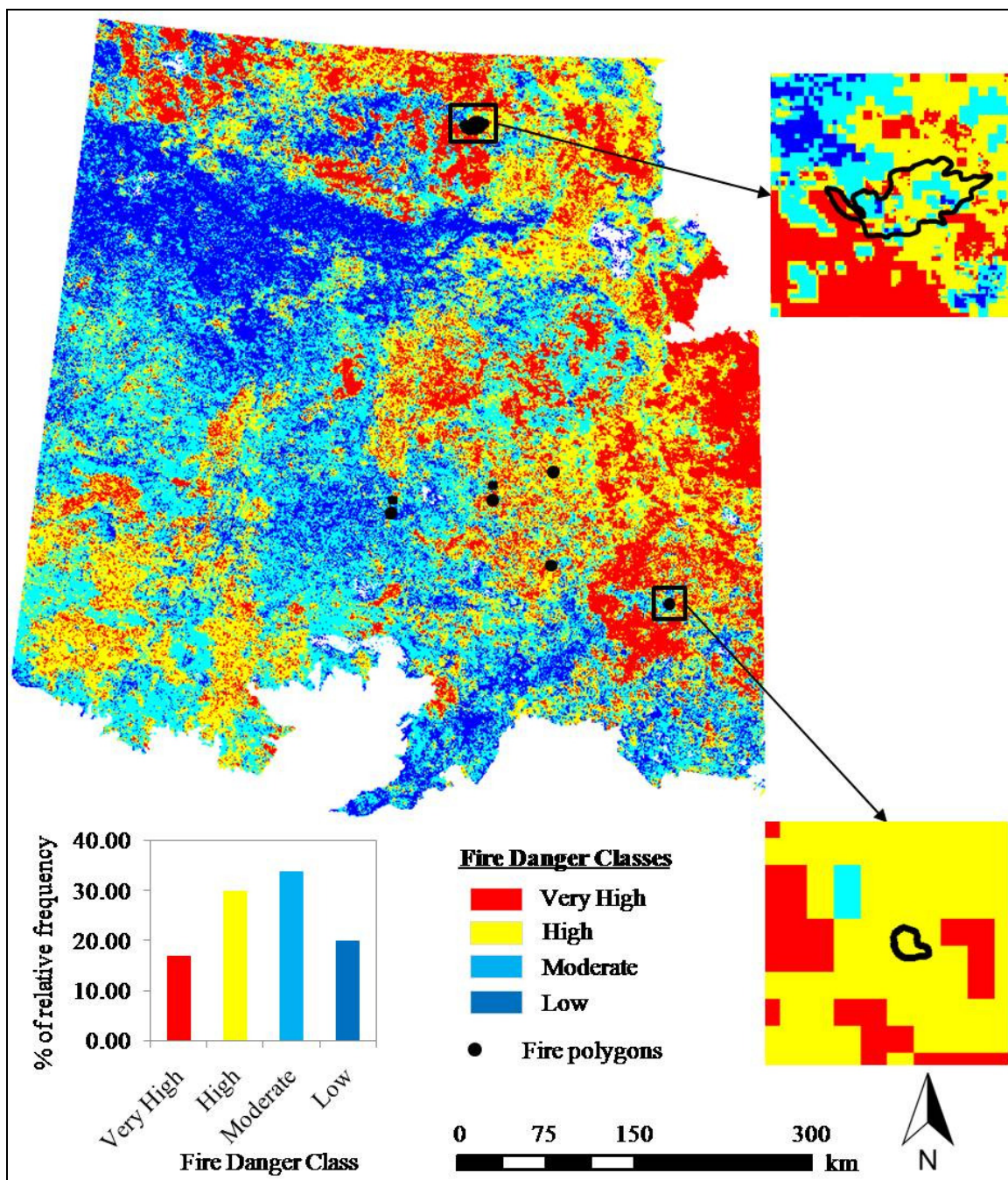


Figure AIII.7: Fire danger mapping for the period 04 July-11 July, 2007 produced by combining all of three variables of T_s , NMDI, and TVWI from the previous period 26 June-03 July 2007.

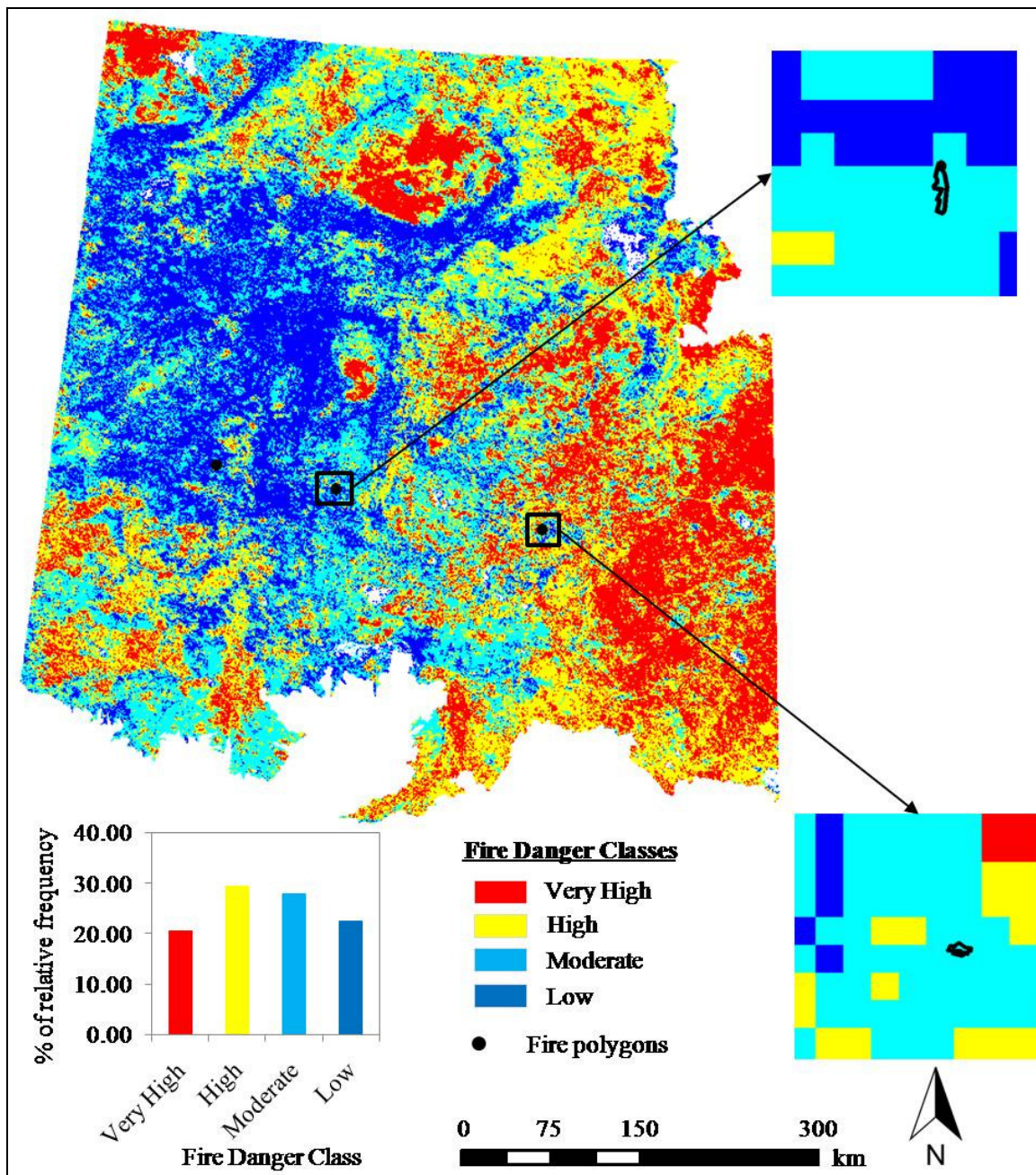


Figure AIII.8: Fire danger mapping for the period 28 July-04 August, 2007 produced by combining all of three variables of T_s , NMDI, and TVWI from the previous period 20 July-27 July 2007.

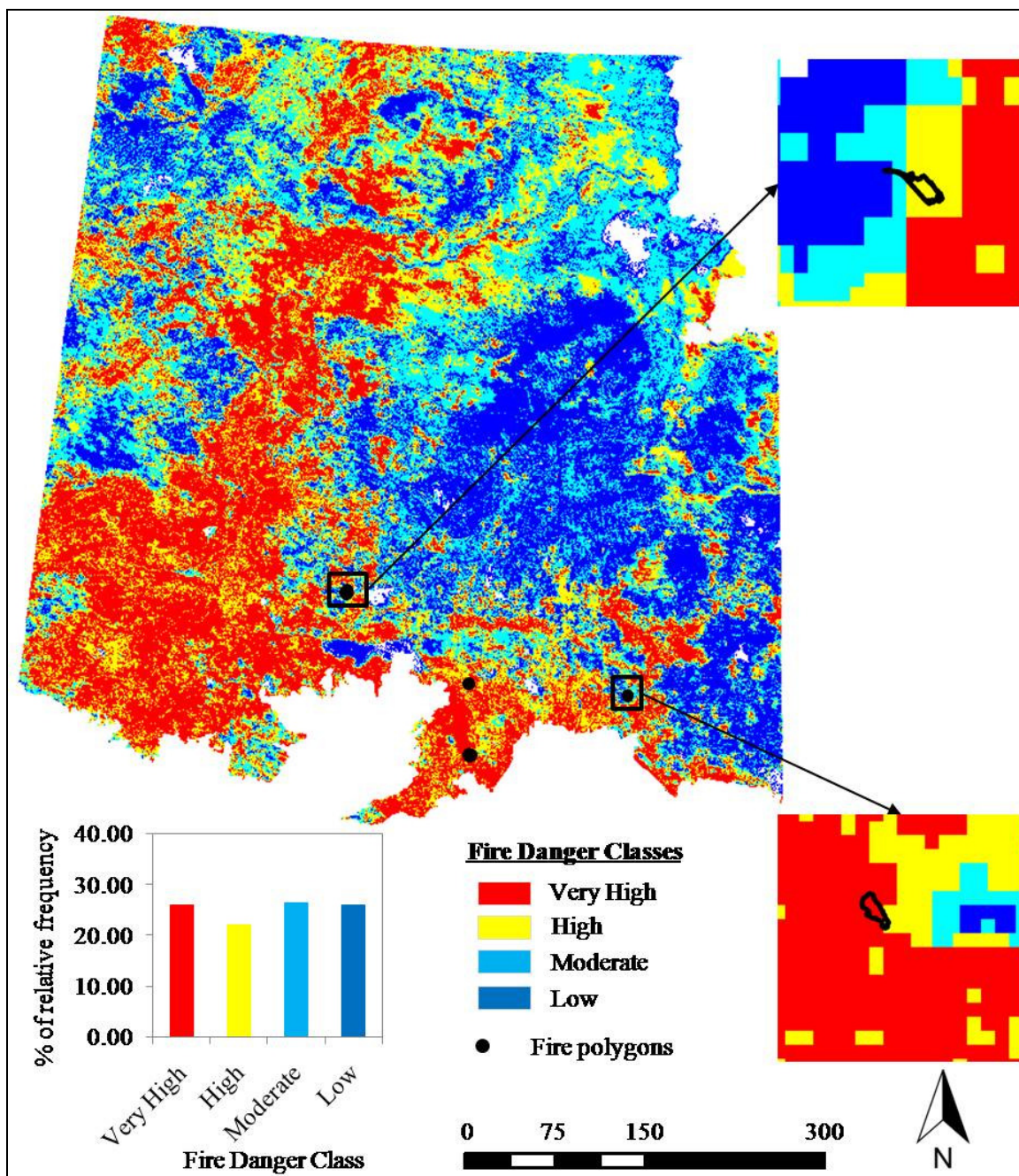


Figure AIII.9: Fire danger mapping for the period 16 May-23 May, 2008 produced by combining all of three variables of T_s , NMDI, and TVWI from the previous period 8 May-15 May 2008.

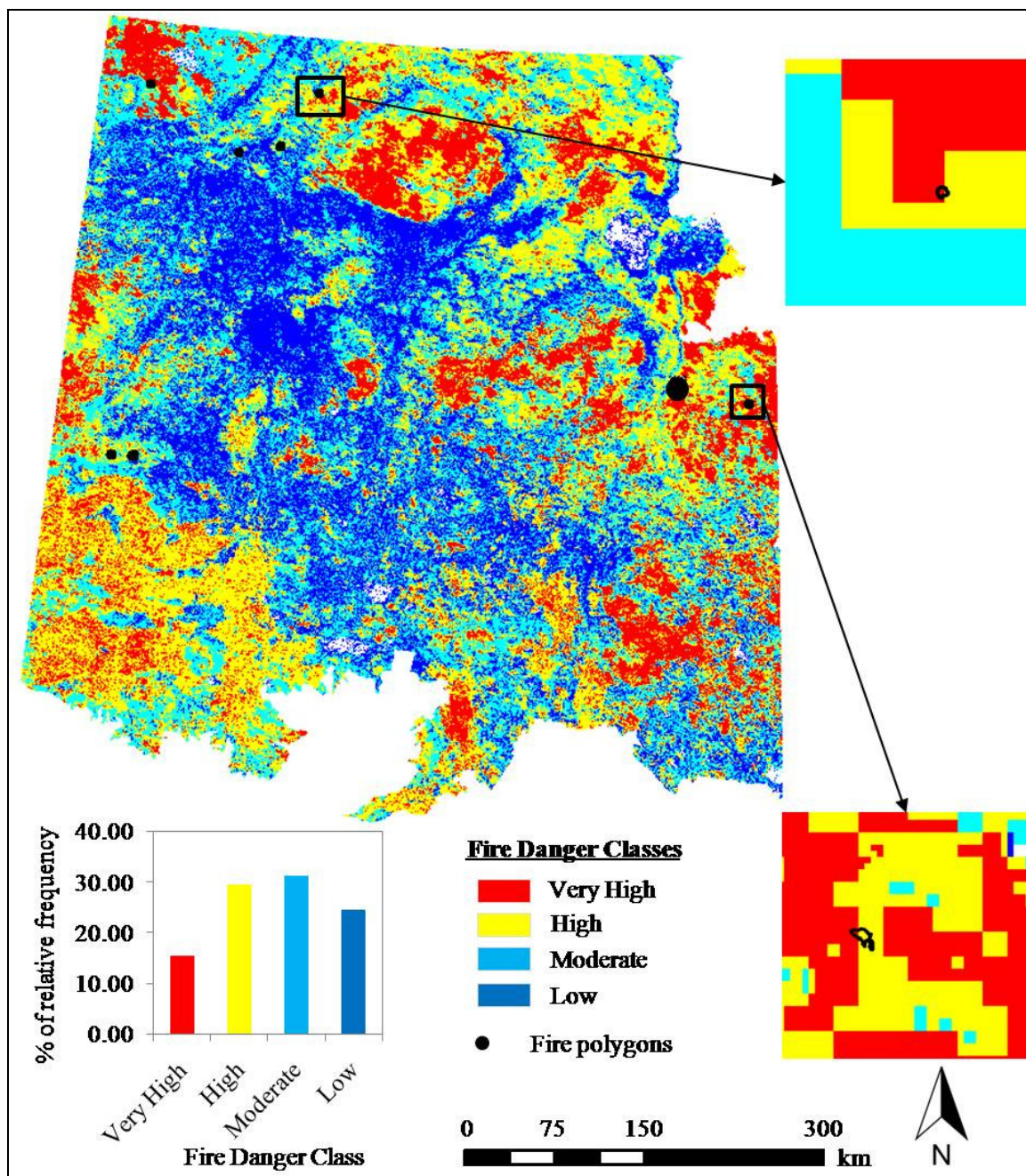


Figure AIII.10: Fire danger mapping for the period 03 July-10 July, 2008 produced by combining all of three variables of T_s , NMDI, and TVWI from the previous period 25 June-02 July 2008.

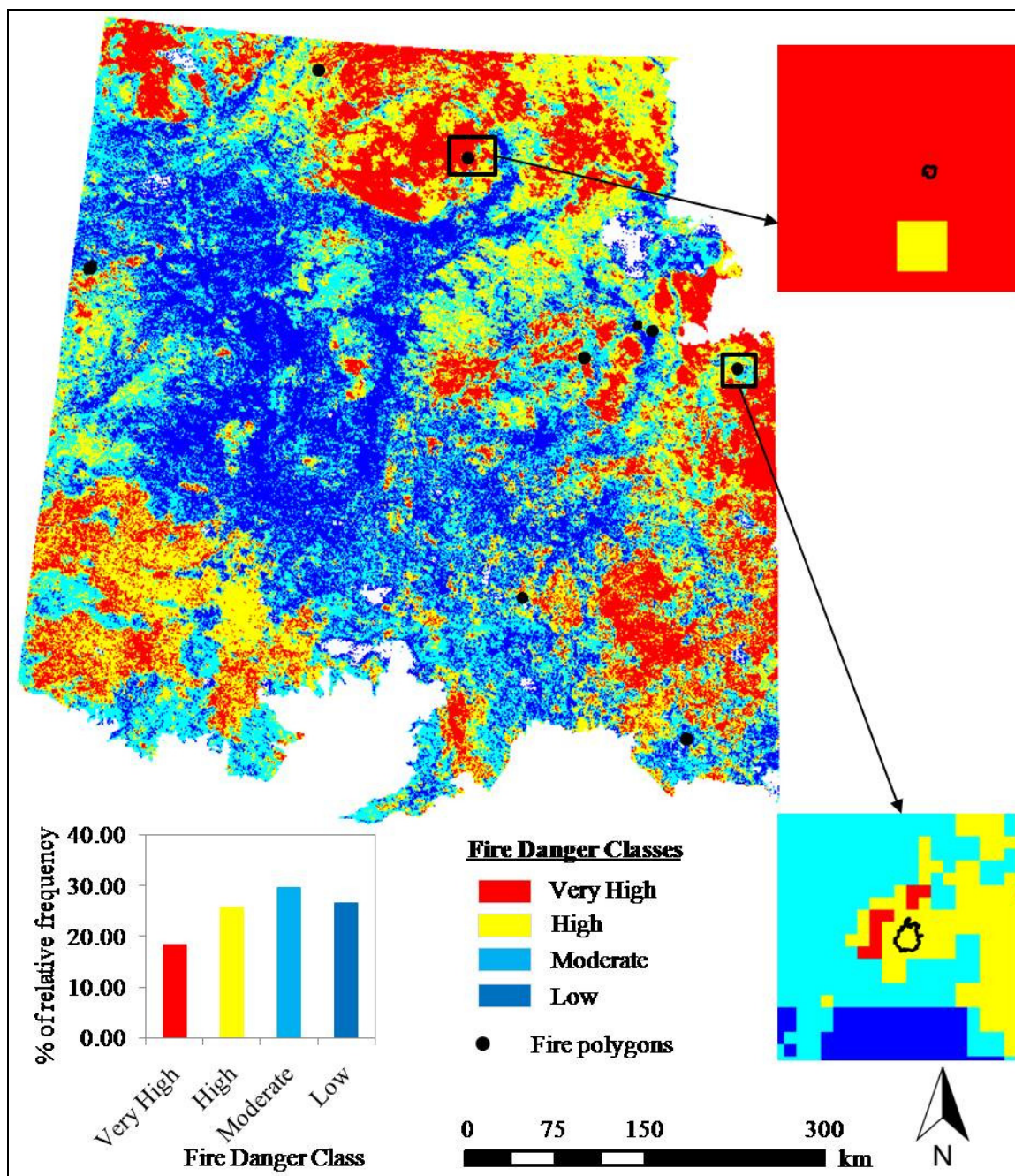


Figure AIII.11: Fire danger mapping for the period 27 July-03 August, 2008
 produced by combining all of three variables of T_s , NMDI, and TVWI from the
 previous period 19 July-26 July 2008.

Appendix V

ERDAS Imagine Step-by-Step modeling

In this study, the “Spatial Modeller” module of the ERDAS Imaging Software (ERDAS 2011) was used.

1. Image mosaick: The two scenes of Geo-TIFF images per period for each of the data set (i.e., T_S and surface reflectance) were mosaicked together using the following model. For example:

Input data: \$n1_361 and \$n1_361 Tiff Images (.tif) of surface temperature of the desired study area of Alberta.

Output data: surface temperatures at 1 km resolution, Imagine Image (.img) file format.

Data type: Integer Unsigned 16 bit. The images were mosaicked for the periods from 97 to 297 DOY during 2006-2008 both for surface temperature and surface reflectance.

Equations for Mosaicking:

\$n1_361_left * 2

\$n1_361_right * 2

EITHER \$n5_memory IF (\$n6_memory ==0) OR \$n6_memory OTHERWISE

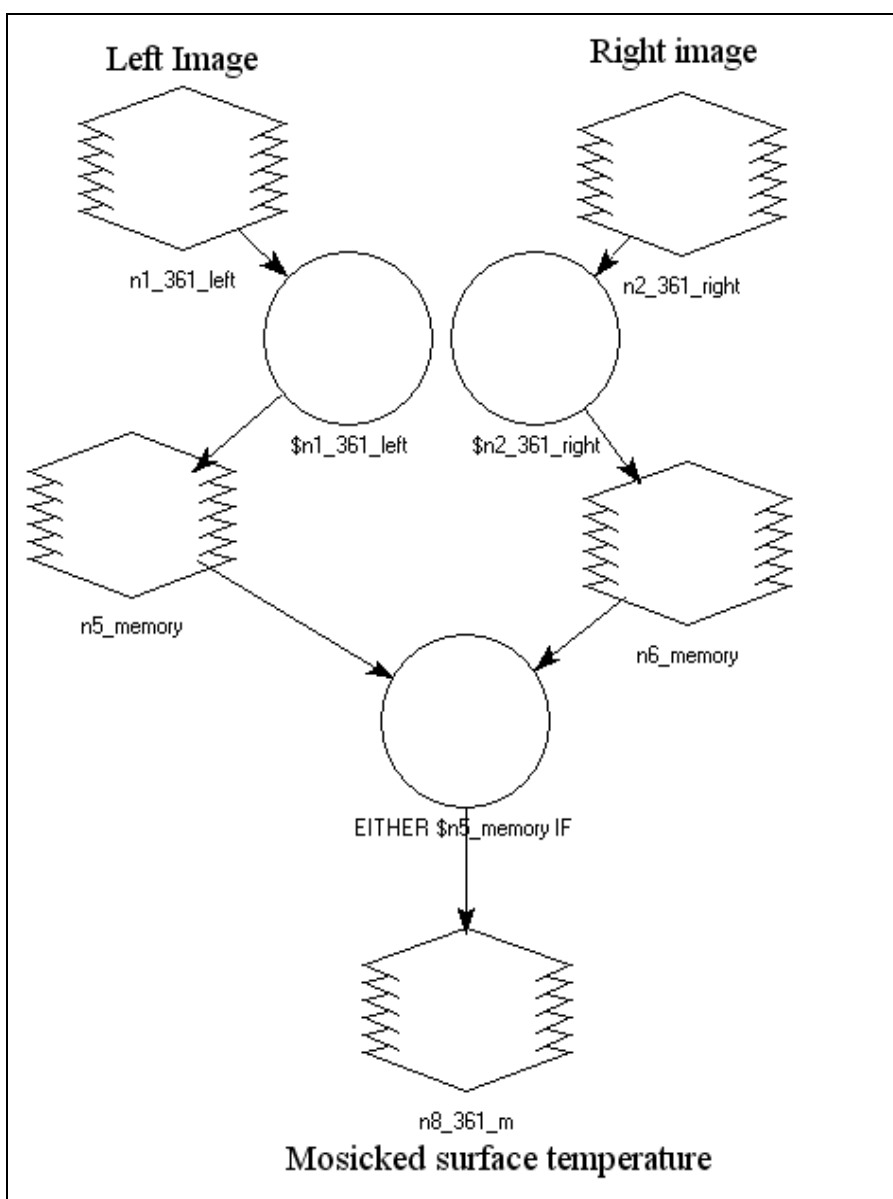


Figure AIV.1: The spatial model showing the formulated workflow with data inputs to produce mosaicked images.

2. Cloud contamination algorithm: Due to the cloud some pixels of the images were contaminated so need to apply an image correction algorithm. This involved the following steps:

- (i) **Layer Stacking:** 26 layers of images of each period for each individual year were stacked together using the built-in model of ERDAS.

Input image: n7_spots and n15_dmtm, (Images from 89 to 297 DOY)

Output image: n17_stacklayer

Equations for layer stacking: STACKLAYERS (\$n7_spots(1) , \$n15_dmtm (2 :
NUMLAYERS (\$n15_dmtm))) (Variable LAYERSTACK using Spatial Modeler
syntax)

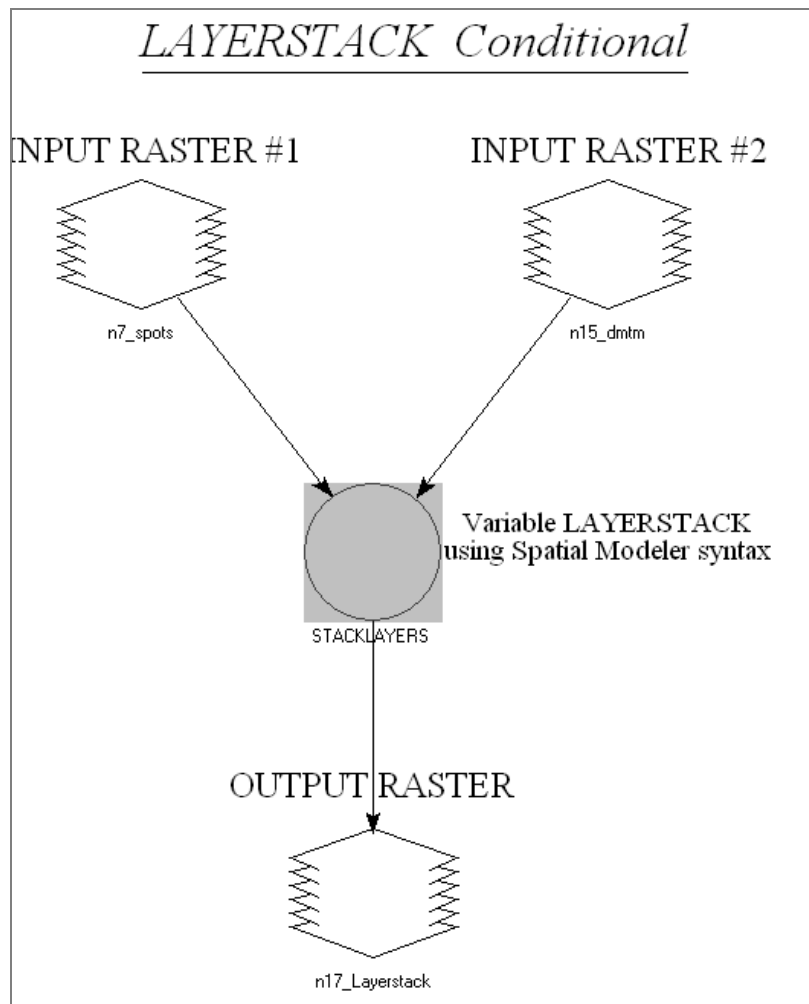


Figure AIV.2: The spatial model showing the formulated workflow with data inputs to produce stacked images.

(ii) Converting pixel values to binary number:

Input image: n17_stacklayer (n1_stack_097_297_05)

Output image: n3_convert_0_1. Data type: Integer Unsigned 8 bit

Equation for converting in binary numbers: EITHER 0 IF (\$n1_stack_97_297_05 ==0) OR 1 OTHERWISE

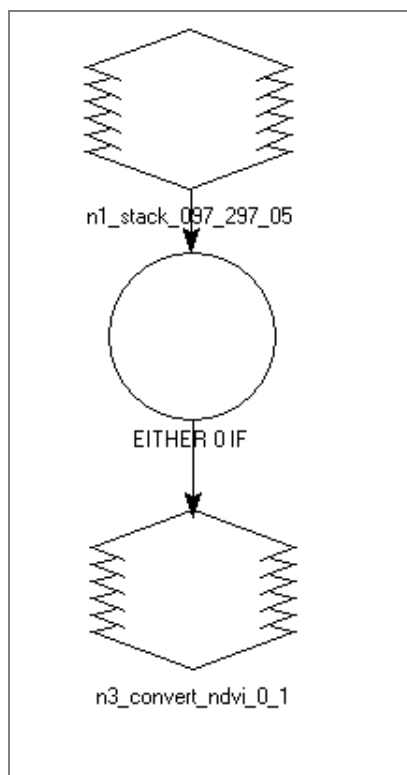


Figure AIV.3: The spatial model showing the formulated workflow with data inputs to produce the binary images.

(iii) Calculating total cloud free numbers (m) from binary numbers:

Input image: n1_convert_0_1

Output image: n3_total_cloud_free

Equation for calculating total cloud free numbers (m): STACK SUM

($n1_convert_0_1$)

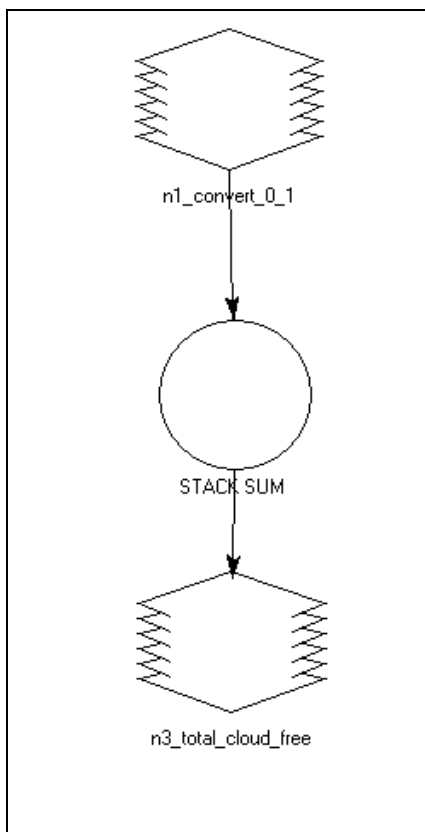


Figure AIV.4: The spatial model showing the formulated workflow with data inputs to produce the total cloud free number images.

(iv) Calculating mean and sum mean deviation:

Input image: n1_stack_97-297 & n2_Custom-integer (mean values of the layers of 97 to 297 DOY)

Output image: n4_mean & n5_sum_mean. Data type: Signed 16 bit

Equation for calculating mean and sum mean deviation:

EITHER 0 IF (\$n1_stack_97_297 ==0) OR (\$n2_Custom_Integer - \$n1_stack_97_297) OTHERWISE

STACK SUM (\$n4_mean)

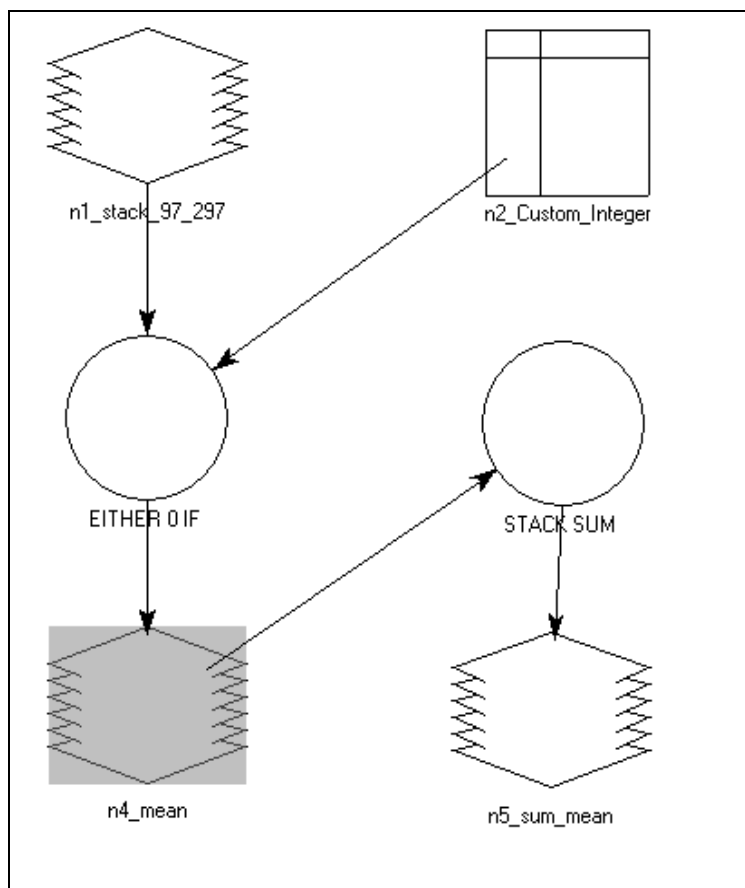


Figure AIV.5: The spatial model showing the formulated workflow with data inputs to produce the mean and sum mean deviation images.

(v) Calculating average deviation:

Input image: \$n1_sum_mean and \$n2_total_cloud_free

Output image: \$n1_avg_of_mean, Data type: Float single

Equation for calculating average deviation:

EITHER 0 IF ((\$n1_sum_mean ==0) or (\$n2_total_cloud_free ==0)) OR

\$n1_sum_mean/\$n2_total_cloud_free OTHERWISE

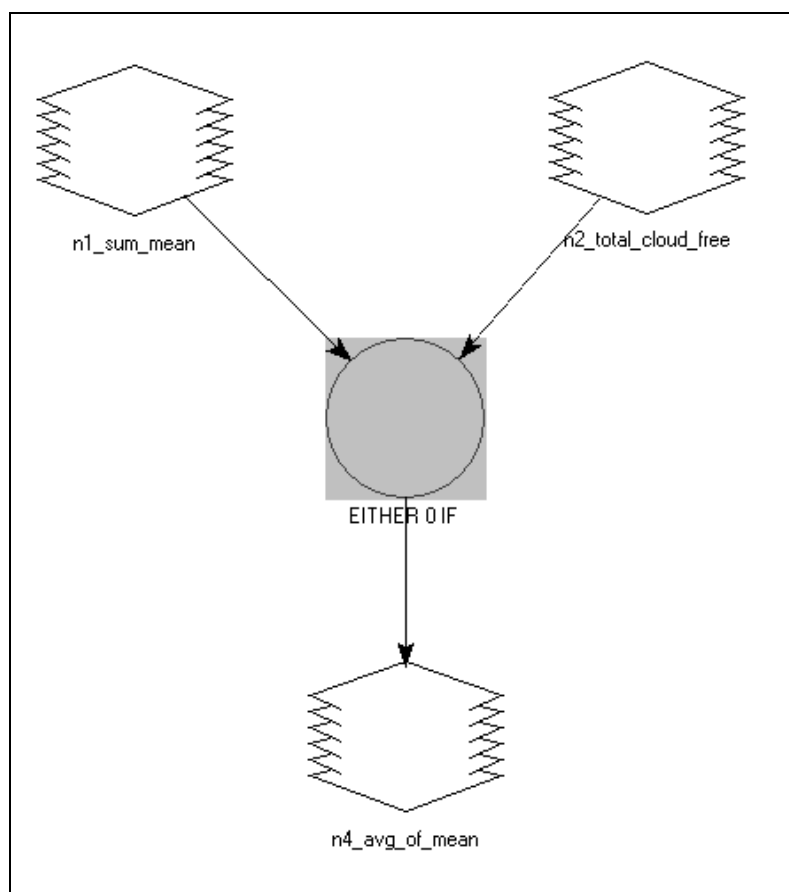


Figure AIV.6: The spatial model showing the formulated workflow with data inputs to produce the average deviation images.

(i) Calculating cloud corrected pixels:

Input image: \$n1_total_cloud_free, \$n8_stack_97_297, \$n2_Custom_Integer, \$n8_stack_97_297

Output image: n4_gap_filled_stack, Data type: Un-signed 16 bit

Equation for calculating cloud corrected pixels: $\text{CONDITIONAL}\{ (\$n1_total_cloud_free == 0) 0, (\$n8_stack_97_297 == 0) (\$n2_Custom_Integer - \$n7_avg_of_mean), (\$n8_stack_97_297 > 0) \$n8_stack_97_297 \}$

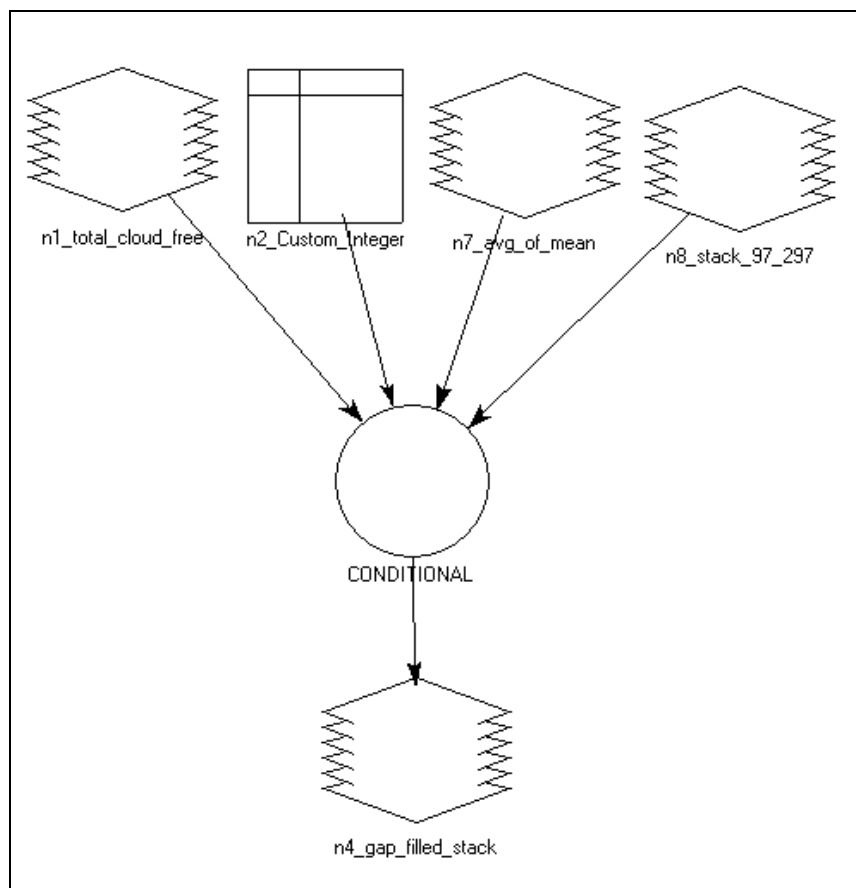


Figure AIV.7: The spatial model showing the formulated workflow with data inputs to produce the cloud corrected images.

3. Calculating NDVI:

Input image: \$n1_097_sur_refl_b01, \$n2_097_sur_refl_b02

Output image: n7_097_ndvi, Data type: Un-signed 16 bit

Equation for calculating NDVI: EITHER 0 IF ((\$n1_097_sur_refl_b01 <=0) or (\$n2_097_sur_refl_b02 <=0)) OR $10000 * (\$n2_097_sur_refl_b02 - \$n1_097_sur_refl_b01) / (\$n2_097_sur_refl_b02 + \$n1_097_sur_refl_b01)$

OTHERWISE

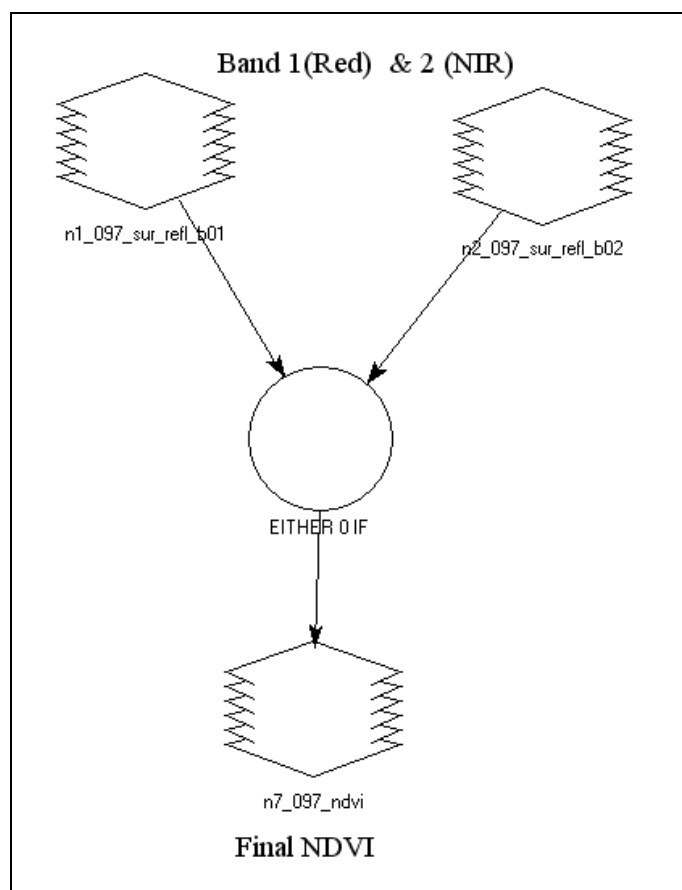


Figure AIV.8: The spatial model showing the formulated workflow with data inputs to produce the NDVI images.

4. Calculating NMDI:

Input image: \$n1_mod092008137 (stacked surface reflectance of band 1-7)

Output image: nmdi_137_08.img, data type: unsigned 16-bit

Equation for calculating NMDI:

EITHER 0 IF ((\$n1_mod092008137(2) <=0) or (\$n1_mod092008137(6) <=0) or
 (\$n1_mod092008137(7) <=0)) OR 10000*(((\$n1_mod092008137(2)-
 (\$n1_mod092008137(6)-
 \$n1_mod092008137(7)))/(\$n1_mod092008137(2)+(\$n1_mod092008137(6)-
 \$n1_mod092008137(7)))) OTHERWISE

EITHER 10000 IF (\$n3_memory >=10000) OR \$n3_memory OTHERWISE

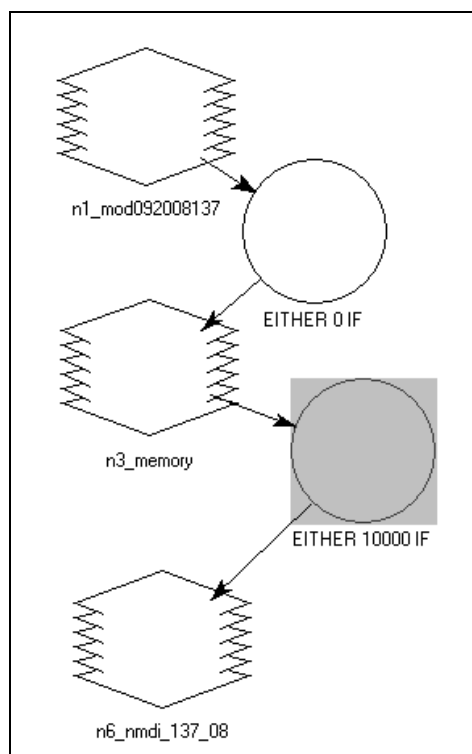


Figure AIV.9: The spatial model showing the formulated workflow with data inputs to produce the NMDI images.

5. Calculating TVWI:

The following steps were employed to calculate TVWI:

(i) Calculating atmospheric pressure

Input image: \$n1_alberta_dem250m

Output image: n3_atmos_press_ab_250m

Equation for calculating cloud corrected pixels: `CONDITIONAL { ($n1_alberta_dem250m == 0) 0, ($n1_alberta_dem250m >0) 101.3* ((293 - (0.0065*$n1_alberta_dem250m))/293)**5.26}`

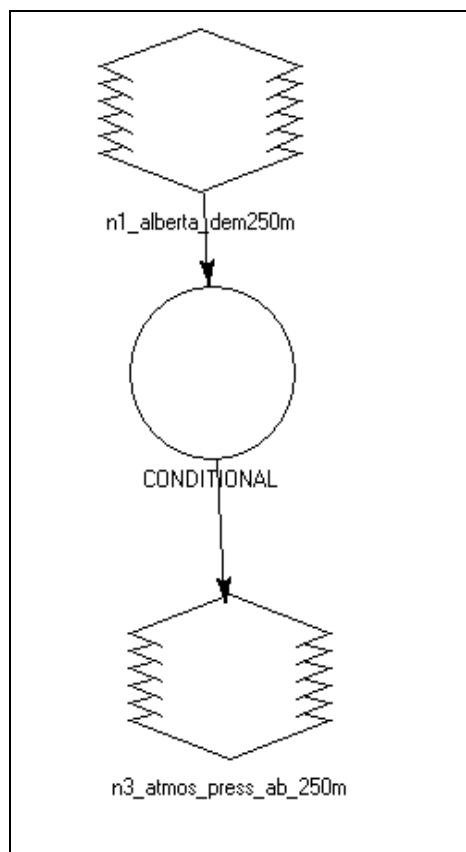


Figure AIV.10: The spatial model showing the formulated workflow with data inputs to produce the atmospheric pressure images.

(ii) Calculating potential temperature

Input image: \$n3_atmos_p_nb_ns_pei_250m,

\$n6_cloud_filled_8day_097_297_ts

Output image: n4_potstack_097_297

Equation for calculating potential temperature: $\text{CONDITIONAL } \{$
 $(\$n3_atmos_p_nb_ns_pei_250m == 0) 0, (\$n3_atmos_p_nb_ns_pei_250m > 0)$
 $((\$n6_cloud_filled_8day_097_297_ts/100)$
 $*((101.3/\$n3_atmos_p_nb_ns_pei_250m)**0.286))\}$

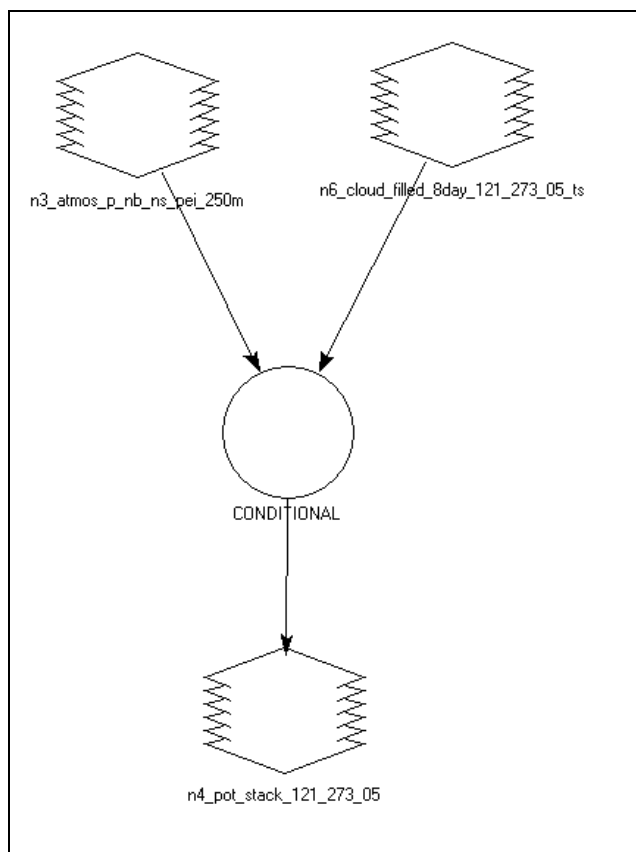


Figure AIV.11: The spatial model showing the formulated workflow with data inputs to produce the potential temperature images.

(iii) Stacking NDVI and potential surface temperature

Input image: \$n1_097_ndvi, \$n2_pot_temp_097

Output image: stack_ndvi_pot_temp_097.img

Equation for stacking the NDVI and potential temperature: STACKLAYERS (
\$n1_097_ndvi , \$n2_pot_temp_097)

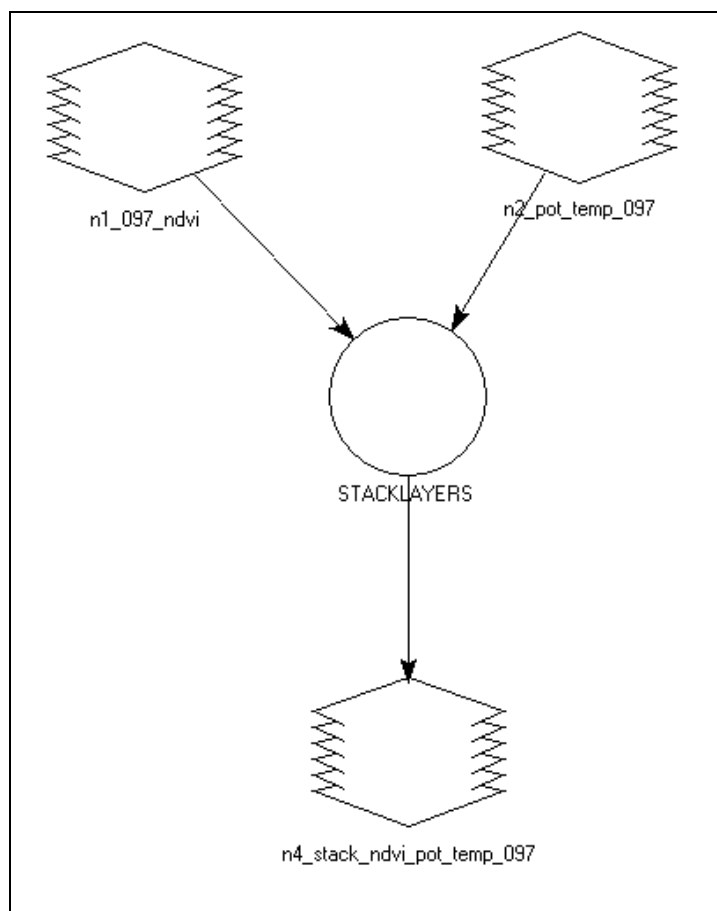


Figure AIV.12: The spatial model showing the formulated workflow with data inputs to produce the stack image of NDVI and potential temperature.

(iv) Creating Feature Space Image

Input image: 01_97_ndvi_pot_06.img

Output image: ndvi_pot_097_1_2.fsp.img

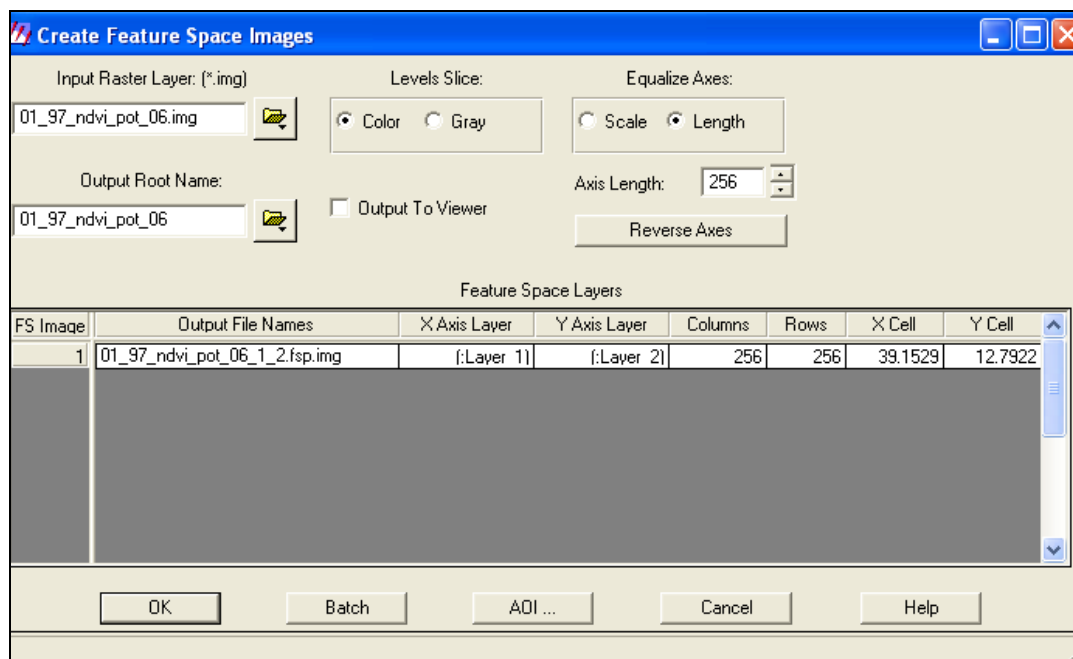


Figure AIV.13: The ERDAS built-in model interface of Creating Feature Space Image.

(v) Converting Pixels to ASCII (.asc)

Input image: ndvi_pot_097_1_2.fsp.img

Output image: ndvi_pot_temp_097.asc

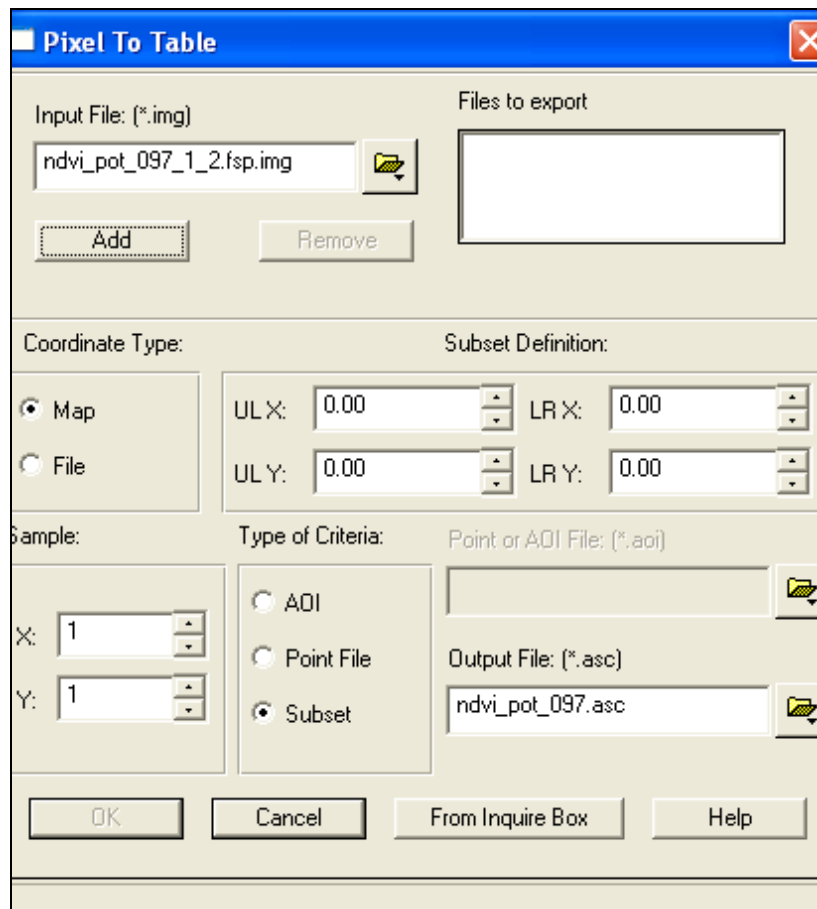


Figure AIV.14: The ERDAS built-in model interface of converting pixel values to ASCII.

(i) Calculating TVWI values

Input image: \$n2_ndvi_pot_08_193, values of dryline1 and dryline2 interpreted from the trapezoidal shape of the scatter plot of NDVI and potential surface temperature using Microsoft spreadsheet from the generated ASCII file.

Example: 193 DOY of 2008 the dryline was 317.00 and the dryline2 was [375.59-(0.0071*NDVI)]

Intermediate image (dryline): \$n4_08_193_273.img

Output image (TVWI): 193_tvwi_08.img

Intermediate equation for calculating dryline:

```
CONDITIONAL { ($n2_ndvi_pot_08_193(1) ==0) 0,
($n2_ndvi_pot_08_193(1) >=8300) 375.59-(0.0071*$n2_ndvi_pot_08_193(1)),
($n2_ndvi_pot_08_193(1) <8300) 317
}
```

Equation for calculating TVWI:

```
CONDITIONAL { ($n4_08_193_273 ==0) 0,
($n2_ndvi_pot_08_193(2) >$n4_08_193_273) 0,
($n2_ndvi_pot_08_193(2) <=273) 1,
($n2_ndvi_pot_08_193(2) > 273) ((($n4_08_193_273 -
$n2_ndvi_pot_08_193(2))/($n4_08_193_273 - 273))}
```

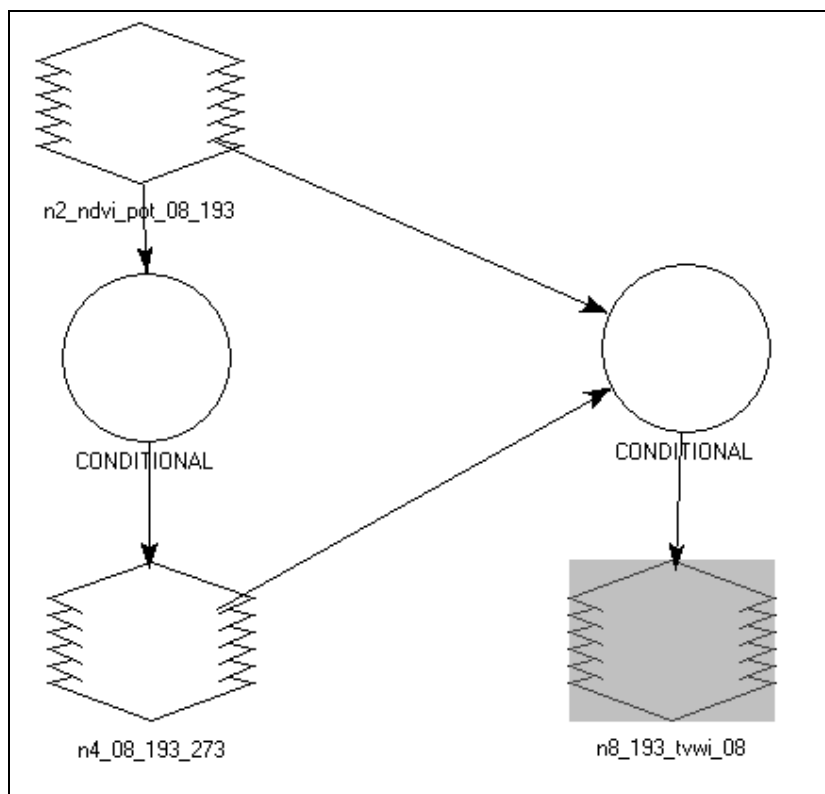


Figure AIV.15: The spatial model showing the formulated workflow with data inputs to produce the TVWI images.

6. Calculating global mean and standard deviation:

Input image: \$n1_forest_tvwi_stack_097_297_08 (Example of TVWI 2008 after clipping the images according to boreal forested zone)

Output image: Global mean, Global standard deviation in .tbl format

Equation:

GLOBAL MEAN (\$n1_forest_tvwi_stack_097_297_08 , IGNORE 0)

GLOBAL STANDARD DEVIATION (\$n1_forest_tvwi_stack_097_297_08 ,
IGNORE 0)

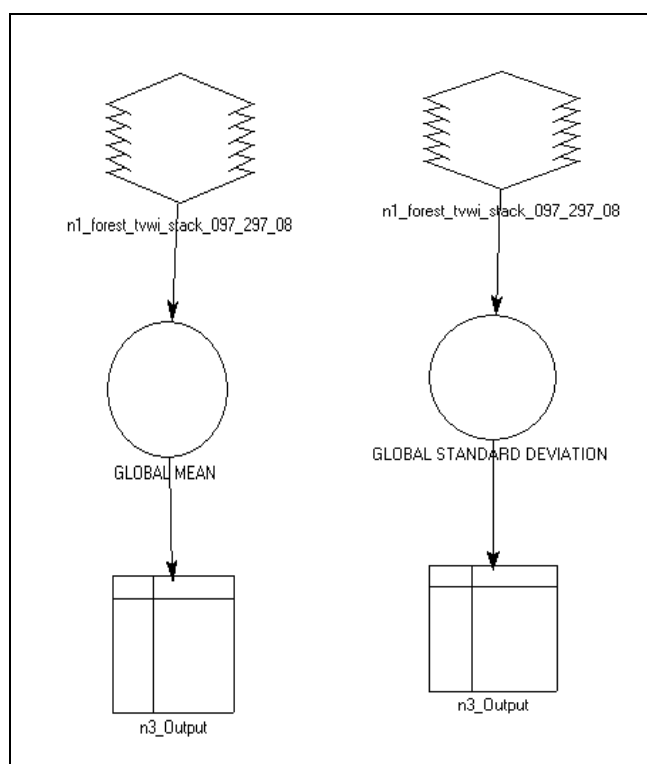


Figure AIV.16: The spatial model showing the formulated workflow with data inputs to calculate the global mean and standard deviation.

7. **Generating fire danger maps:**

Example of 169 DOY of year 2008 to forecast 177 DOY fire danger2008

Input image: \$n1_gap_filled_stack_lst_08, \$n4_nmdi_stack_097_297_2008, \$n7_tvwi_stack_097_297_2008, global mean values for the three variables in 169 DOY of 2008.

Output image: fire_danger_class_169_08.img, data type: unsigned 4 bit

Equations:

```
CONDITIONAL{($n1_gap_filled_stack_lst_08(10)==0)0,
($n1_gap_filled_stack_lst_08(10) >29377) 1 , ($n1_gap_filled_stack_lst_08(10)
<=29377) 2 }
```

```
CONDITIONAL{($n4_nmdi_stack_097_297_2008(10)==0)0,
($n4_nmdi_stack_097_297_2008(10)<4731)1,
($n4_nmdi_stack_097_297_2008(10) >= 4731) 2 }
```

```
CONDITIONAL { ($n7_tvwi_stack_097_297_2008(10) ==0) 0 ,
($n7_tvwi_stack_097_297_2008(10) < 4359) 1 ,
($n7_tvwi_stack_097_297_2008(10) >= 4359) 2 }
```

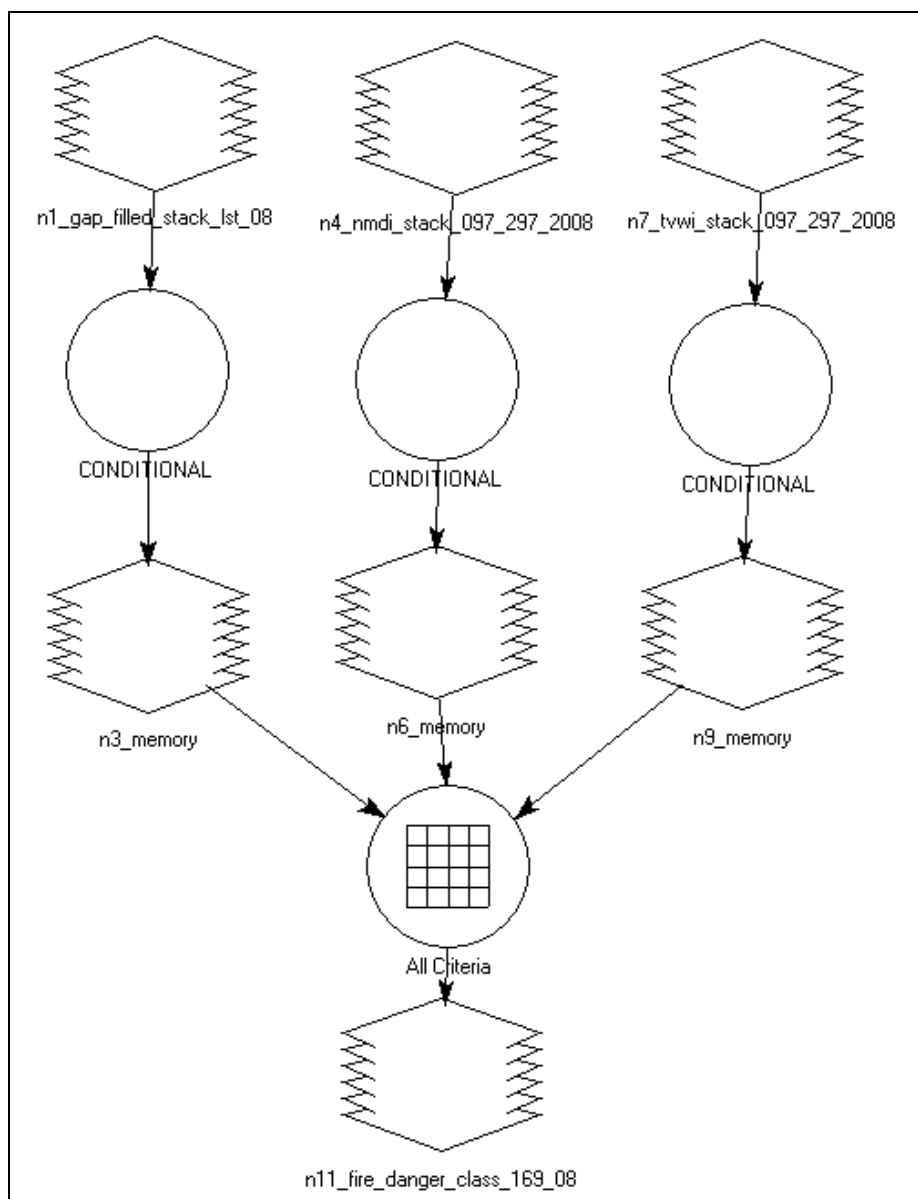


Figure AIV.17: The spatial model showing the formulated workflow with data inputs to produce the fire danger maps.

Appendix V

Copyright permission document for Wang and Qu 2007:

Usage Permissions	3
AGU - Earth Oceans Atmosphere Space Planets	
Home » Publications » Authors » Usage Permissions	
<h2>Usage Permissions</h2>	 Alerts 
<h3>Usage Permissions</h3>	 Publications Contacts
<p>Permission is granted for individuals to make single copies for personal use in research, study, or teaching and to use figures, tables, and short quotes from the journal for republication in scientific books and journals. This permission does not extend to posting a copy of the PDF or HTML created by AGU for publication. There is no charge for any of these uses, but the material must be cited appropriately.</p>	Author Help E-mail: author.help@agu.org
<h3>Rights Granted to Authors</h3>	Graphics Help E-mail: graphics-help@agu.org
<p>AGU's philosophy recognizes the need to ensure that authors have a say in how their works are used and the necessity to foster broad dissemination of scientific literature while protecting the viability of the publication system. The following nonexclusive rights are granted to AGU authors:</p>	Customer Service E-mail: service@agu.org
<ul style="list-style-type: none"> • All proprietary rights other than copyright (such as patent rights) • The right to present the material orally • The right to reproduce figures, tables, and extracts properly cited • The right to make paper copies of all or part of the contribution for classroom use • The right to deny subsequent commercial use of the contribution • The right to place the contribution or its abstract on his/her personal Web site as described below. 	
http://www.agu.org/pubs/authors/usage_permissions.shtml	9/7/2011